TECHNICAL REPORT Report No.:ESSO-INCOIS-OMDA-TR-02(2024)

Improvements in Regional Analysis of Indian OceaN (RAIN) with sea-level anomaly (SLA) assimilation

by

Balaji Baduru, Biswamoy Paul, Arya Paul & P.A. Francis

Indian National Centre for Ocean Information Services (INCOIS)
Earth System Science Organization (ESSO)
Ministry of Earth Sciences (MoES)
HYDERABAD, INDIA
www.incois.gov.in

May 2024

DOCUMENT CONTROL SHEET

Earth System Science Organization (ESSO)
Ministry of Earth Sciences (MoES)
Indian National Centre for Ocean Information Services (INCOIS)

ESSO Document Number: ESSO-INCOIS-OMDA-TR-02(2024)

Title of the report: Improvements in Regional Analysis of Indian OceaN (RAIN) with sea-level anomaly (SLA) assimilation

Author(s) [Last name, First name]:

Balaji B., Biswamoy Paul, Arya Paul & P.A.Francis

Originating unit : Ocean Modeling and Data Assimilation (OMDA) Division, Ocean Modeling, Applied Research & Services (OMARS) Group, INCOIS.

Type of Document: Technical Report (TR)

Number of pages and figures: 97, 140

Number of references: 19

Keywords: Data Assimilation, Local Ensemble Transform Kalman Filter, Regional Ocean Modeling System, Indian Ocean.

Security classification: Open

Distribution: Open

Date of publication: 22 May, 2024

Abstract

We had developed the assimilation system RAIN (Regional Analysis of Indian OceaN) using Local Ensemble Transform Kalman Filter (LETKF) and interfaced with the Regional Ocean Modeling System (ROMS) that assimilates in-situ temperature and salinity from RAMA moorings, NIOT buoys and Argo floats. The system also assimilate satellite track data of sea-surface temperature from GHRSST. The speciality of this assimilation system is that it comprises ensembles that are initialized with different model coefficients like diffusion parameters and the ensemble members also respond to two different mixing schemes - K profile parameterization and Mellor-Yamada. This helps to maintain the ensemble's spread, which has always been a difficult challenge. RAIN provides an improved initial condition to the operational ocean forecast model ROMS. In order to improve the ocean state forecast, the RAIN system has now been modified to assimilate sea-level anomaly (SLA). The RAIN system is modified to sequentially assimilate corrected SLA observations along with assimilation of in-situ temperature, salinity profiles and SST and we call it the RAIN-SLA system.

We validate the RAIN-SLA system extensively against multiple observations ranging from RAMA moorings to ADCP observations across both dependent variables like temperature and salinity and independent variables like currents. We show that SLA assimilation improves the overall ocean state except at a few isolated locations. It improves the correlation with respect to observations and reduces the root-mean-squared error. We also show that SLA assimilation improves the estimation of currents.

Improvements in Regional Analysis of Indian OceaN (RAIN) with sea-level anomaly (SLA) assimilation

Balaji Baduru, Biswamoy Paul, Arya Paul, P.A. Francis

Indian National Centre for Ocean Information Services (INCOIS)
Earth System Science Organization (ESSO)
Ministry of Earth Sciences (MoES)
HYDERABAD, INDIA

Acknowledgements

The Data Assimilation (DA) team wishes to acknowledge Prof. Eugenia Kalnay and Dr. Steve Penny from University of Maryland, USA. The LETKF-ROMS is built on the foundation of LETKF-MOM which Steve had developed for MOM. We are grateful to them for sharing the code of LETKF-MOM and introducing us to rocoto which is an excellent tool for firing parallel jobs. Arya Paul also wishes to thank Ministry of Earth Sciences (MOES) for funding the visit. The DA team thank OOS team, INCOIS for providing us the ocean state analysis from operational RAIN against which RAIN-SLA is compared with. The team would also like to thank the ODM and OON Division, INCOIS for supplying us with the observations, without which this program would not have been possible. We also acknowledge the support received from the ICT Division, INCOIS and the support staff from NCMRWF overseeing the upkeep and maintenance of the high performance computer Mihir and a special thanks to Dr. V.S.Prasad and Dr. Johny C. J from NCMRWF for providing us the ensemble atmospheric fluxes. The team concludes by thanking our Director for continuing to believe in us and providing assistance in every way possible.

Author Contribution

AP has developed the LETKF-ROMS code and the submission scripts. BB developed the steric correction and reference level adjustment code for sequential assimilation of SLA observations. BB and BP have carried out the experiments. BB, BP, AP and PAF have analyzed the results. BB has written the technical report assisted by BP, AP and PAF.

Abstract

We have developed the assimilation system RAIN (Regional Analysis of Indian OceaN) [7-8] using Local Ensemble Transform Kalman Filter (LETKF) and interfaced with the Regional Ocean Modeling System (ROMS) that assimilates in-situ temperature and salinity from RAMA moorings, NIOT buoys and Argo floats. The system also assimilate satellite track data of sea-surface temperature from GHRSST. The speciality of this assimilation system is that it comprises ensembles that are initialized with different model coefficients like diffusion parameters and the ensemble members also respond to two different mixing schemes - K profile parameterization and Mellor-Yamada. This helps to maintain the ensemble's spread, which has always been a difficult challenge. RAIN provides an improved initial condition to the operational ocean forecast model ROMS. In order to improve the ocean state forecast, the RAIN system has been modified to assimilate sea-level anomaly (SLA). The RAIN system is modified to sequentially assimilate corrected SLA observations along with assimilation of in-situ temperature, salinity profiles and SST.

We validate the RAIN-SLA system extensively against multiple observations ranging from RAMA moorings to ADCP observations across both dependent variables like temperature and salinity and independent variables like currents. We show that SLA assimilation improves the overall ocean state except at a few isolated locations. It improves the correlation with respect to observations and reduces the root-mean-squared error. We also show that SLA assimilation improves the estimation of currents.

Contents

1. The System

1.1 Introduction

The objective of Indian National Centre for Ocean Information Services (INCOIS) is to provide the best possible ocean information and advisory services to society, industry, government agencies and the scientific community through sustained ocean observations and constant improvements through systematic and focused research. The ocean state forecast is provided by implementing ocean general circulation models. There are multiple ways in which the forecast may be improved. One of the approaches is to implement a high resolution general circulation model that can resolve finer length scales and hence simulate processes that were not properly resolved in low resolution models. Under the project High-resolution Operational Ocean Forecast and reanalysis System for the Indian Ocean (HOOFS), these high-resolution ocean model setups provide operational forecasts of various oceanographic parameters for the Indian Ocean. Regional Ocean Modeling System (ROMS) [1-4], which is a state-of-the art ocean circulation model, is used as the general circulation model for the HOOFS setups [5-6]. Due to uncertainty in the initial condition the forecast is still off from reality. The model trajectory will most likely be restrained from drifting from the truth if the initial conditions are corrected on a regular basis. The most prominent way to periodically adjust the initial condition is through the technique of data assimilation (DA). In terms of uncertainty and root-mean-squared error, data assimilation is a method that takes information from both the model state and the observation, statistically churns it to reduce the cost function (errors), and provides out an initial condition that is closer to the truth than either the input prior model state or the input observation.

RAIN (Regional Analysis of Indian OceaN) [7-9] is a data assimilation system developed in-house using Local Ensemble Transform Kalman Filter (LETKF) algorithm [10] and interfaced with ROMS model for Indian Ocean region to improve the accuracy of the model forecast. The data assimilation system LETKF-ROMS assimilates satellite track data of sea-surface temperature (SST), temperature and salinity profiles from various observation networks like RAMA moorings, NIOT buoys, ARGO floats and ship data. RAIN has improved the ocean state forecast, the Implementation and evaluation of RAIN is presented in [8] and detailed validation results are presented in technical report [7]. RAIN comprises 80 ensemble members, i.e., 80 similar replicas of the model evolve in time starting from slightly different initial conditions. The physical parameters like tracer diffusion coefficients, viscosity coefficients etc and mixing parameterization schemes also slightly differ across the ensemble members. This strategy aids in exploiting the benefits of varied mixing parameterizations and also helps in maintaining a healthy spread across the ensemble members. A healthy spread plays a pivotal role in arresting filter divergence. The ensemble members are forced every 6 hourly by 80 ensembles of fluxes from the atmospheric model GFS operated by National Centre for Medium Range Weather Forecasting (NCMRWF). Identical boundary conditions, derived from INCOIS-GODAS, are fed to all the ensemble members. This system generates ocean state vectors of the Indian Ocean basin (30°N -

30°S; 30°E - 120°E) on a regular grid with an horizontal length scale of ~ 9 km and the ocean, on the other hand, is divided into 40 layers vertically.

The forecast model used in RAIN (Regional Analysis of Indian OceaN) for the Indian Ocean is the Regional Ocean Modeling System (ROMS) [1-4], developed by Rutgers University, New Jersey, USA. ROMS is a free surface, terrain following general circulation model which solves a set of primitive equations in an orthogonal curvilinear coordinate system. The domain and bathymetry in the model domain for the RAIN setup is shown in Fig.1.1. The domain extends from 30^{O}E to 120^{O}E in the east-west direction and from 30^{O}S to 30^{O}N in the north-south direction. The horizontal resolution is $1/12^{O}$ (approximately 9 km) and it has 40 sigma levels in the vertical. A detailed description of RAIN setup is provided in [6-9]. The in-situ temperature and salinity profiles and satellite observed sea surface temperature (SST) are assimilated (henceforth called RAIN) with a provision to assimilate sea-level anomaly (SLA) and sea surface salinity (SSS).

To ameliorate the ocean state forecast the RAIN system is upgraded to assimilate sea-level anomaly (SLA). Results from the RAIN system with SLA assimilation are presented in this work. In section 2, we describe the RAIN set-up followed by a description of the observation that went into the assimilation system in section 3. Finally at the end of this chapter, we briefly describe the data assimilation scheme in section 4.

1.2 RAIN-SLA

Even though our RAIN system is capable of assimilating sea-surface salinity (SSS) and sea-level anomaly (SLA), we did not assimilate these observations since SSS is not available during the period of our interest and assimilating SLA will incur errors due to absence of steric signal in ROMS. The steric effect associated with thermal expansion of the water column is observed by altimeters, so included in the SLA satellite observation, but in ROMS this is neglected. So the steric correction is to be applied to observations before being provided to the RAIN system. The RAIN system is tweaked to assimilate modified SLA observations along with in-situ temperature and salinity profiles and satellite observed SST (henceforth called RAIN-SLA). The sequential assimilation strategy is used for assimilating SLA observation and to handle steric height. Firstly the quality controlled in-situ temperature and salinity profiles and sea surface temperature observations were assimilated to get improved analysis and followed by computation of steric height for assimilation of SLA observations with steric correction. The chief characteristics of the model configuration of RAIN and RAIN-SLA are identical. These systems are compared and evaluated with 40 ensembles in state estimation of prognostic variables and some diagnostic variables.

1.3 Observation

We assimilate in-situ temperature and salinity profiles from observation networks that include Argo and moored buoys within the Indian Ocean domain. We however discard assimilating observations that are too close to the domain boundaries or too close to any landmass. We also assimilate satellite track data of sea-surface temperature (SST) from Group for High Resolution Sea Surface Temperature (GHRSST). We also assimilate sea-level anomaly (SLA) track data from Archiving Validation and Interpretation of Satellite Oceanography

(AVISO) Altimetry in the RAIN-SLA system. For the assimilation system, we coarse-grain the data over a length-scale of 50 km due to the extremely dense data along the track. This ”super-obbing” is routinely done in many assimilation systems [11].

In Fig 1.1, we show the model domain for Indian Ocean along with the location of the in-situ instruments that record temperature, salinity and currents. In Fig 1.2, the location of daily pop-up of Argo floats is plotted in the Arabian Sea, Bay of Bengal and Indian Ocean which were used later for validating the results. In Fig.1.3, we show a typical SST track data (after being coarse-grained) that enters into the assimilation system. In Fig 1.4, we show a sample SLA track data captured on a single day and accumulated observations captured over 5 days. The SLA observations combined for 5 days were assimilated on the 5th day in the RAIN-SLA system and no SLA observation assimilated in the RAIN system.

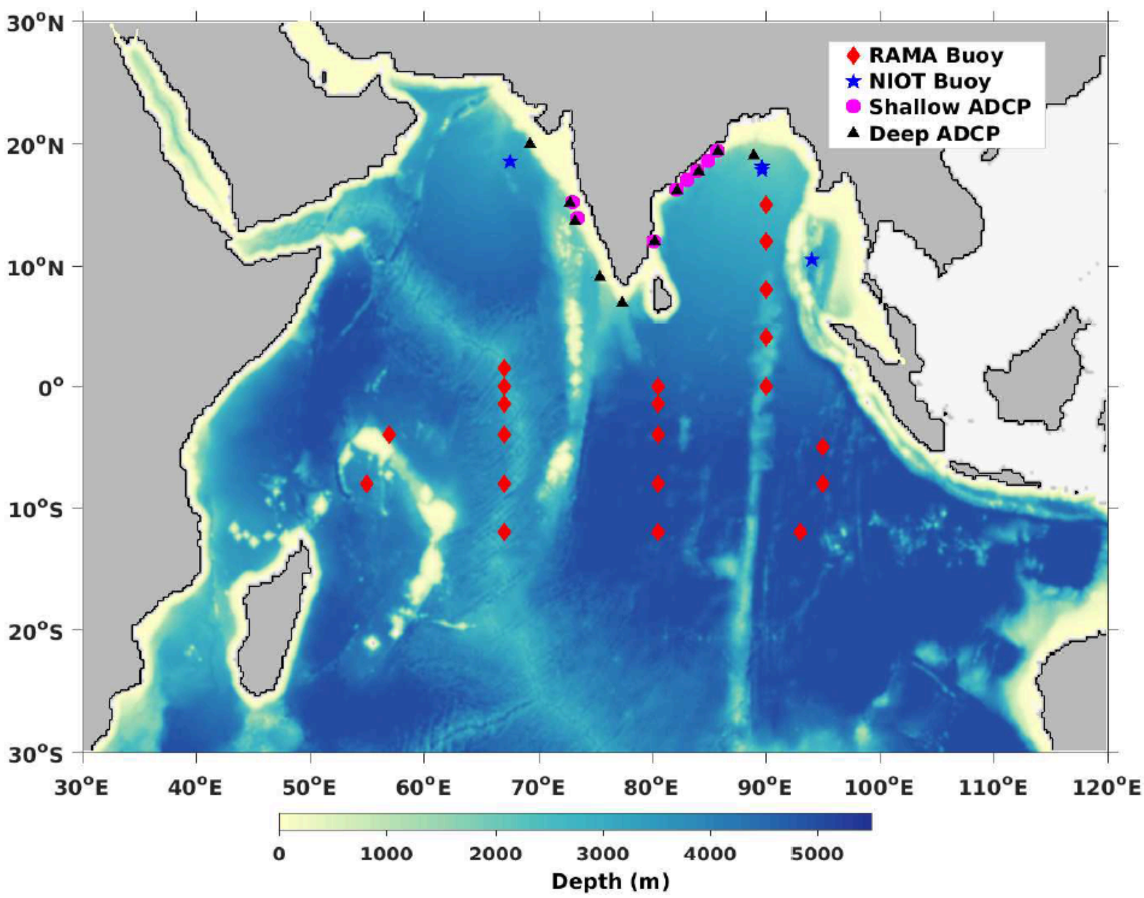

Figure 1.1: Picture of the Indian Ocean domain along with the bathymetry. The location of in-situ RAMA moorings, NIOT buoys and ADCPs are also pointed out.

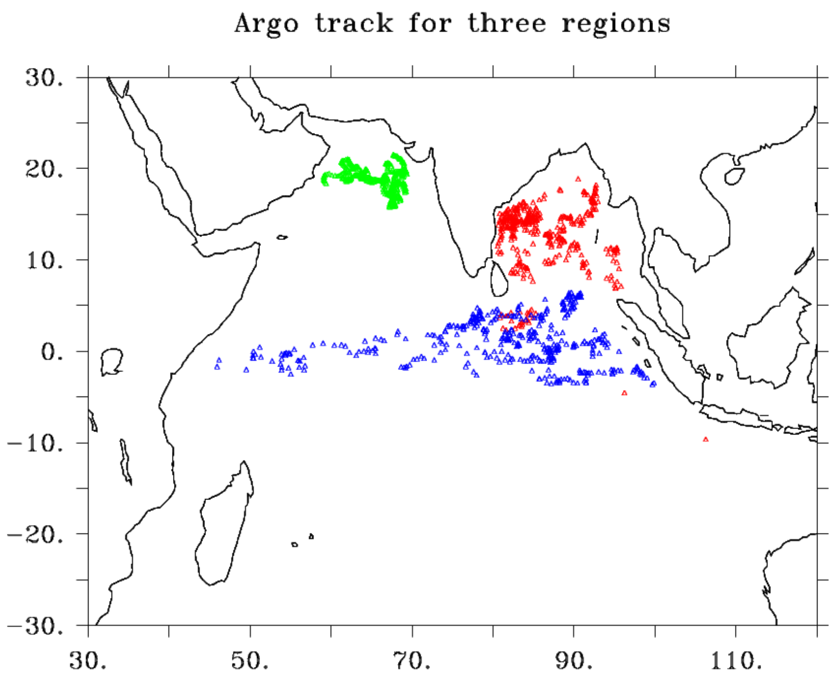

Figure 1.2: Daily pop-up of Argo floats in the Indian Ocean - primarily in the Northern Indian Ocean - is plotted which were used for validation. Daily pop-up were segregated according to the location of their pop-ups - green in Arabian Sea, red in Bay of Bengal and blue in Equatorial Indian Ocean.

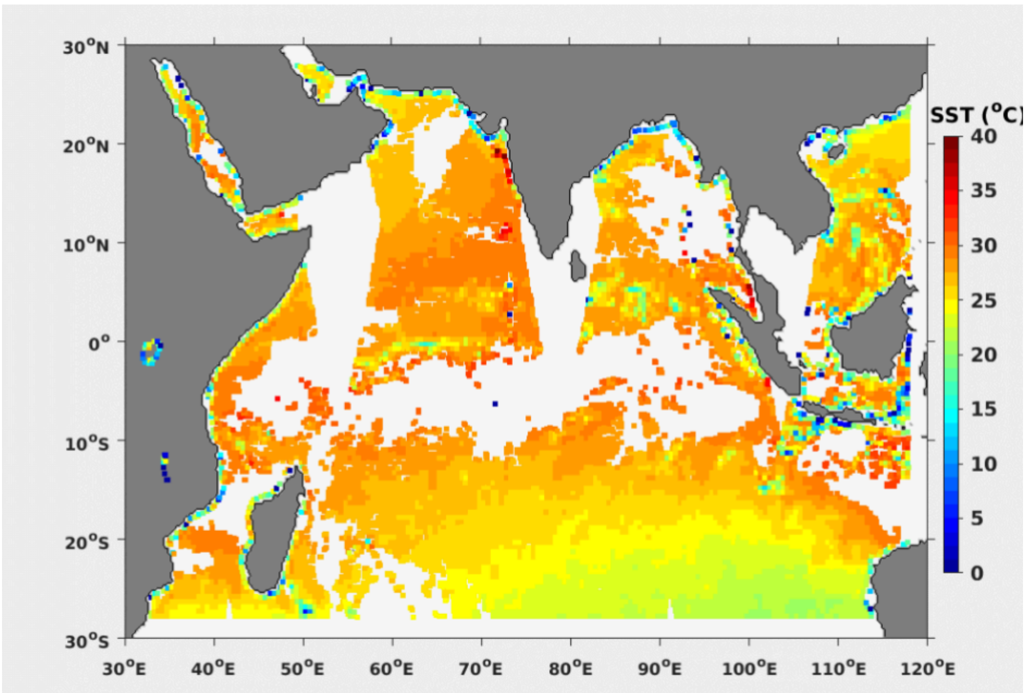

Figure 1.3: Sample satellite track (after superobbing) capturing SST over Indian Ocean.

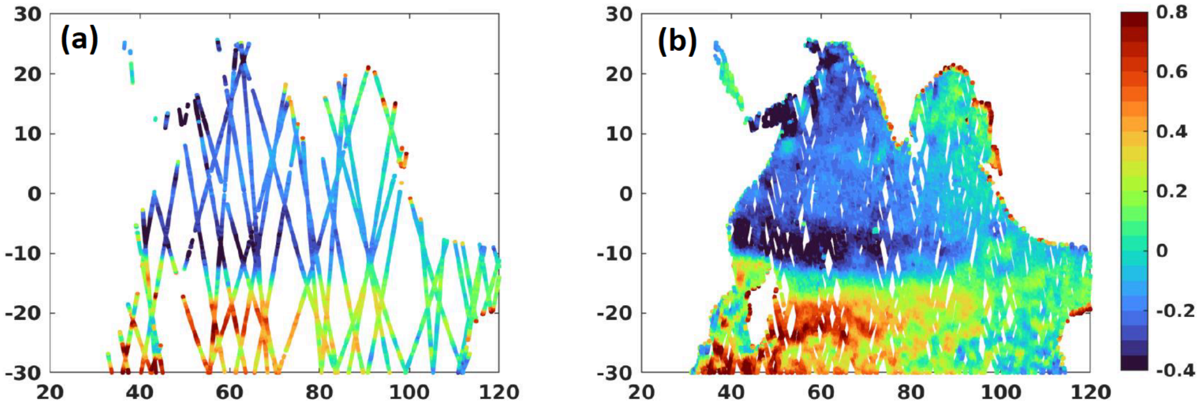

Figure 1.4: Sample satellite track (after superobbing) capturing SLA over Indian Ocean. (a) observations captured on a single day and (b) Observations captured over 5 days.

1.4 Data Assimilation - LETKF

We employ Local Ensemble Transform Kalman Filter [10] as the data assimilation technique. LETKF has its origin to the Local Ensemble Kalman Filter (LEKF) [12] and the Ensemble Transform Kalman Filter (ETKF) [13] and is an insightful amalgamation of these two techniques. The major advantage of LETKF is that it can produce analysis that is qualitatively similar to LEKF whereas the efficiency is as good as ETKF thereby exploiting the virtues of both the systems. Nevertheless, it is a variant of Ensemble Kalman Filter wherein the model error covariance is approximated as a sample covariance derived from the ensemble members and whose rank is roughly equal to the number of ensemble members (k) used in the study when the ensemble size is large. For an infinite number of ensemble members, this reduces exactly to model error covariance. We have used 40 ensemble members and hence the rank of the model error covariance matrix is 39. The inaccuracy introduced due to this approximation is traded off with the sharp decrease in computational resources and runtime. The configuration details like initial ensemble generation, boundary condition, strategies employed to maintain the ensemble spread, covariance inflation, localization radius and spatio-temporal varying representation error (RE) [9] supplied to observation error covariance are discussed in [7-8]. The settings are identical for both RAIN and RAIN-SLA systems.

In the next few chapters, we will present comparisons of RAIN and RAIN-SLA with a variety of observation networks of various state variables like SST, temperature, salinity, SLA and currents. It is important to reiterate that the RAIN-SLA, which is designed as a 40 ensemble system, is compared with RAIN system.

2. Sea Surface Temperature

2.1 Introduction

We validate Sea Surface Temperature (SST) with respect to observations from multiple sources RAMA moorings [14], NIOT buoys and Advanced Very High Resolution Radiometer (AVHRR) satellite [15]. It is to be noted that ROMS does not relax its SST to any climatological field. This has the advantage that SST obtained during analysis will likely not drift away during forecasting when relaxation fields of SST (reanalysis) are unavailable. We will compare the quality of states obtained from RAIN and RAIN-SLA. We emphasize that SST is not an independent variable.

2.2 Comparison with AVHRR

We present here the comparison of the two systems - RAIN and RAIN-SLA - with respect to gridded SST obtained from AVHRR during the period September 2017 - December 2018. AVHRR provides daily SST over a resolution of about 25 km. The model states were projected onto the observation state and compared.

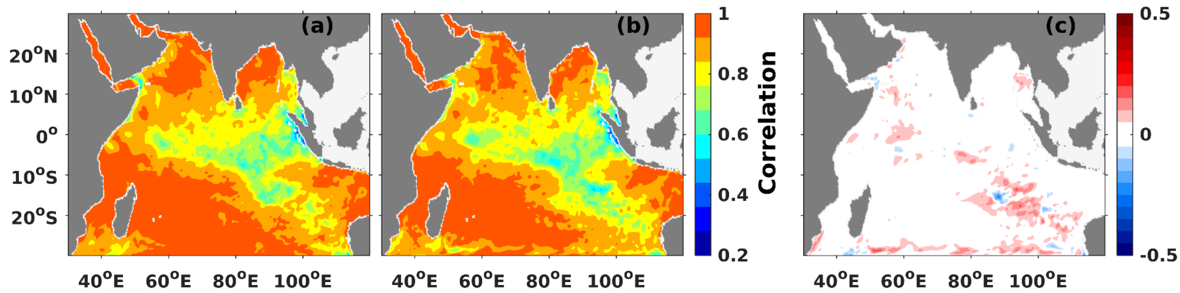

Figure 2.1: Spatial plot of correlation with respect to AVHRR for (a) RAIN, (b) RAIN-SLA assimilation and (c) Difference of (a)-(b). The Correlation is same in most of the regions over the Indian ocean domain with few patches of minor improvements and degradation.

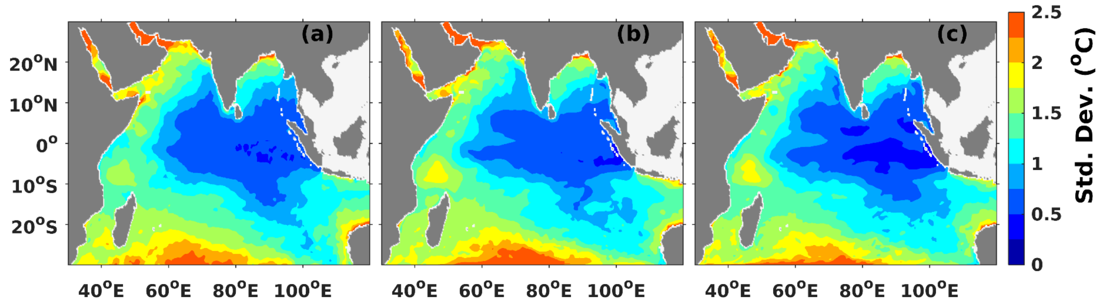

Figure 2.2: Spatial plot of standard deviation for (a) Observation, (b) RAIN and (C) RAIN-SLA. Both the systems appear to reproduce the large-scale variability of the observation.

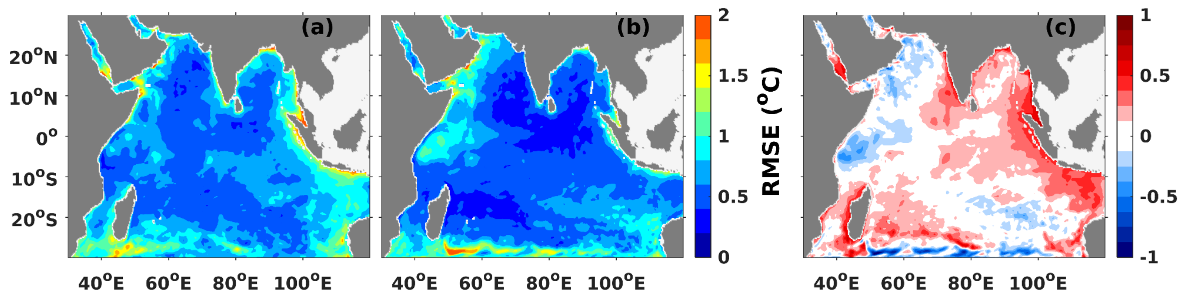

Figure 2.3: Spatial plot of root-mean-squared error (RMSE) with respect to AVHRR for (a) RAIN, (b) RAIN-SLA and (c) Difference of (a)-(b). SLA Assimilation has significantly brought down the rmse at all places in Bay of Bengal and part of eastern Arabian sea. SLA assimilation has reduced RMSE in most of the regions over the Indian ocean domain except the Somali coast region, western Arabian Sea and the southern Indian Ocean.

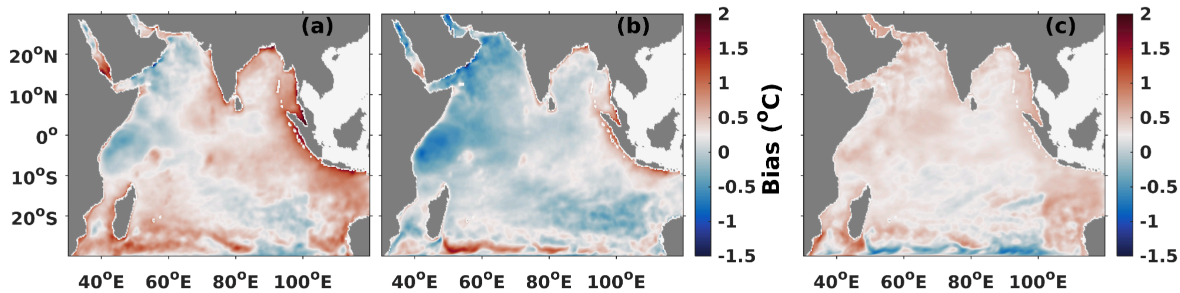

Figure 2.4: Spatial plot of bias with respect to AVHRR for (a) RAIN, (b) RAIN-SLA and (c) Difference of (a) - (b). Assimilating SLA has reduced the bias across the Indian Ocean.

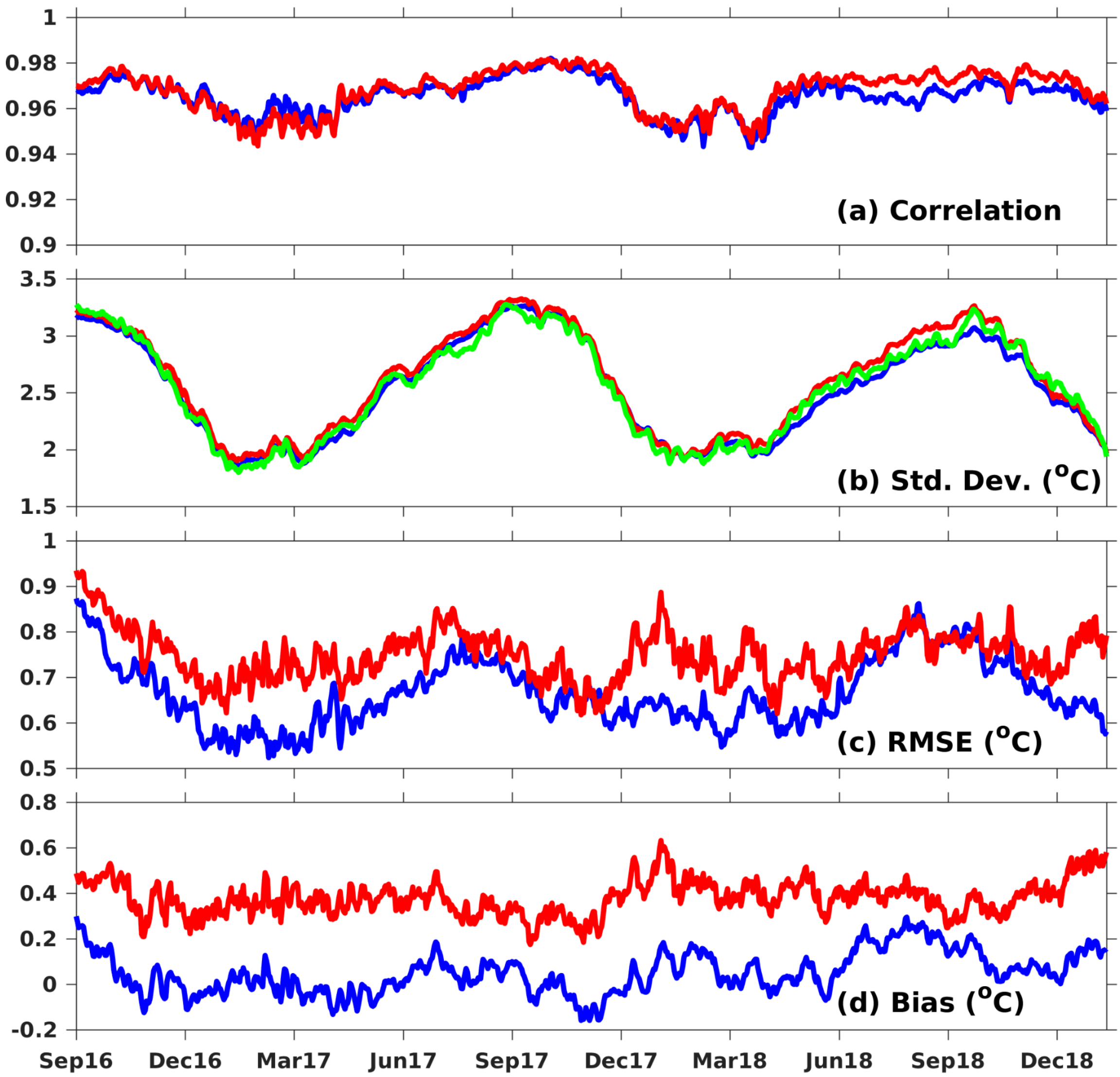

Figure 2.5: Temporal plot of (a) correlation, (b) standard deviation, (c) rmse and (d) bias from RAIN-SLA (blue), RAIN (red) and Observations (green). SLA Assimilation significantly improves the sea-surface temperature by reducing rmse and bias. The standard deviation of observation in (b) is shown in green.

2.3 Comparison with RAMA moorings

We present a comparison of the two systems with respect to various RAMA moorings (24 in number) [14] stationed in the Indian Ocean.

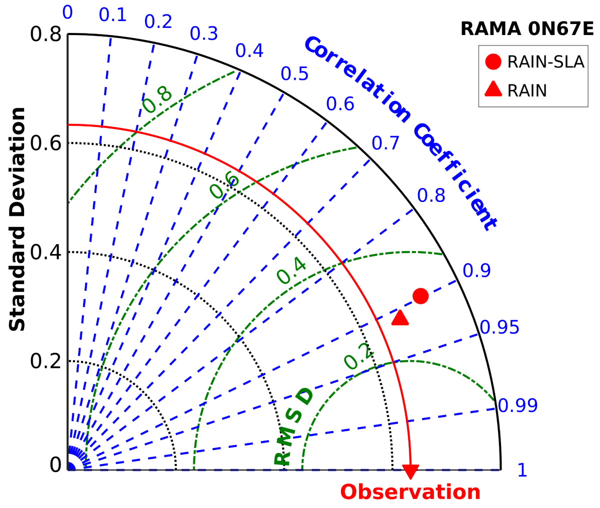

Figure 2.6:Taylor Diagram of SST from RAIN-SLA and RAIN with respect to RAMA mooring at 0° N, 67° E.

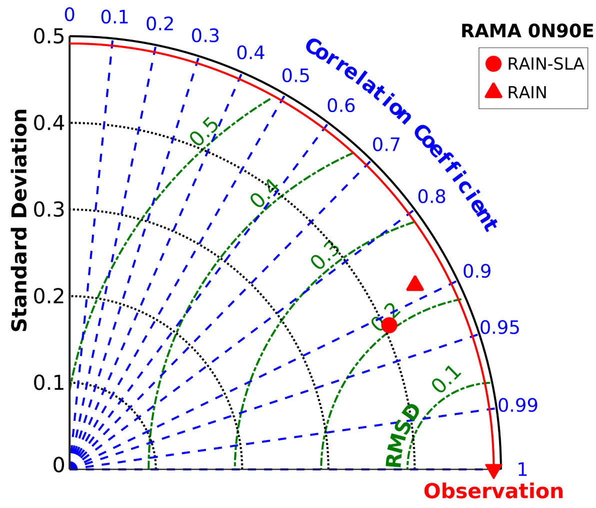

Figure 2.7:Taylor Diagram of SST from RAIN-SLA and RAIN with respect to RAMA mooring at 0° N, 90° E.

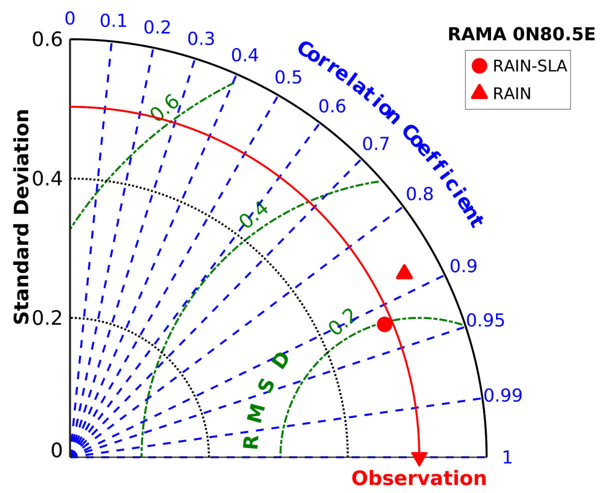

Figure 2.8:Taylor Diagram of SST from RAIN-SLA and RAIN with respect to RAMA mooring at 0° N, 80.5° E.

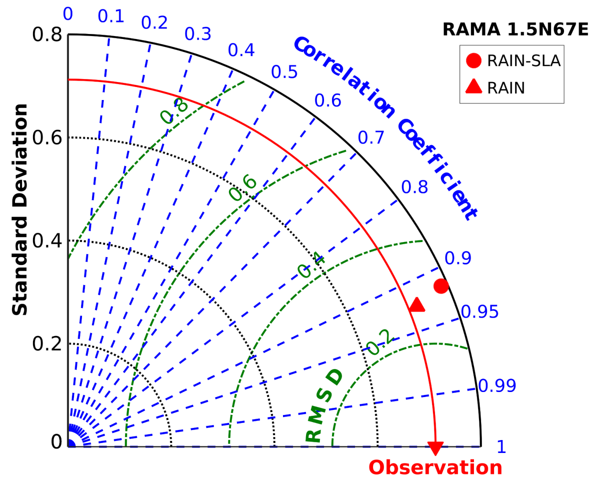

Figure 2.9:Taylor Diagram of SST from RAIN-SLA and RAIN with respect to RAMA mooring at 1.5° N, 67° E.

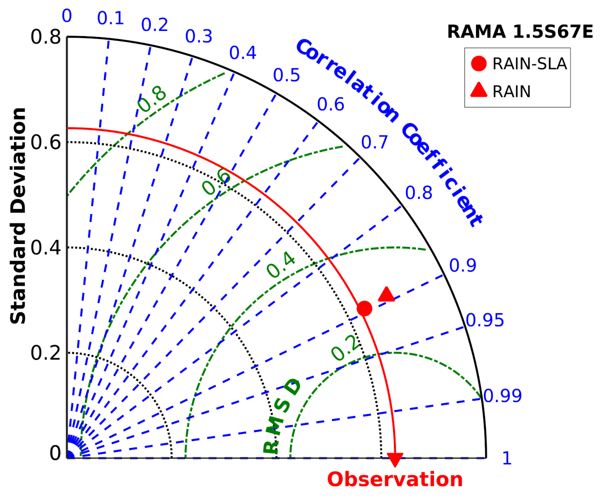

Figure 2.10:Taylor Diagram of SST from RAIN-SLA and RAIN with respect to RAMA mooring at 1.5° S, 67° E.

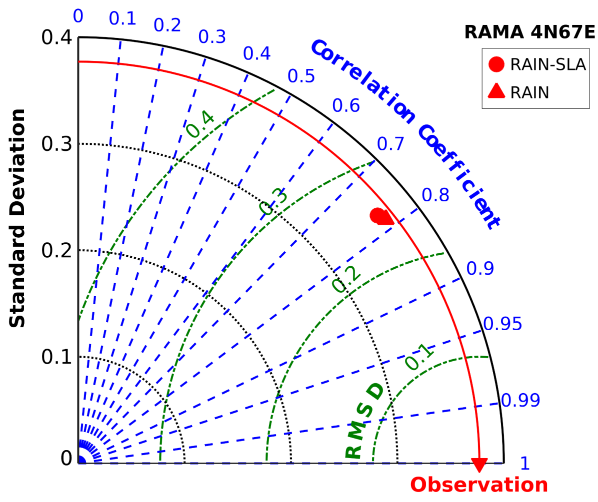

Figure 2.11:Taylor Diagram of SST from RAIN-SLA and RAIN with respect to RAMA mooring at 4° N, 67° E.

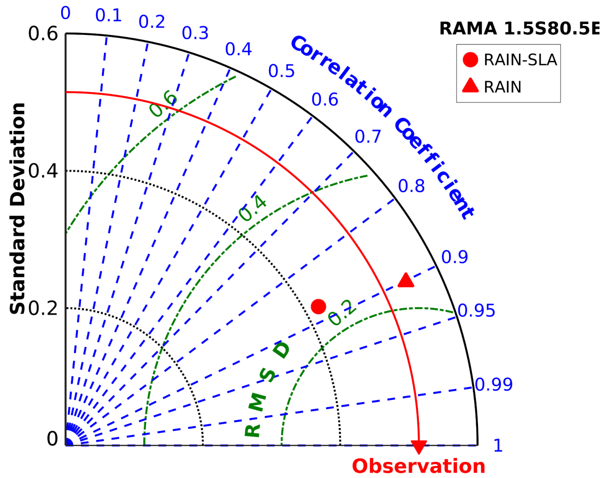

Figure 2.12:Taylor Diagram of SST from RAIN-SLA and RAIN with respect to RAMA mooring at 1.5° S, 80.5° E.

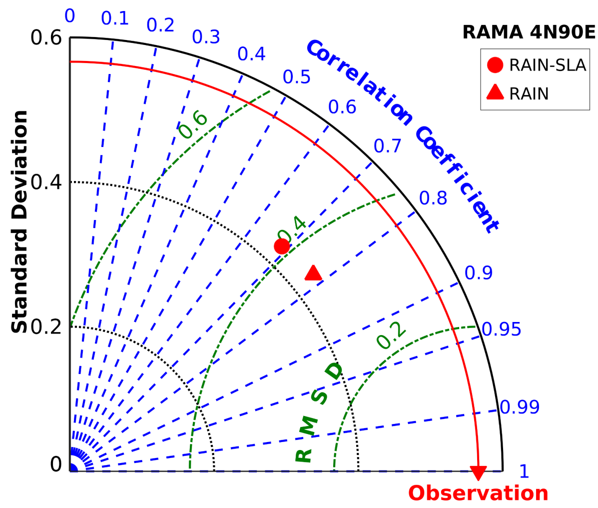

Figure 2.13:Taylor Diagram of SST from RAIN-SLA and RAIN with respect to RAMA mooring at 4° N, 90° E.

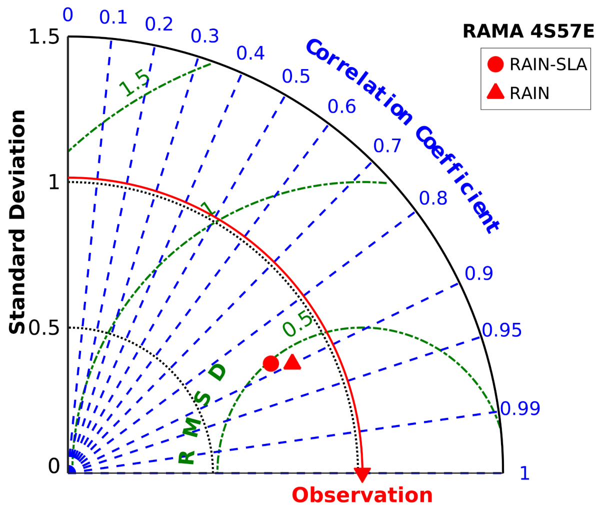

Figure 2.14:Taylor Diagram of SST from RAIN-SLA and RAIN with respect to RAMA mooring at 4° S, 57° E.

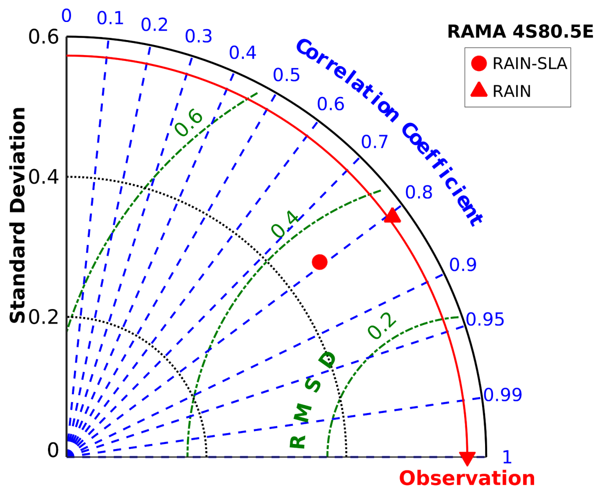

Figure 2.15:Taylor Diagram of SST from RAIN-SLA and RAIN with respect to RAMA mooring at 4° S, 80.5° E.

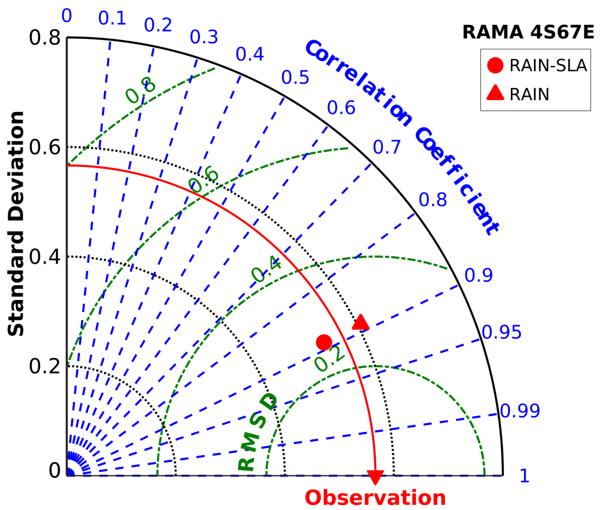

Figure 2.16:Taylor Diagram of SST from RAIN-SLA and RAIN with respect to RAMA mooring at 4° S, 67° E.

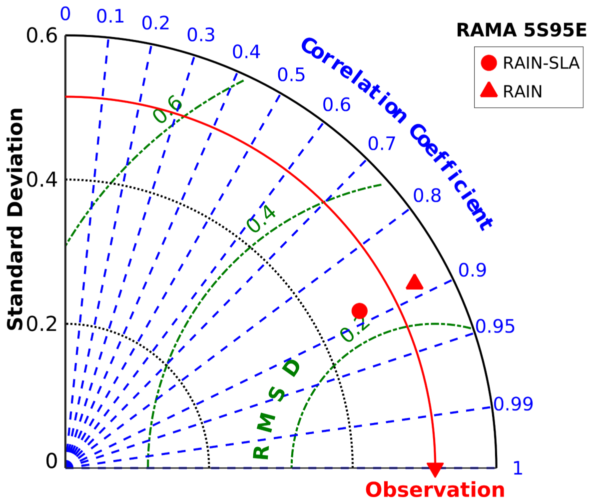

Figure 2.17:Taylor Diagram of SST from RAIN-SLA and RAIN with respect to RAMA mooring at 5° S, 95° E.

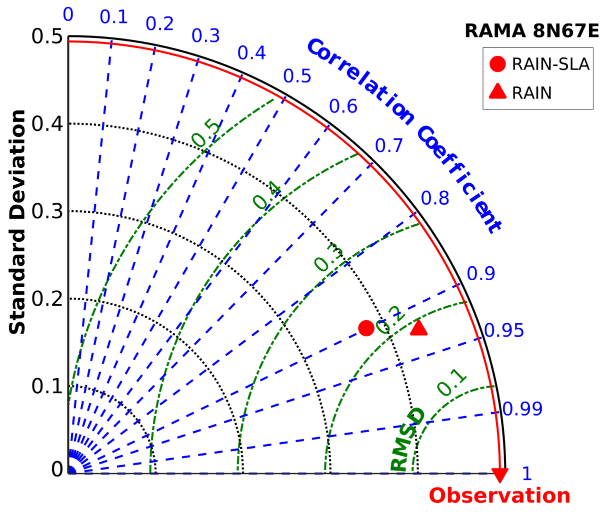

Figure 2.18:Taylor Diagram of SST from RAIN-SLA and RAIN with respect to RAMA mooring at 8° N, 67° E.

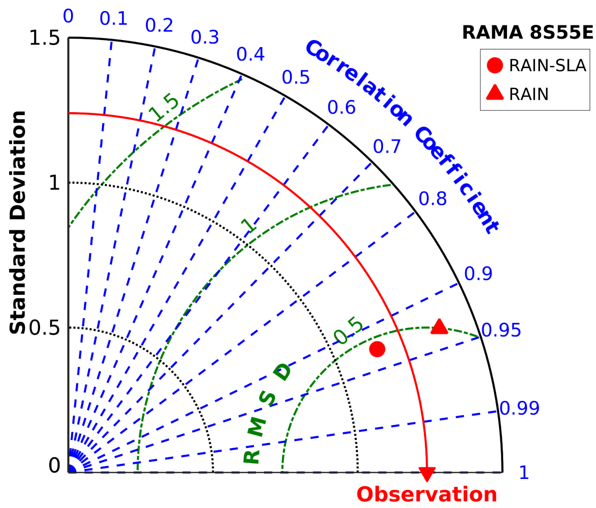

Figure 2.19:Taylor Diagram of SST from RAIN-SLA and RAIN with respect to RAMA mooring at 8° S, 55° E.

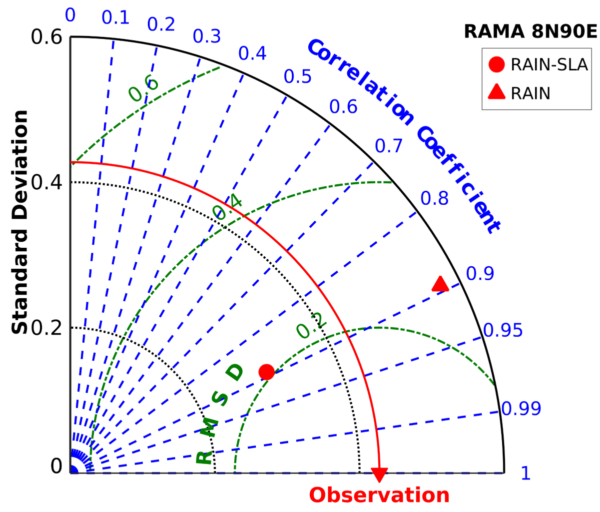

Figure 2.20:Taylor Diagram of SST from RAIN-SLA and RAIN with respect to RAMA mooring at 8° N, 90° E.

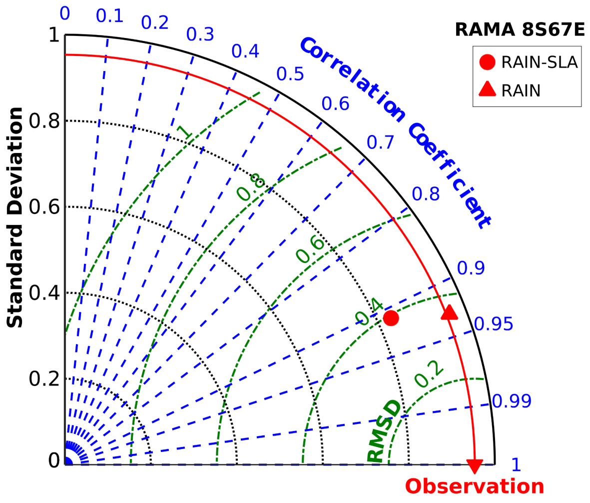

Figure 2.21:Taylor Diagram of SST from RAIN-SLA and RAIN with respect to RAMA mooring at 8° S, 67° E.

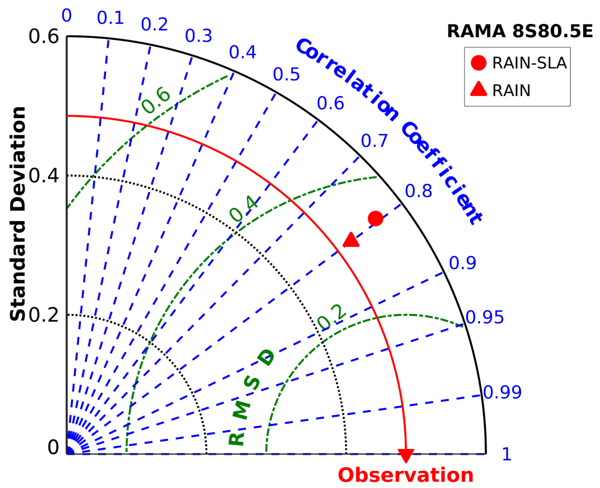

Figure 2.22:Taylor Diagram of SST from RAIN-SLA and RAIN with respect to RAMA mooring at 8° S, 80.5° E.

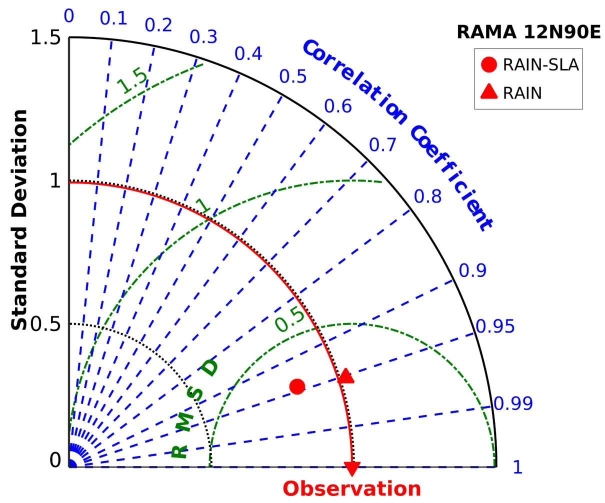

Figure 2.23:Taylor Diagram of SST from RAIN-SLA and RAIN with respect to RAMA mooring at 12° N, 90° E.

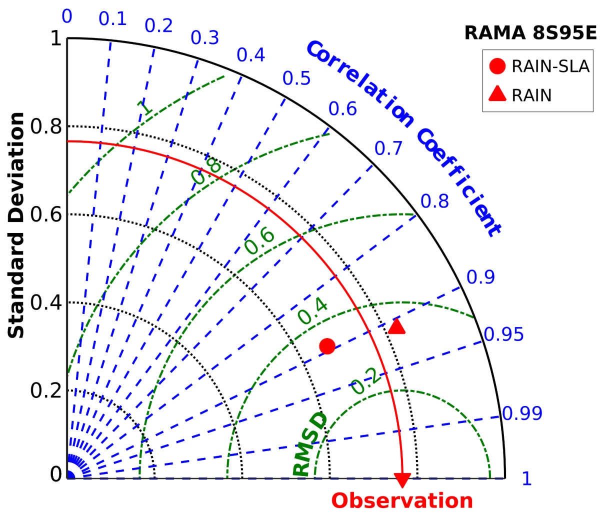

Figure 2.24:Taylor Diagram of SST from RAIN-SLA and RAIN with respect to RAMA mooring at 8° S, 95° E.

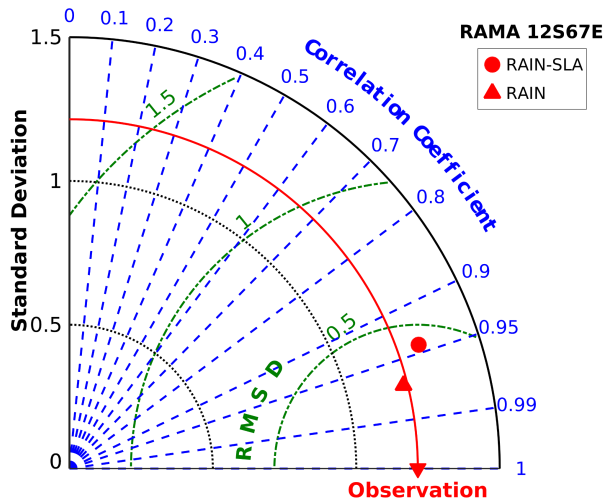

Figure 2.25:Taylor Diagram of SST from RAIN-SLA and RAIN with respect to RAMA mooring at 12° S, 67° E.

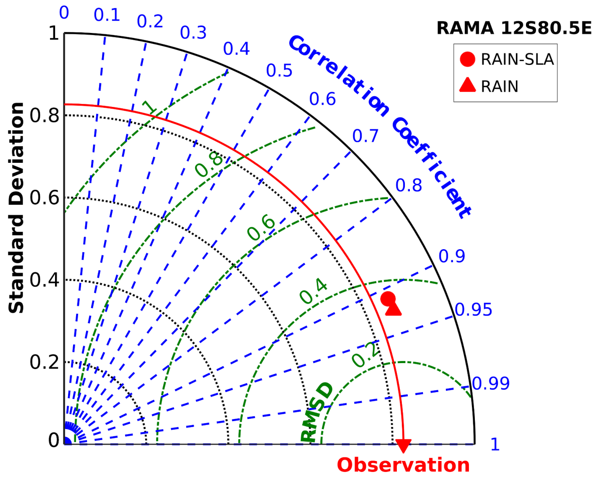

Figure 2.26:Taylor Diagram of SST from RAIN-SLA and RAIN with respect to RAMA mooring at 12° S, 80.5° E.

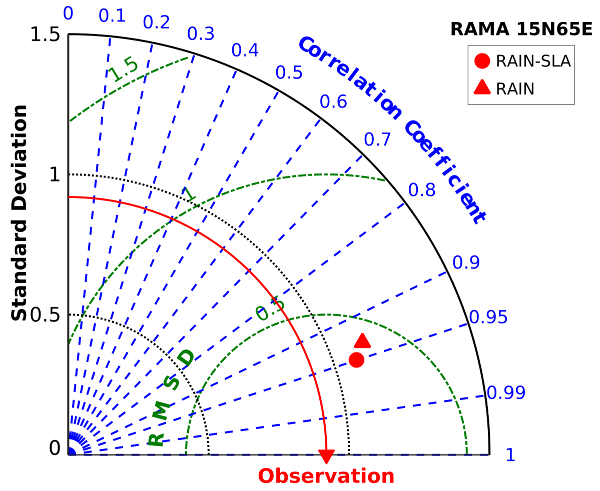

Figure 2.27:Taylor Diagram of SST from RAIN-SLA and RAIN with respect to RAMA mooring at 15° N, 65° E.

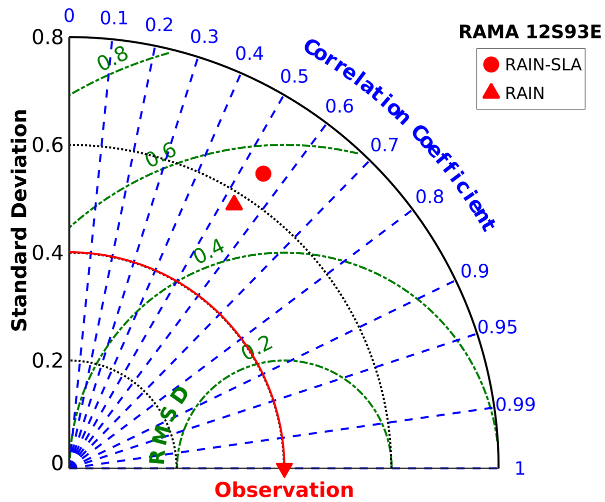

Figure 2.28:Taylor Diagram of SST from RAIN-SLA and RAIN with respect to RAMA mooring at 12° S, 93° E.

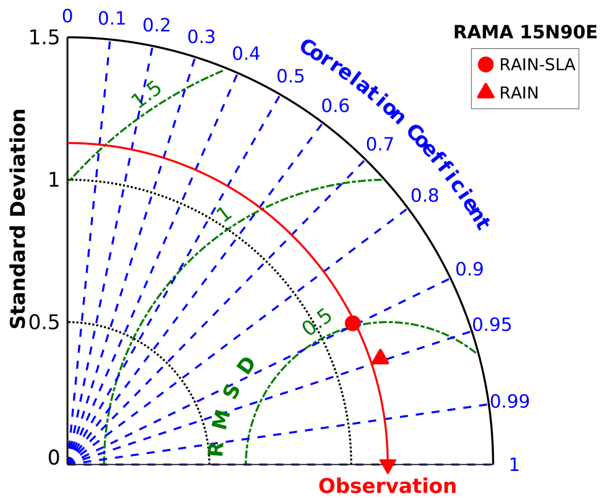

Figure 2.29:Taylor Diagram of SST from RAIN-SLA and RAIN with respect to RAMA mooring at ° N, 90° E.

2.4 Conclusion

We observe that assimilating SLA has improved the domain-averaged RMSE and bias of SST. There is very little impact on the correlation though. When compared with RAMA moorings, assimilating SLA does not show a significant improvement.

3 Temperature

3.1 Introduction

We validate temperature profiles obtained from RAIN and RAIN-SLA with respect to observations from RAMA moorings [14].

3.2 Comparison with RAMA moorings

We present here the comparison of temperature from RAIN and RAIN-SLA with respect to 16 RAMA moorings during the period January 2017 - December 2018. Only those moorings were chosen which had 50% or more data availability during this period.

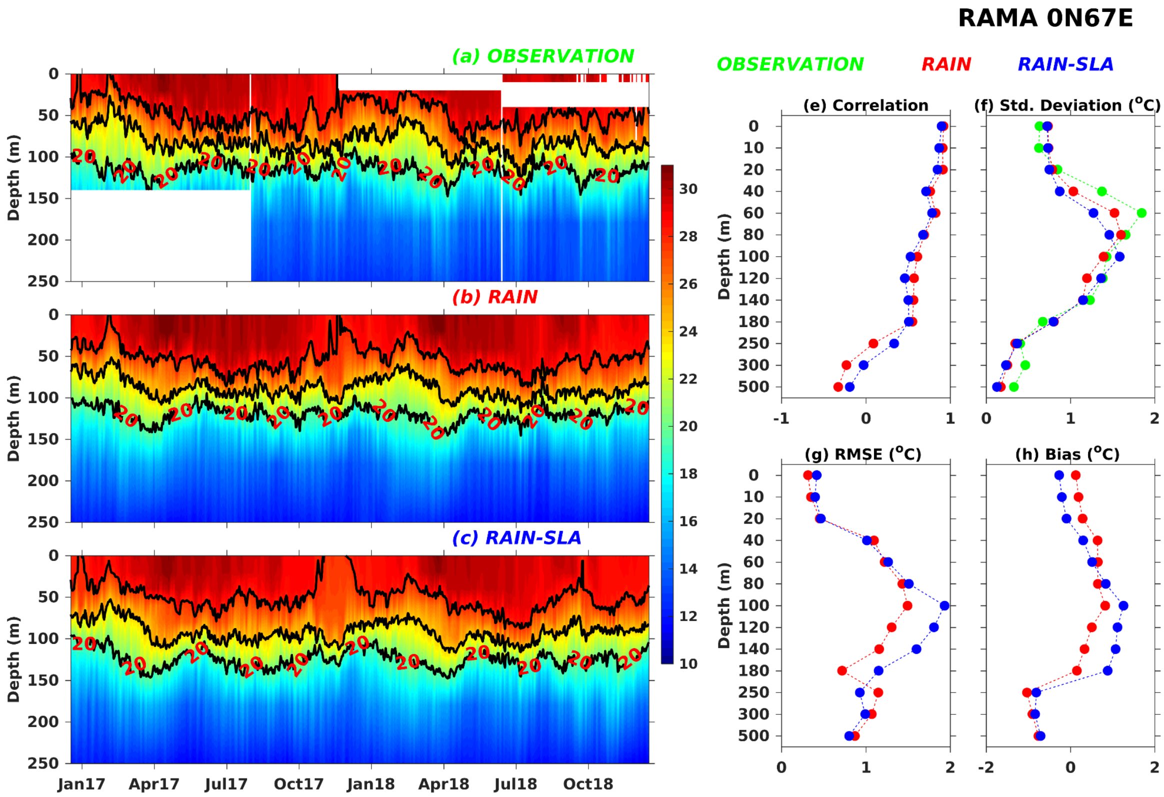

Figure 3.1: Time-depth section of temperature at 0° N, 67° E. from (a) RAMA, (b) RAIN and (c) RAIN-SLA. (e) Correlation of RAMA with RAIN (red) and RAIN-SLA (blue). (f) Standard deviation of RAMA (green), RAIN (red) and RAIN-SLA (blue). (g) RMSE with respect to RAMA for RAIN (red) and RAIN-SLA (blue). (h) Bias of RAIN (red) and RAIN-SLA (blue) with respect to RAMA. The white shades represent data unavailability.

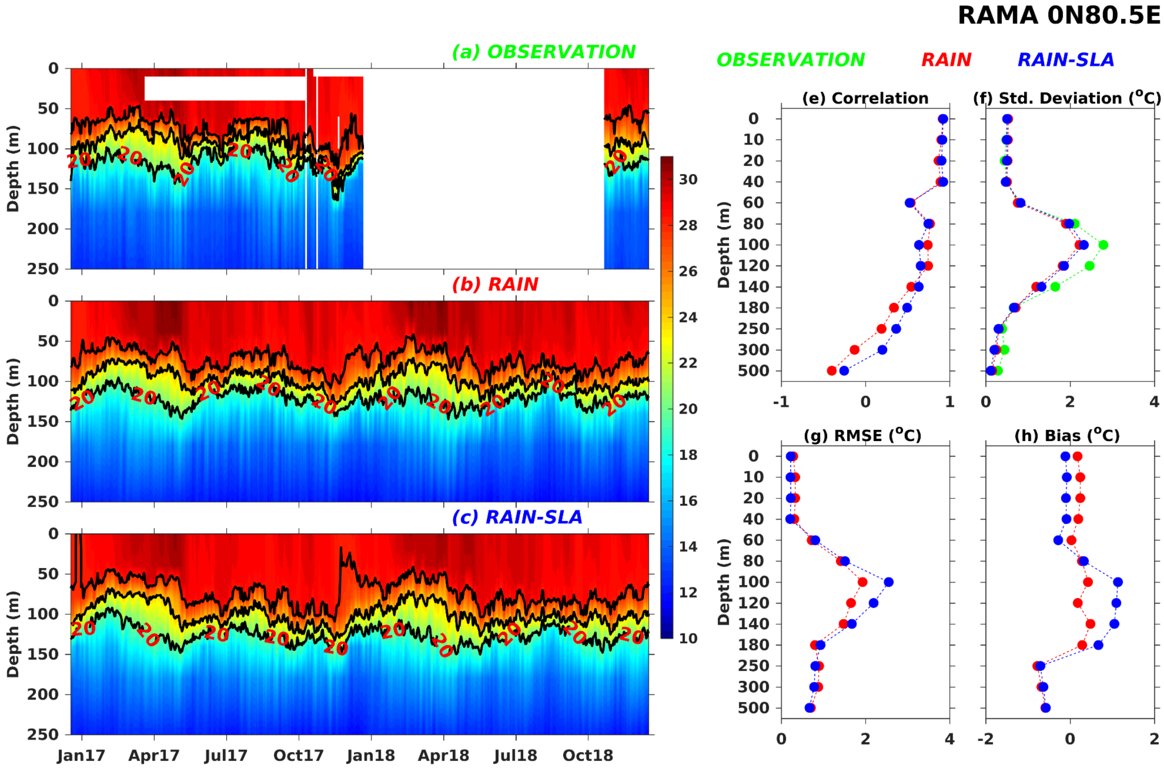

Figure 3.2: Time-depth section of temperature at 0° N, 80.5° E. from (a) RAMA, (b) RAIN and (c) RAIN-SLA. (e) Correlation of RAMA with RAIN (red) and RAIN-SLA (blue). (f) Standard deviation of RAMA (green), RAIN (red) and RAIN-SLA (blue). (g) RMSE with respect to RAMA for RAIN (red) and RAIN-SLA (blue). (h) Bias of RAIN (red) and RAIN-SLA (blue) with respect to RAMA. The white shades represent data unavailability.

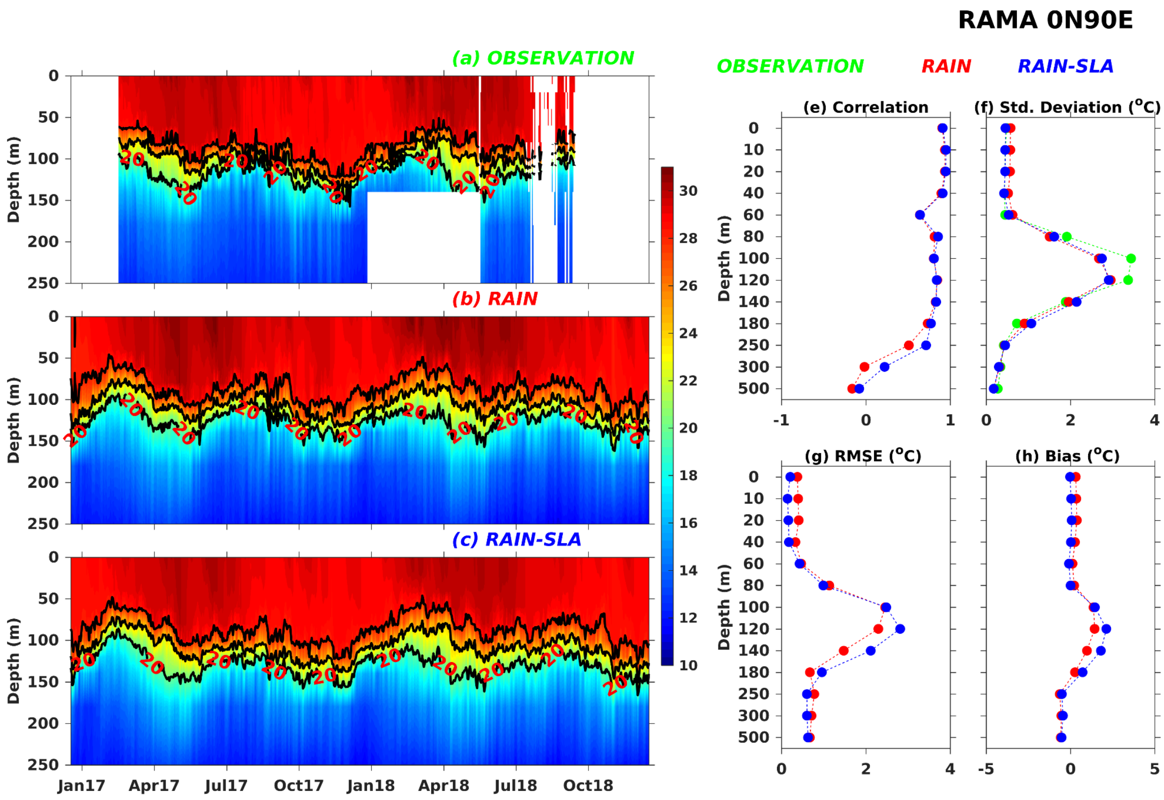

Figure 3.3: Time-depth section of temperature at 0° N, 90° E. from (a) RAMA, (b) RAIN and (c) RAIN-SLA. (e) Correlation of RAMA with RAIN (red) and RAIN-SLA (blue). (f) Standard deviation of RAMA (green), RAIN (red) and RAIN-SLA (blue). (g) RMSE with respect to RAMA for RAIN (red) and RAIN-SLA (blue). (h) Bias of RAIN (red) and RAIN-SLA (blue) with respect to RAMA. The white shades represent data unavailability.

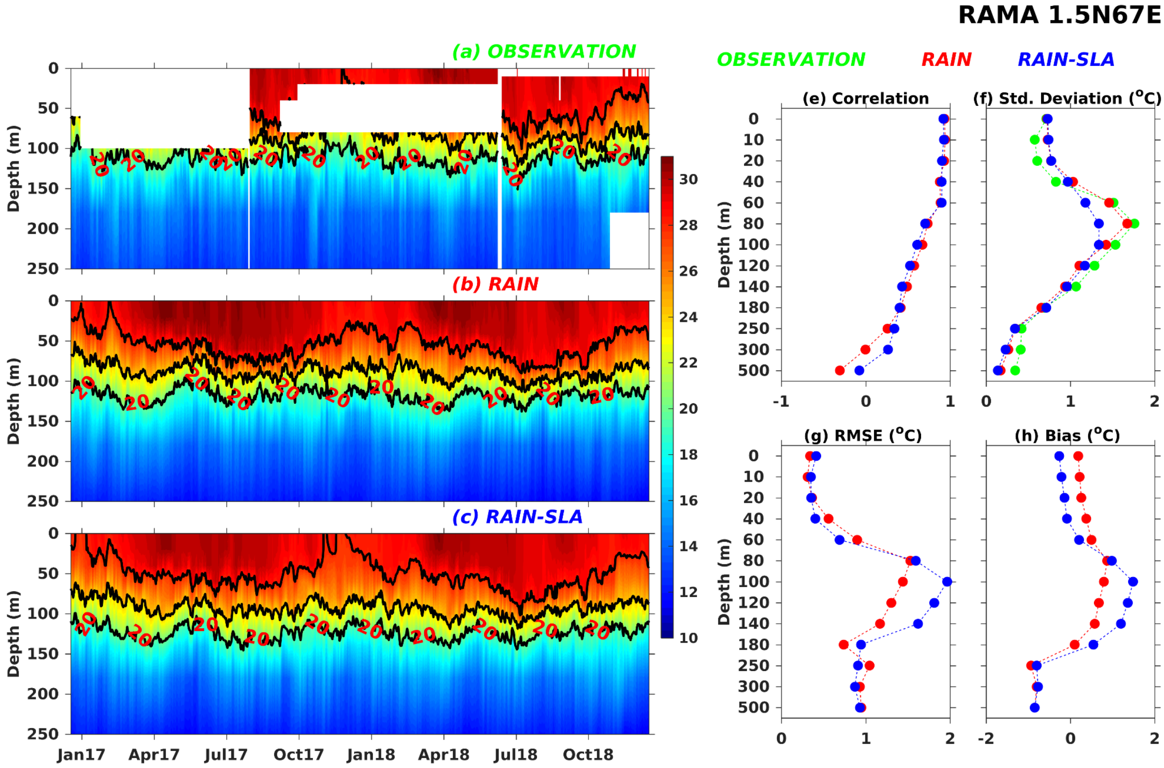

Figure 3.4: Time-depth section of temperature at 1.5° N, 67° E. from (a) RAMA, (b) RAIN and (c) RAIN-SLA. (e) Correlation of RAMA with RAIN (red) and RAIN-SLA (blue). (f) Standard deviation of RAMA (green), RAIN (red) and RAIN-SLA (blue). (g) RMSE with respect to RAMA for RAIN (red) and RAIN-SLA (blue). (h) Bias of RAIN (red) and RAIN-SLA (blue) with respect to RAMA. The white shades represent data unavailability.

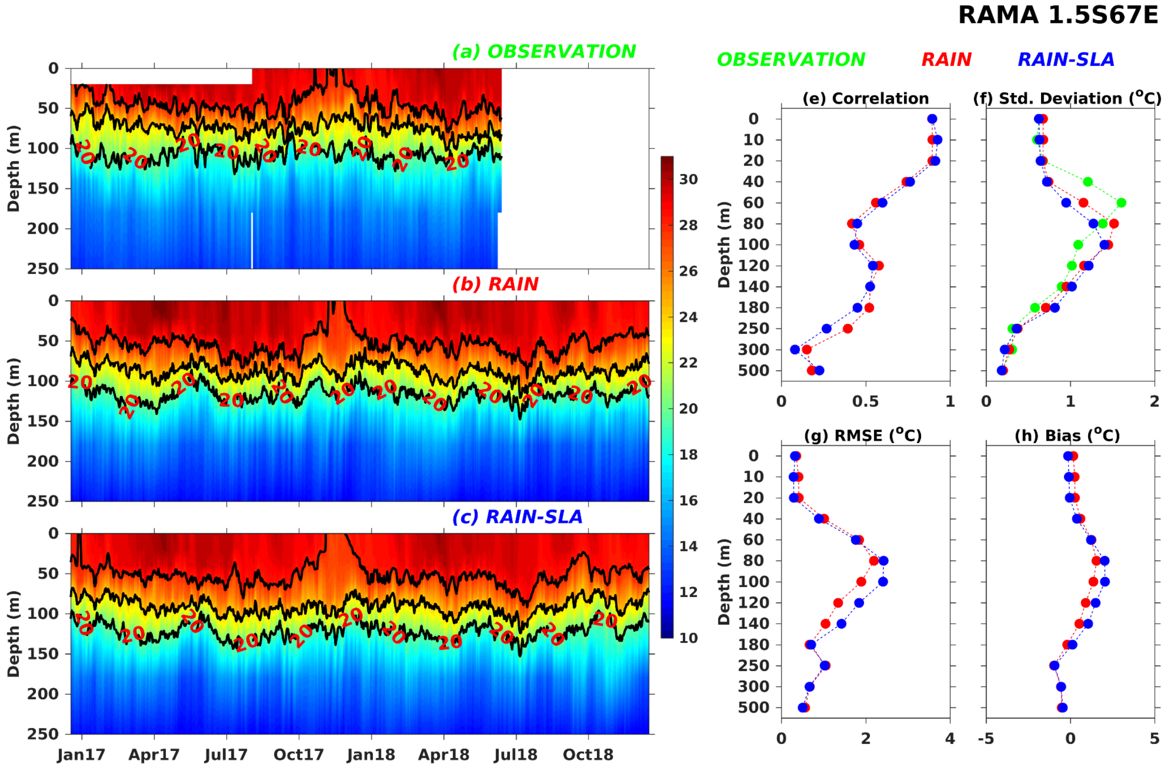

Figure 3.5: Time-depth section of temperature at 1.5° S, 67° E. from (a) RAMA, (b) RAIN and (c) RAIN-SLA. (e) Correlation of RAMA with RAIN (red) and RAIN-SLA (blue). (f) Standard deviation of RAMA (green), RAIN (red) and RAIN-SLA (blue). (g) RMSE with respect to RAMA for RAIN (red) and RAIN-SLA (blue). (h) Bias of RAIN (red) and RAIN-SLA (blue) with respect to RAMA. The white shades represent data unavailability.

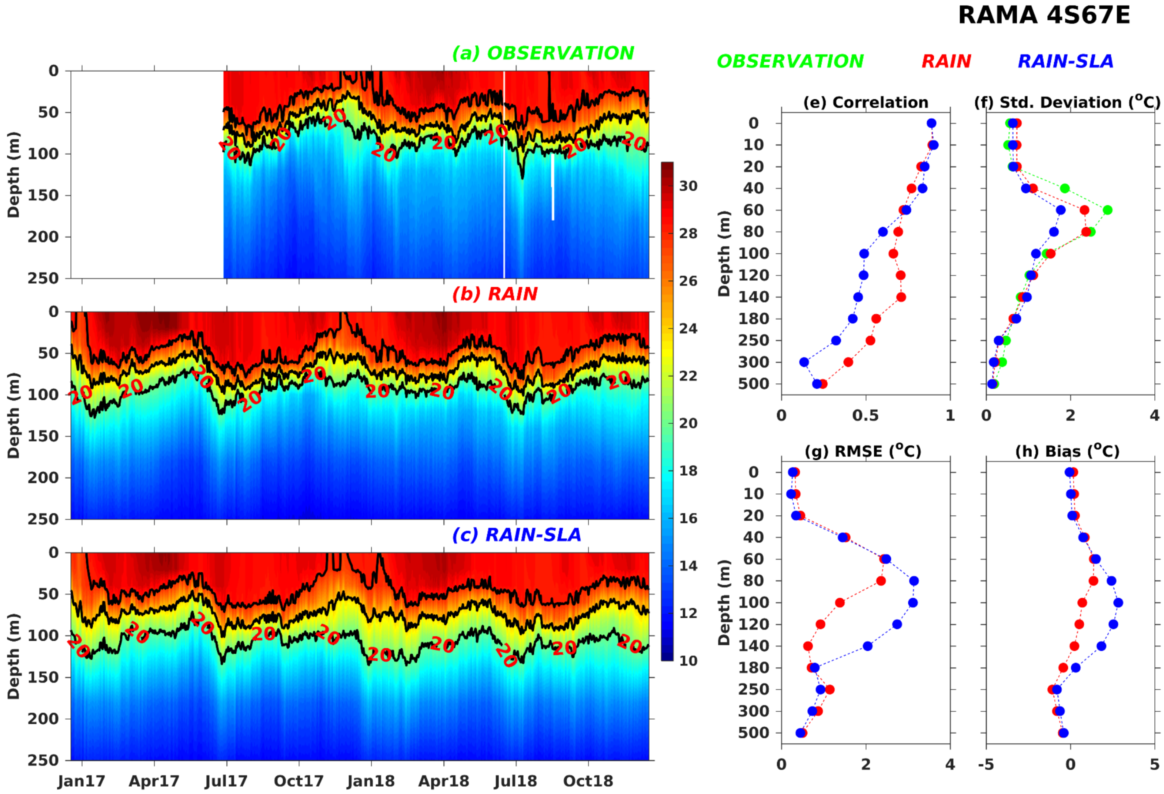

Figure 3.6: Time-depth section of temperature at 4° S, 67° E. from (a) RAMA, (b) RAIN and (c) RAIN-SLA. (e) Correlation of RAMA with RAIN (red) and RAIN-SLA (blue). (f) Standard deviation of RAMA (green), RAIN (red) and RAIN-SLA (blue). (g) RMSE with respect to RAMA for RAIN (red) and RAIN-SLA (blue). (h) Bias of RAIN (red) and RAIN-SLA (blue) with respect to RAMA. The white shades represent data unavailability.

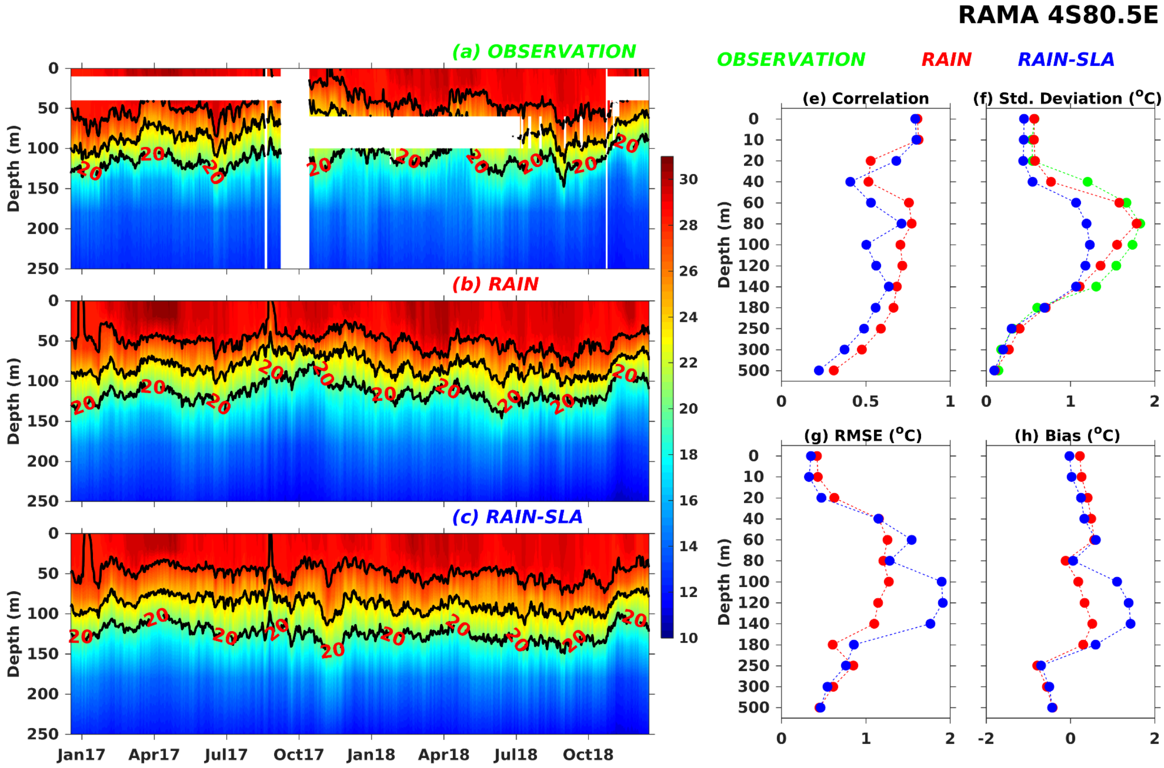

Figure 3.7: Time-depth section of temperature at 4° S, 80.5° E. from (a) RAMA, (b) RAIN and (c) RAIN-SLA. (e) Correlation of RAMA with RAIN (red) and RAIN-SLA (blue). (f) Standard deviation of RAMA (green), RAIN (red) and RAIN-SLA (blue). (g) RMSE with respect to RAMA for RAIN (red) and RAIN-SLA (blue). (h) Bias of RAIN (red) and RAIN-SLA (blue) with respect to RAMA. The white shades represent data unavailability.

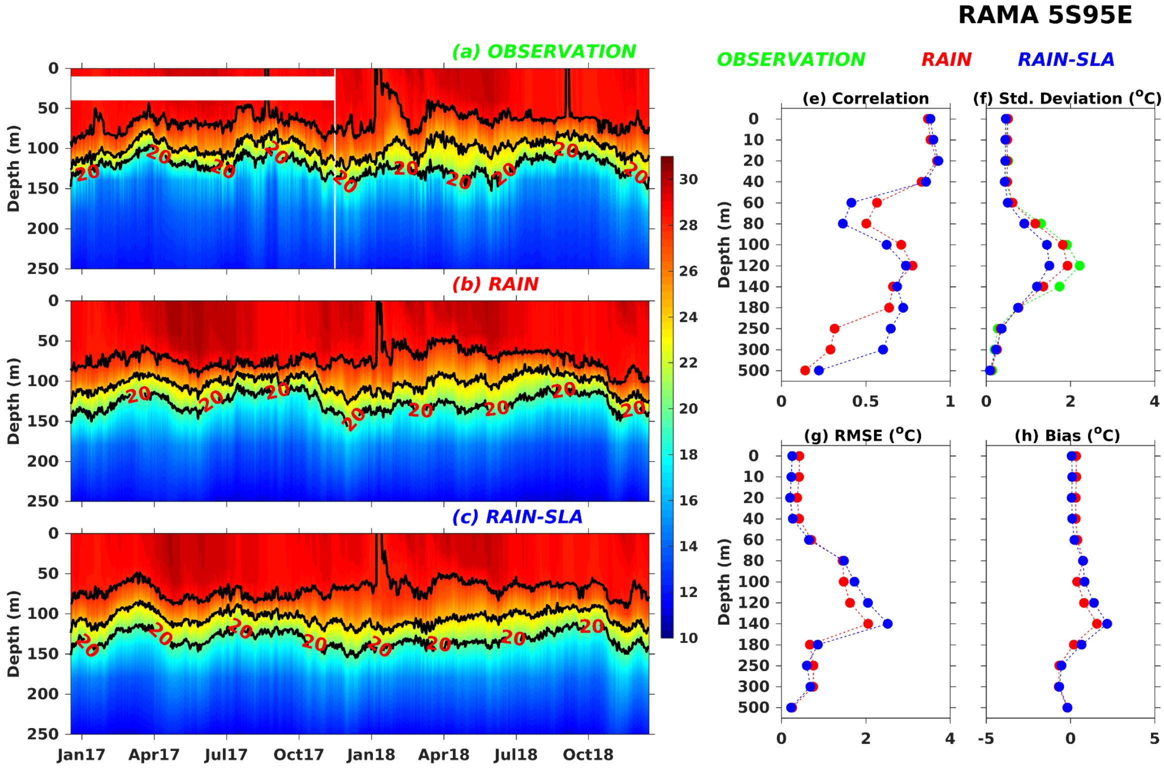

Figure 3.8: Time-depth section of temperature at 5° S, 95° E. from (a) RAMA, (b) RAIN and (c) RAIN-SLA. (e) Correlation of RAMA with RAIN (red) and RAIN-SLA (blue). (f) Standard deviation of RAMA (green), RAIN (red) and RAIN-SLA (blue). (g) RMSE with respect to RAMA for RAIN (red) and RAIN-SLA (blue). (h) Bias of RAIN (red) and RAIN-SLA (blue) with respect to RAMA. The white shades represent data unavailability.

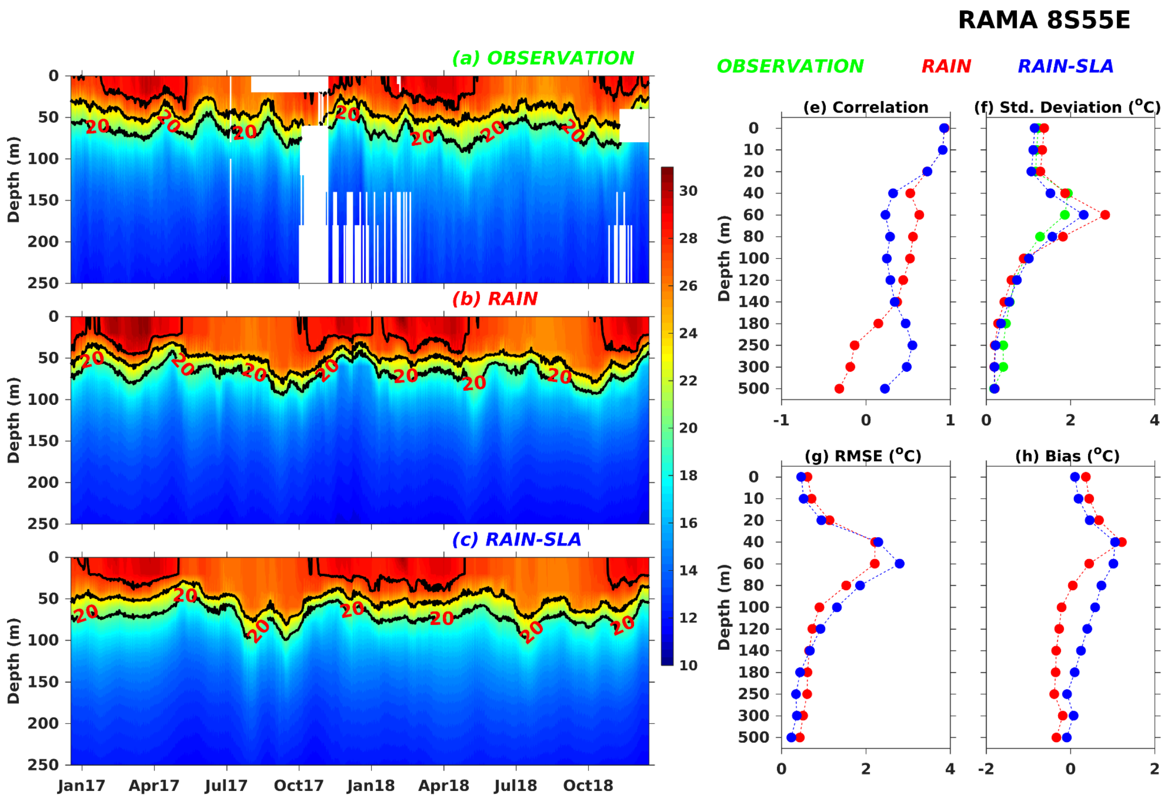

Figure 3.9: Time-depth section of temperature at 8° S, 55° E. from (a) RAMA, (b) RAIN and (c) RAIN-SLA. (e) Correlation of RAMA with RAIN (red) and RAIN-SLA (blue). (f) Standard deviation of RAMA (green), RAIN (red) and RAIN-SLA (blue). (g) RMSE with respect to RAMA for RAIN (red) and RAIN-SLA (blue). (h) Bias of RAIN (red) and RAIN-SLA (blue) with respect to RAMA. The white shades represent data unavailability.

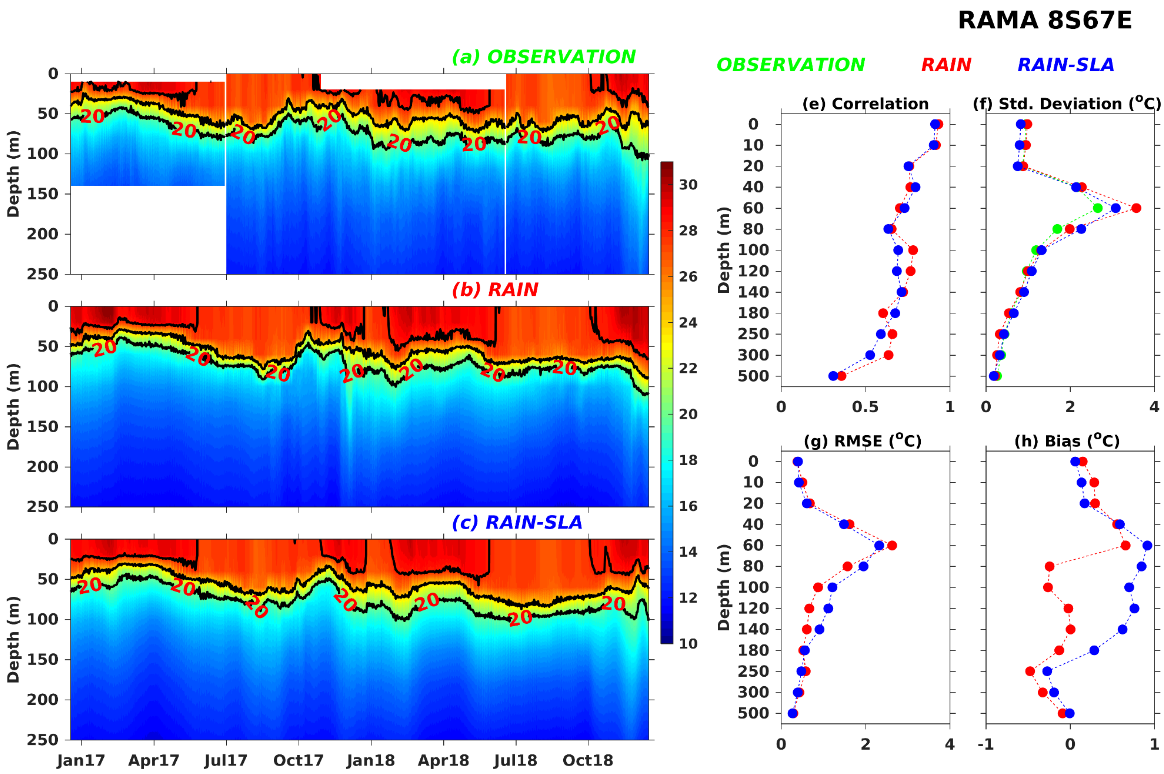

Figure 3.10: Time-depth section of temperature at 8° S, 67° E. from (a) RAMA, (b) RAIN and (c) RAIN-SLA. (e) Correlation of RAMA with RAIN (red) and RAIN-SLA (blue). (f) Standard deviation of RAMA (green), RAIN (red) and RAIN-SLA (blue). (g) RMSE with respect to RAMA for RAIN (red) and RAIN-SLA (blue). (h) Bias of RAIN (red) and RAIN-SLA (blue) with respect to RAMA. The white shades represent data unavailability.

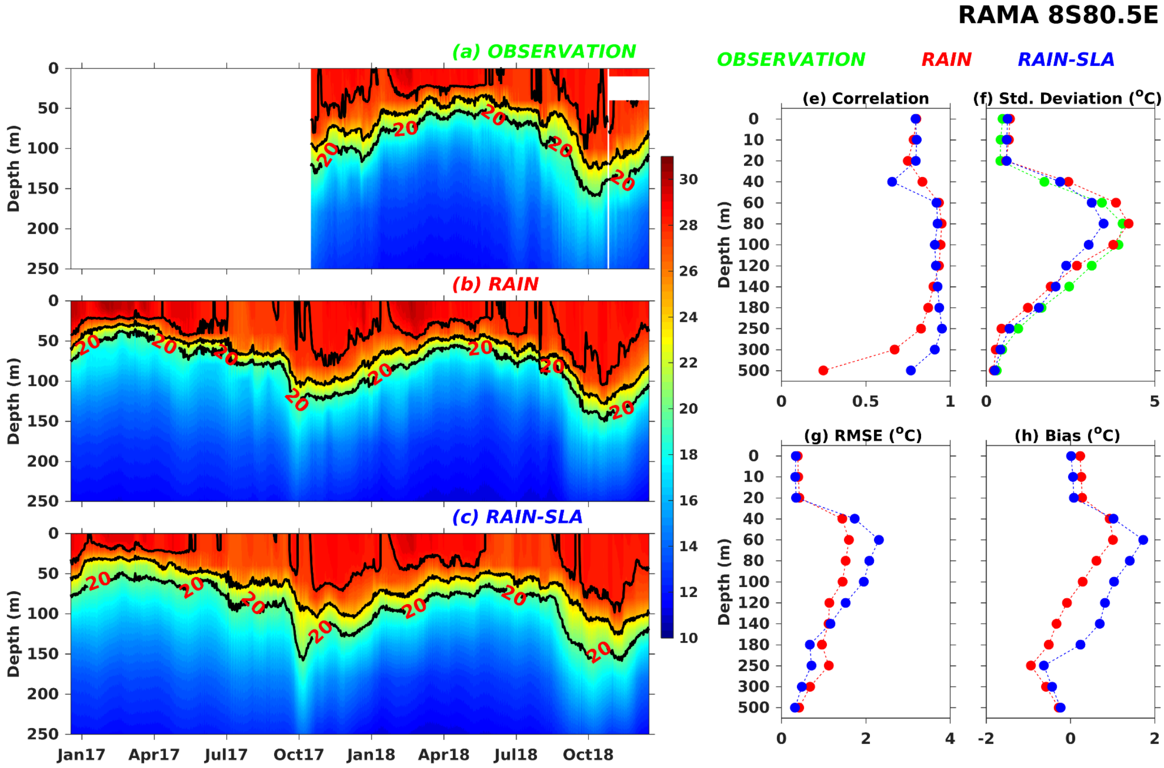

Figure 3.11: Time-depth section of temperature at 8° S, 80.5° E. from (a) RAMA, (b) RAIN and (c) RAIN-SLA. (e) Correlation of RAMA with RAIN (red) and RAIN-SLA (blue). (f) Standard deviation of RAMA (green), RAIN (red) and RAIN-SLA (blue). (g) RMSE with respect to RAMA for RAIN (red) and RAIN-SLA (blue). (h) Bias of RAIN (red) and RAIN-SLA (blue) with respect to RAMA. The white shades represent data unavailability.

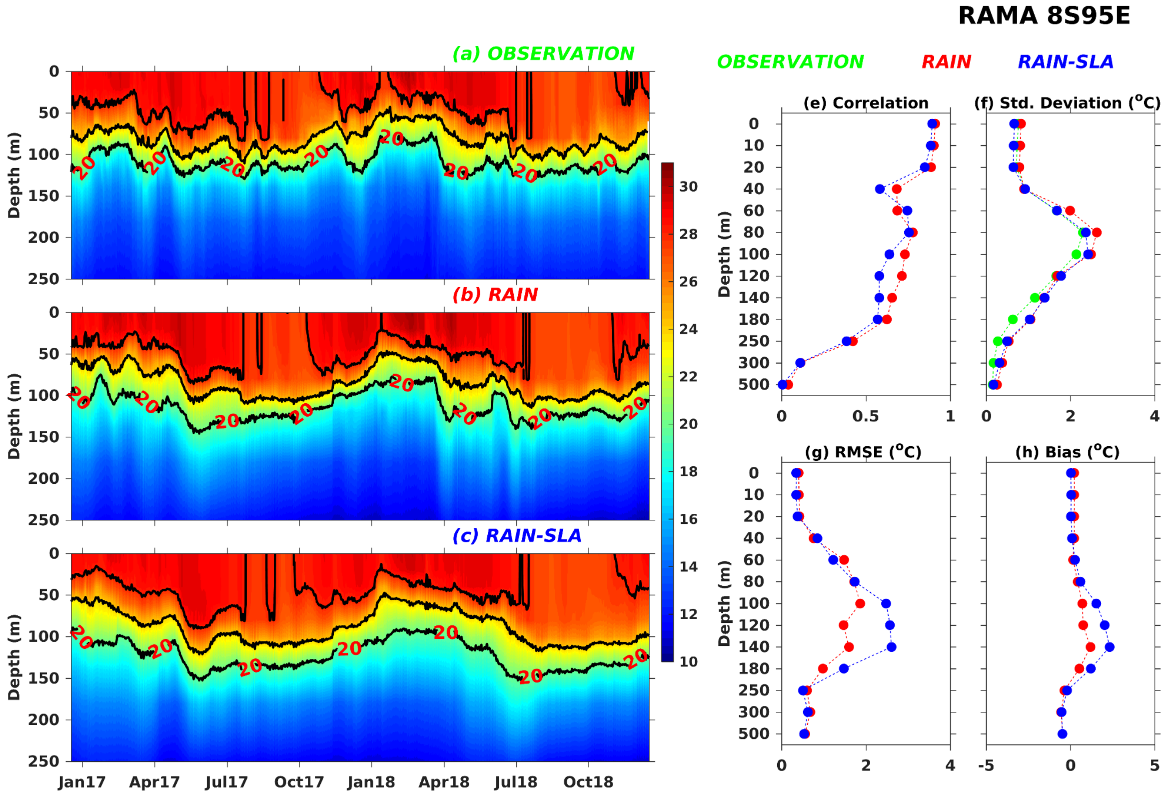

Figure 3.12: Time-depth section of temperature at 8° S, 95° E. from (a) RAMA, (b) RAIN and (c) RAIN-SLA. (e) Correlation of RAMA with RAIN (red) and RAIN-SLA (blue). (f) Standard deviation of RAMA (green), RAIN (red) and RAIN-SLA (blue). (g) RMSE with respect to RAMA for RAIN (red) and RAIN-SLA (blue). (h) Bias of RAIN (red) and RAIN-SLA (blue) with respect to RAMA. The white shades represent data unavailability.

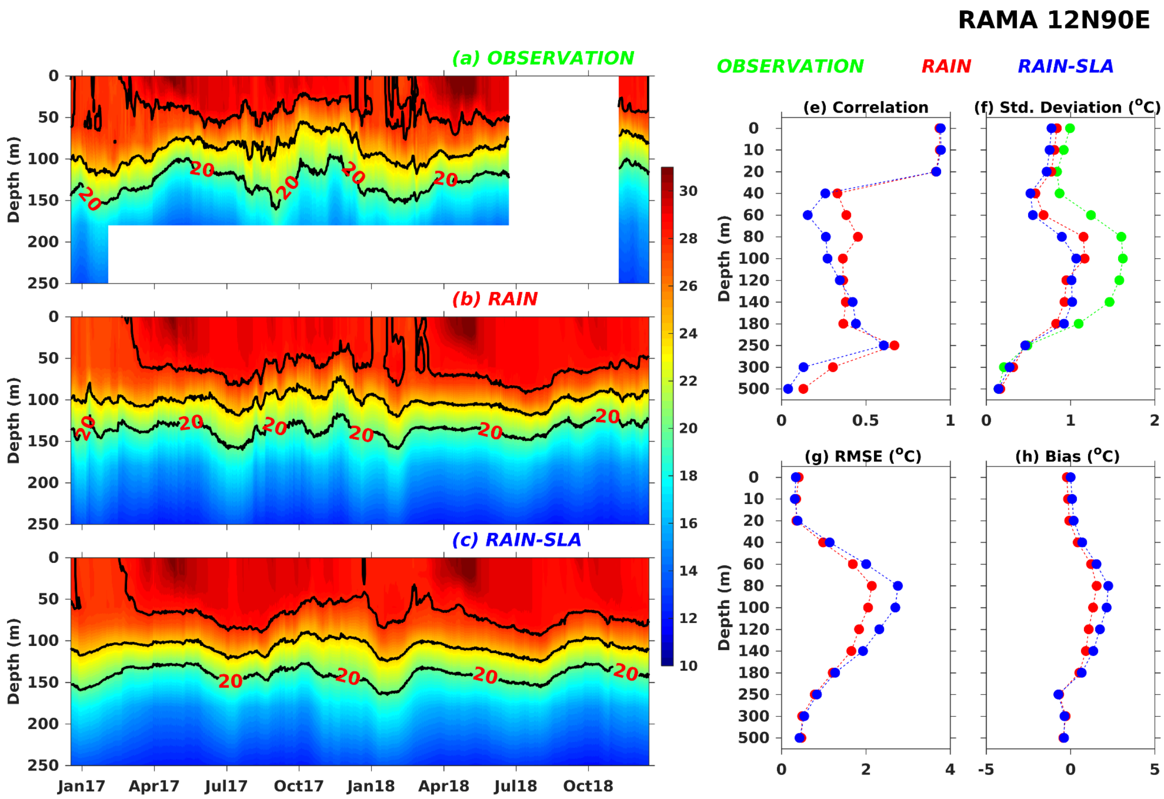

Figure 3.13: Time-depth section of temperature at 12° N, 90° E. from (a) RAMA, (b) RAIN and (c) RAIN-SLA. (e) Correlation of RAMA with RAIN (red) and RAIN-SLA (blue). (f) Standard deviation of RAMA (green), RAIN (red) and RAIN-SLA (blue). (g) RMSE with respect to RAMA for RAIN (red) and RAIN-SLA (blue). (h) Bias of RAIN (red) and RAIN-SLA (blue) with respect to RAMA. The white shades represent data unavailability.

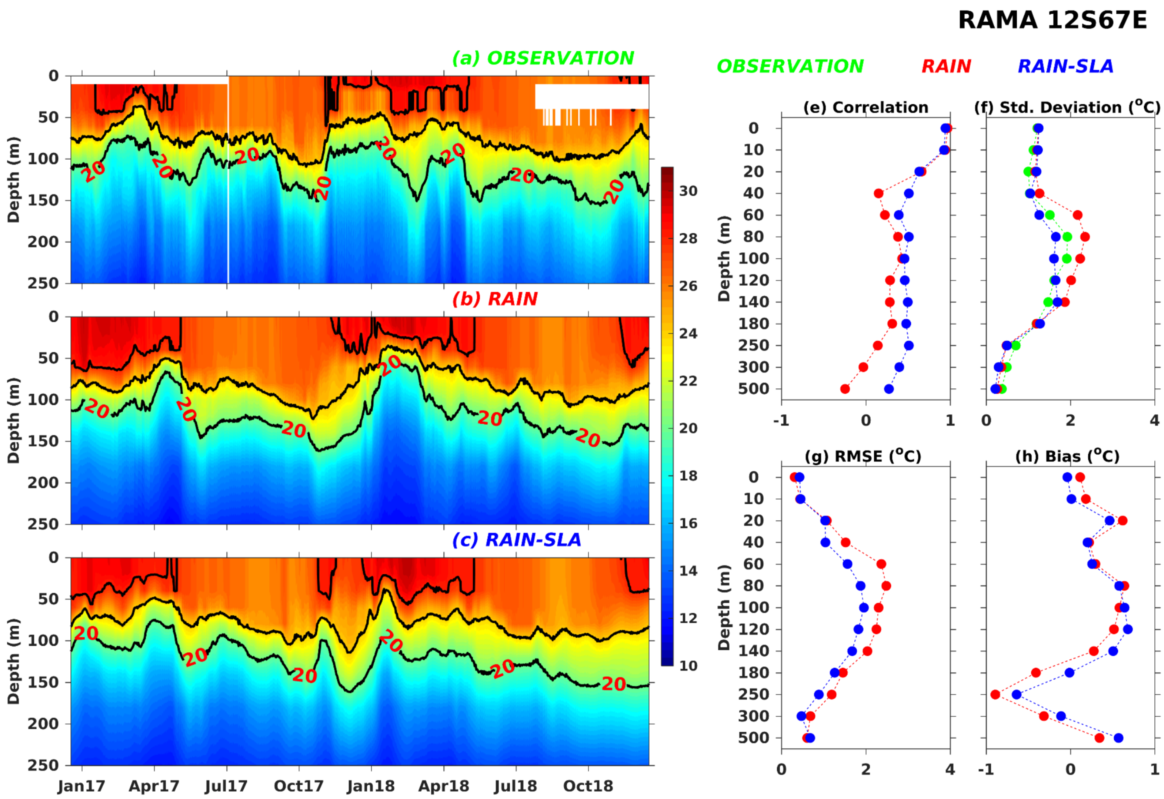

Figure 3.14: Time-depth section of temperature at 12° S, 67° E. from (a) RAMA, (b) RAIN and (c) RAIN-SLA. (e) Correlation of RAMA with RAIN (red) and RAIN-SLA (blue). (f) Standard deviation of RAMA (green), RAIN (red) and RAIN-SLA (blue). (g) RMSE with respect to RAMA for RAIN (red) and RAIN-SLA (blue). (h) Bias of RAIN (red) and RAIN-SLA (blue) with respect to RAMA. The white shades represent data unavailability.

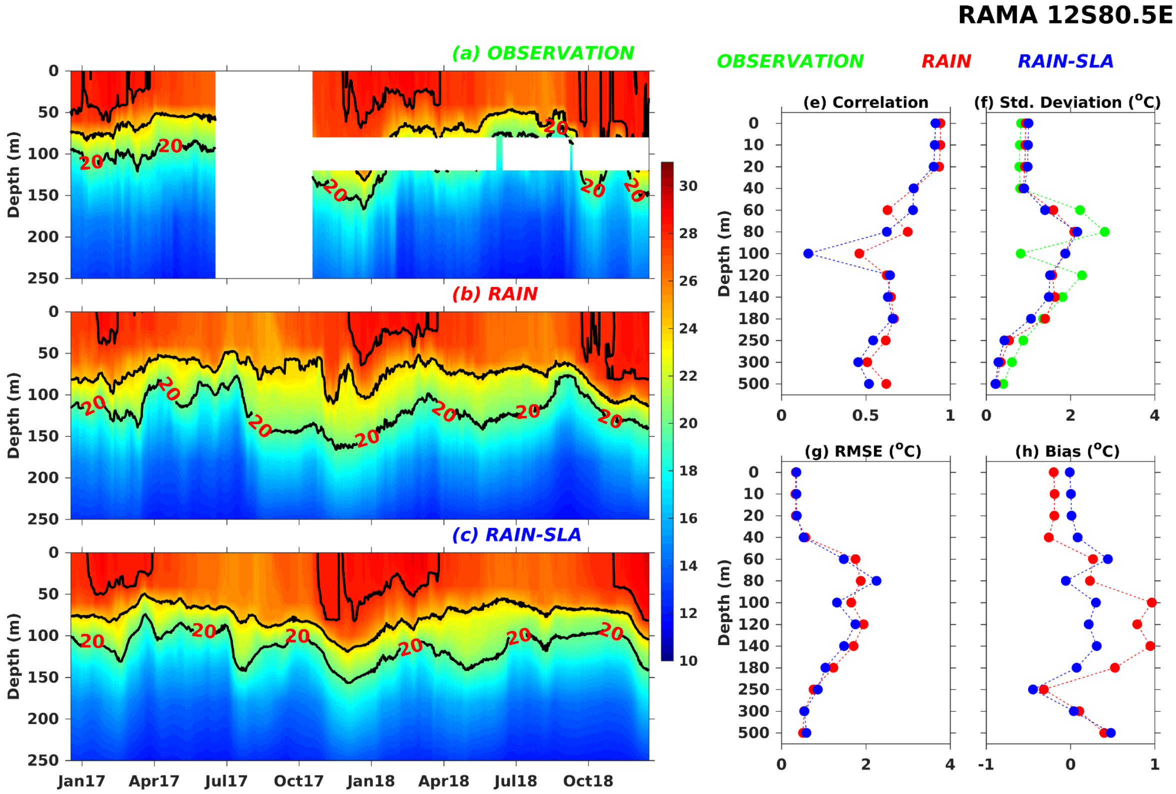

Figure 3.15: Time-depth section of temperature at 12° S, 80.5° E. from (a) RAMA, (b) RAIN and (c) RAIN-SLA. (e) Correlation of RAMA with RAIN (red) and RAIN-SLA (blue). (f) Standard deviation of RAMA (green), RAIN (red) and RAIN-SLA (blue). (g) RMSE with respect to RAMA for RAIN (red) and RAIN-SLA (blue). (h) Bias of RAIN (red) and RAIN-SLA (blue) with respect to RAMA. The white shades represent data unavailability.

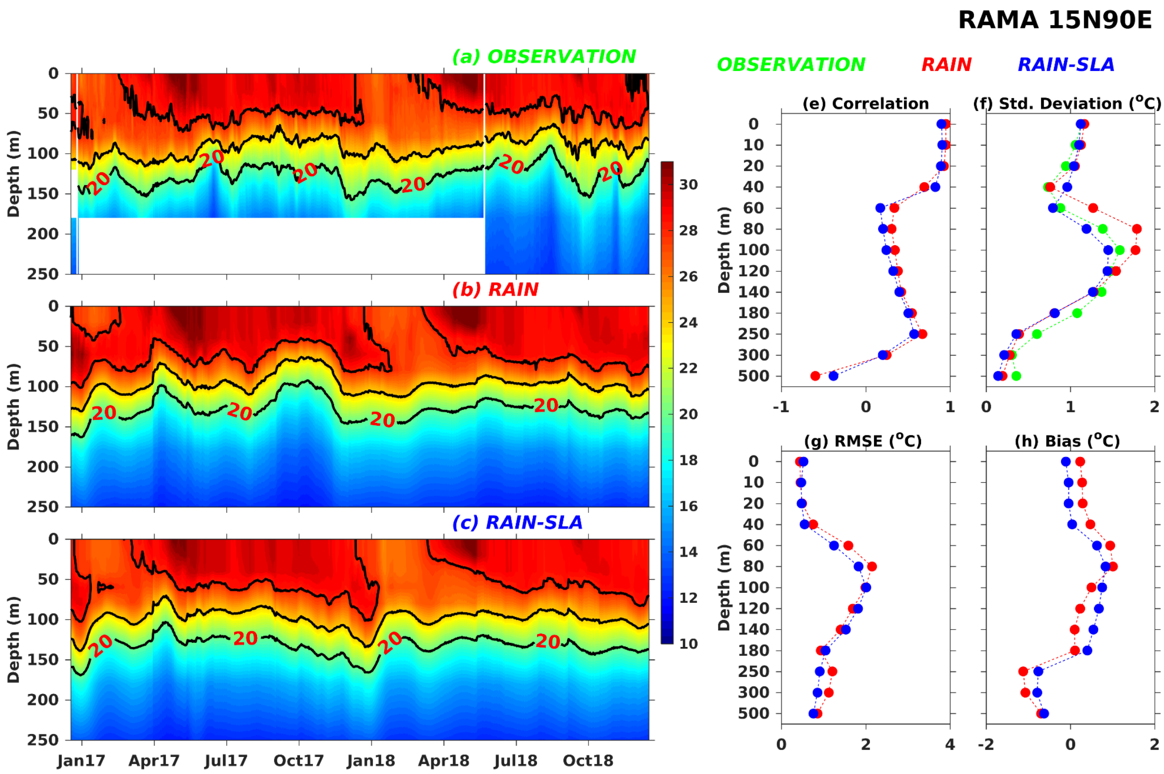

Figure 3.16: Time-depth section of temperature at 15° N, 90° E. from (a) RAMA, (b) RAIN and (c) RAIN-SLA. (e) Correlation of RAMA with RAIN (red) and RAIN-SLA (blue). (f) Standard deviation of RAMA (green), RAIN (red) and RAIN-SLA (blue). (g) RMSE with respect to RAMA for RAIN (red) and RAIN-SLA (blue). (h) Bias of RAIN (red) and RAIN-SLA (blue) with respect to RAMA. The white shades represent data unavailability.

3.3 Comparison with ARGO

Here we quantify the performance of all the three systems with respect to Argo floats in simulating the temperature of the oceans. Since Argo floats traverse in time, we divide the Indian Ocean into three broad regions - Arabian Sea, Bay of Bengal and Equatorial Indian Ocean and perform a collective analysis on the performance. Data from each region is concatenated and a daily Argo observation is obtained for each of the regions. In Fig.1.2, we plot the location of pop-up of Argo floats in the Northern and Equatorial Indian Ocean that were taken into consideration for this validation exercise.

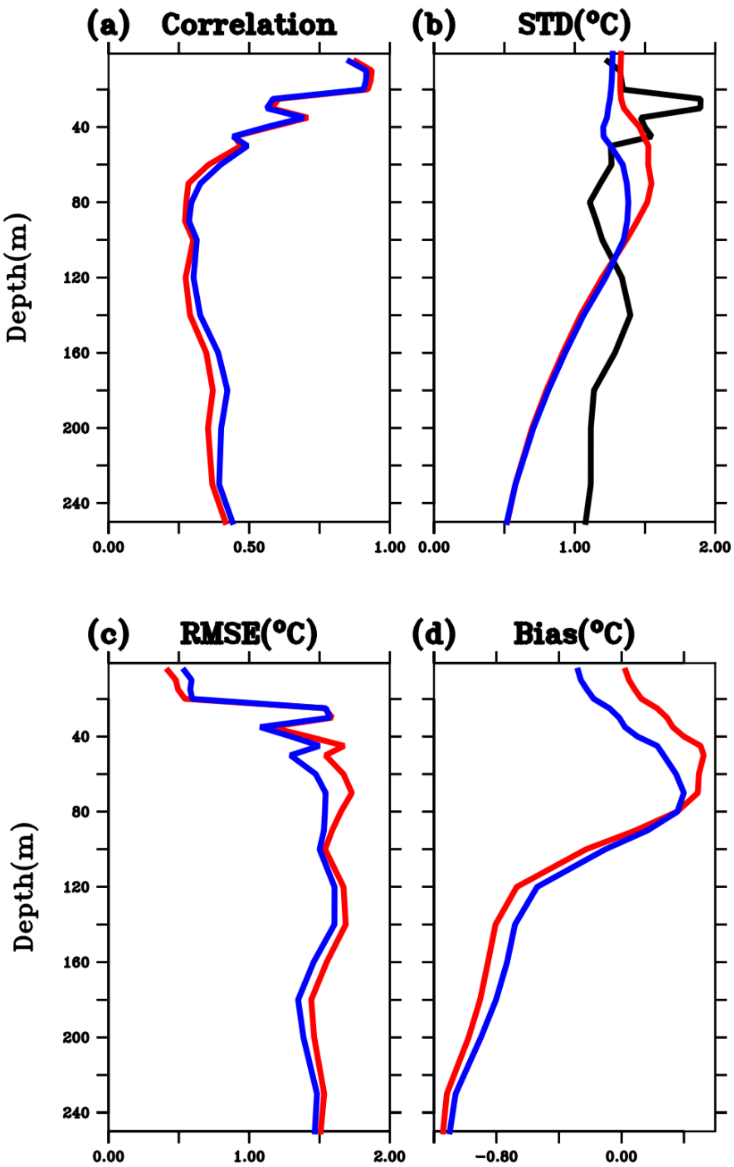

Figure 3.17: (a) Correlation of Argo floats with RAIN (red) and RAIN-SLA (blue) at vertical levels till 260m. (b) Standard deviation of Argo floats (black), RAIN (red) and RAIN-SLA (blue). (c) RMSE with respect to Argo floats for RAIN (red) and RAIN-SLA (blue) at vertical levels till 260m. (d) Bias of RAIN (red) and RAIN-SLA (blue) at vertical levels till 260m with respect to Argo floats in Arabian sea

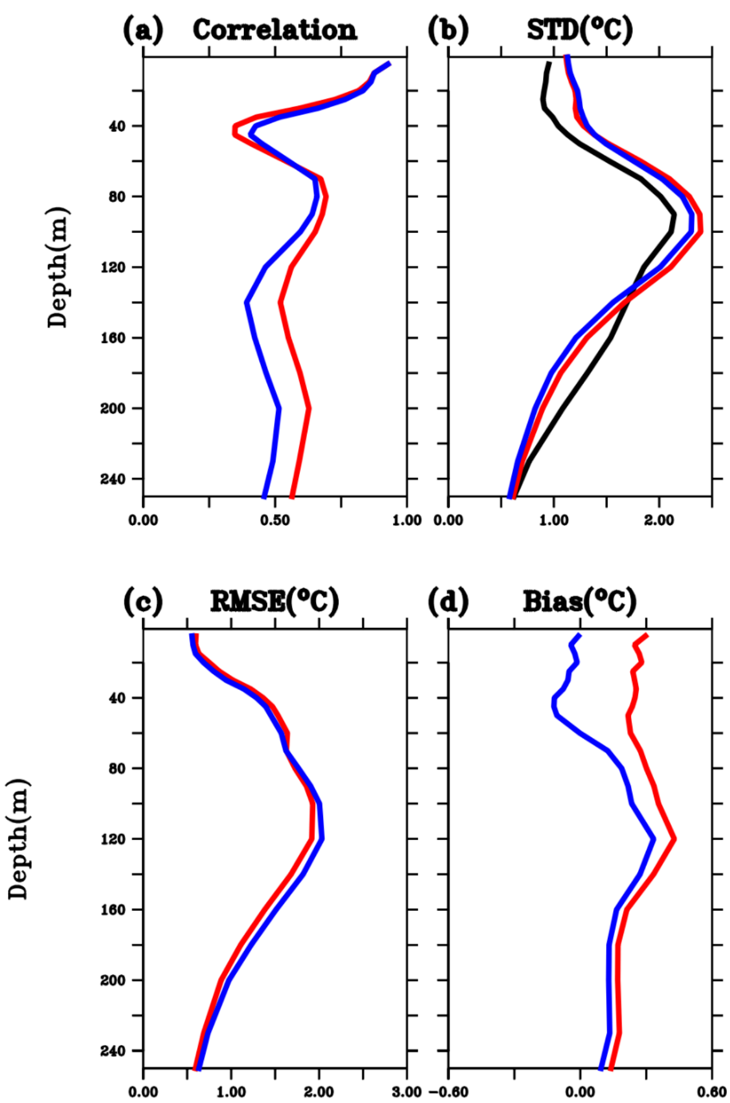

Figure 3.18: (a) Correlation of Argo floats with RAIN (red) and RAIN-SLA (blue) at vertical levels till 260m. (b) Standard deviation of Argo floats (black), RAIN (red) and RAIN-SLA (blue). (c) RMSE with respect to Argo floats for RAIN (red) and RAIN-SLA (blue) at vertical levels till 260m. (d) Bias of RAIN (red) and RAIN-SLA (blue) at vertical levels till 260m with respect to Argo floats in Bay of Bengal

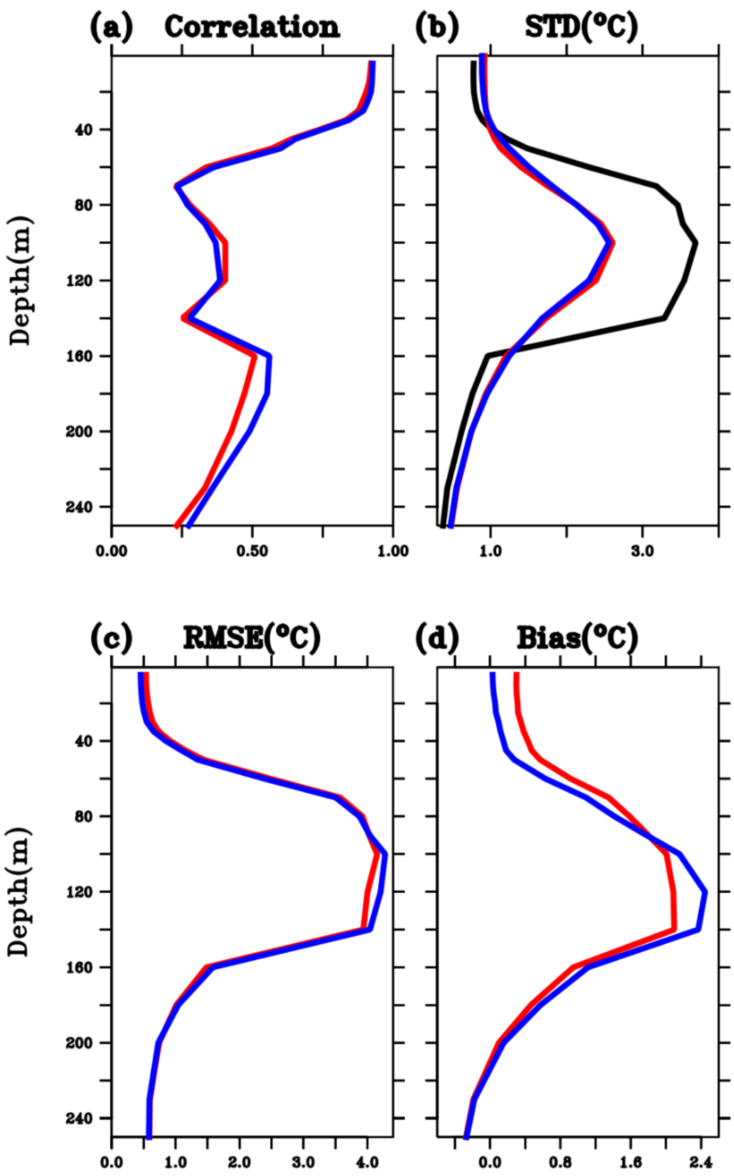

Figure 3.19: (a) Correlation of Argo floats with RAIN (red) and RAIN-SLA (blue) at vertical levels till 260m. (b) Standard deviation of Argo floats (black), RAIN (red) and RAIN-SLA (blue). (c) RMSE with respect to Argo floats for RAIN (red) and RAIN-SLA (blue) at vertical levels till 260m. (d) Bias of RAIN (red) and RAIN-SLA (blue) at vertical levels till 260m with respect to Argo floats in the Equatorial Indian Ocean.

3.4 Conclusion

Assimilating SLA has a positive impact on the temperature profile - particularly in the top layers. Across many locations, we see a reduction in RMSE and bias and a slight increase in correlation.

4 Salinity

4.1 Introduction

We validate salinity profiles obtained from RAIN and RAIN-SLA with respect to observations from RAMA moorings [14]. It is to be noted that the numerical model ROMS do not include effects of river discharge and tides and hence sea-surface salinity is weakly relaxed to World Ocean Atlas monthly salinity climatology [16-17] in ROMS (30 day relaxation time).

4.2 Comparison with RAMA moorings

We present here the comparison of salinity from RAIN and RAIN-SLA with respect to RAMA moorings during the period January 2017 - December 2018. Only those moorings were chosen which had 50% or more data availability during this period.

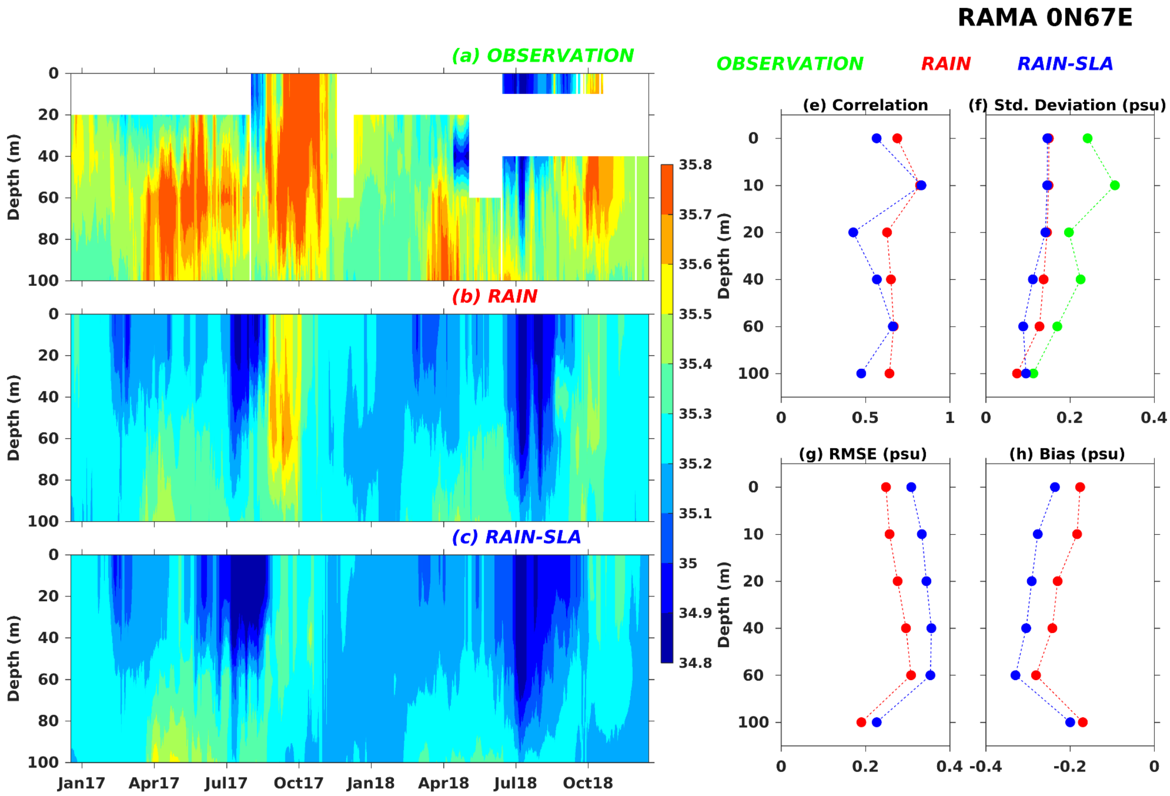

Figure 4.1: Time-depth section of temperature at 0° N, 67° E. from (a) RAMA, (b) RAIN and (c) RAIN-SLA. (e) Correlation of RAMA with RAIN (red) and RAIN-SLA (blue). (f) Standard deviation of RAMA (green), RAIN (red) and RAIN-SLA (blue). (g) RMSE with respect to RAMA for RAIN (red) and RAIN-SLA (blue). (h) Bias of RAIN (red) and RAIN-SLA (blue) with respect to RAMA. The white shades represent data unavailability.

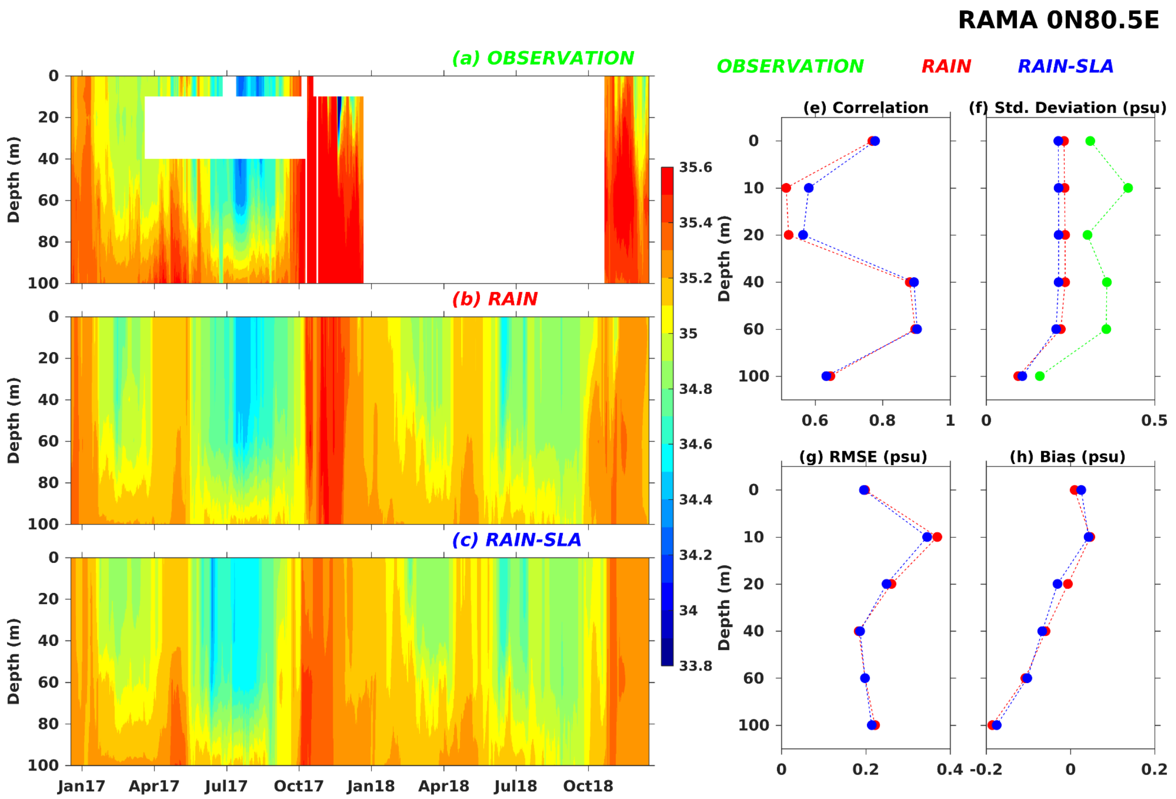

Figure 4.2: Time-depth section of temperature at 0° N, 80.5° E. from (a) RAMA, (b) RAIN and (c) RAIN-SLA. (e) Correlation of RAMA with RAIN (red) and RAIN-SLA (blue). (f) Standard deviation of RAMA (green), RAIN (red) and RAIN-SLA (blue). (g) RMSE with respect to RAMA for RAIN (red) and RAIN-SLA (blue). (h) Bias of RAIN (red) and RAIN-SLA (blue) with respect to RAMA. The white shades represent data unavailability.

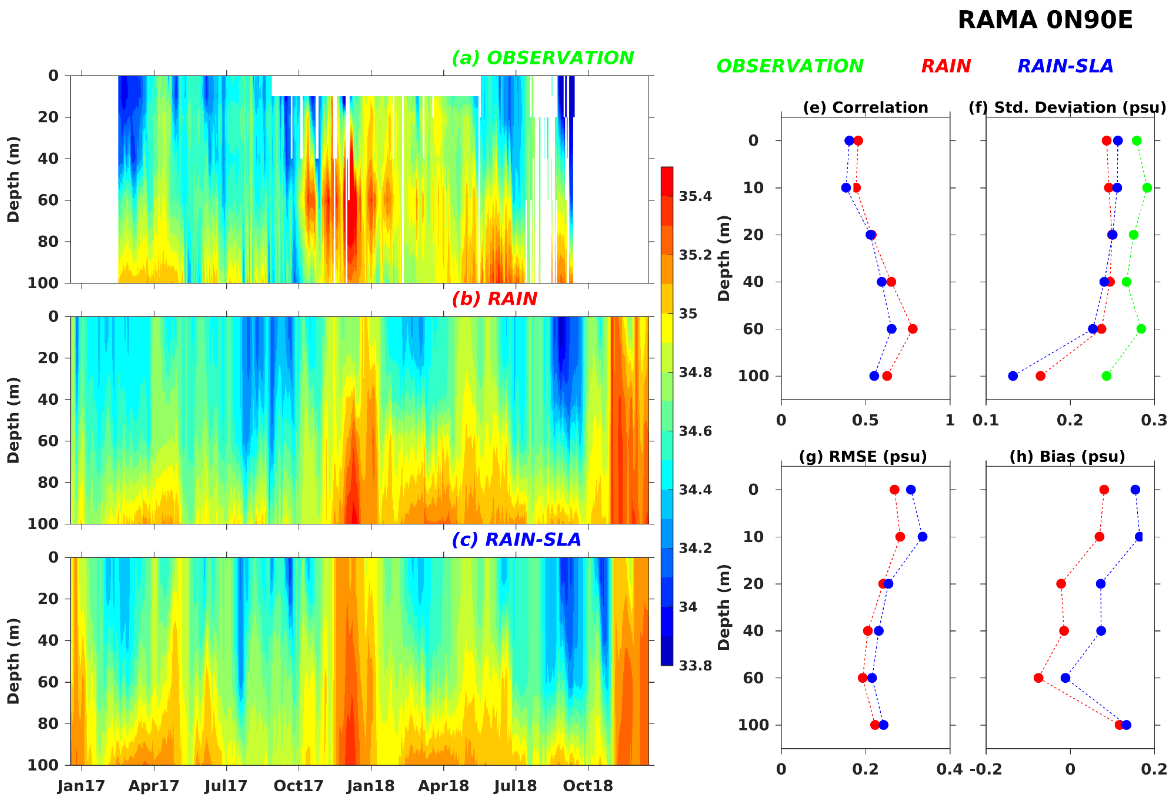

Figure 4.3: Time-depth section of temperature at 0° N, 90° E. from (a) RAMA, (b) RAIN and (c) RAIN-SLA. (e) Correlation of RAMA with RAIN (red) and RAIN-SLA (blue). (f) Standard deviation of RAMA (green), RAIN (red) and RAIN-SLA (blue). (g) RMSE with respect to RAMA for RAIN (red) and RAIN-SLA (blue). (h) Bias of RAIN (red) and RAIN-SLA (blue) with respect to RAMA. The white shades represent data unavailability.

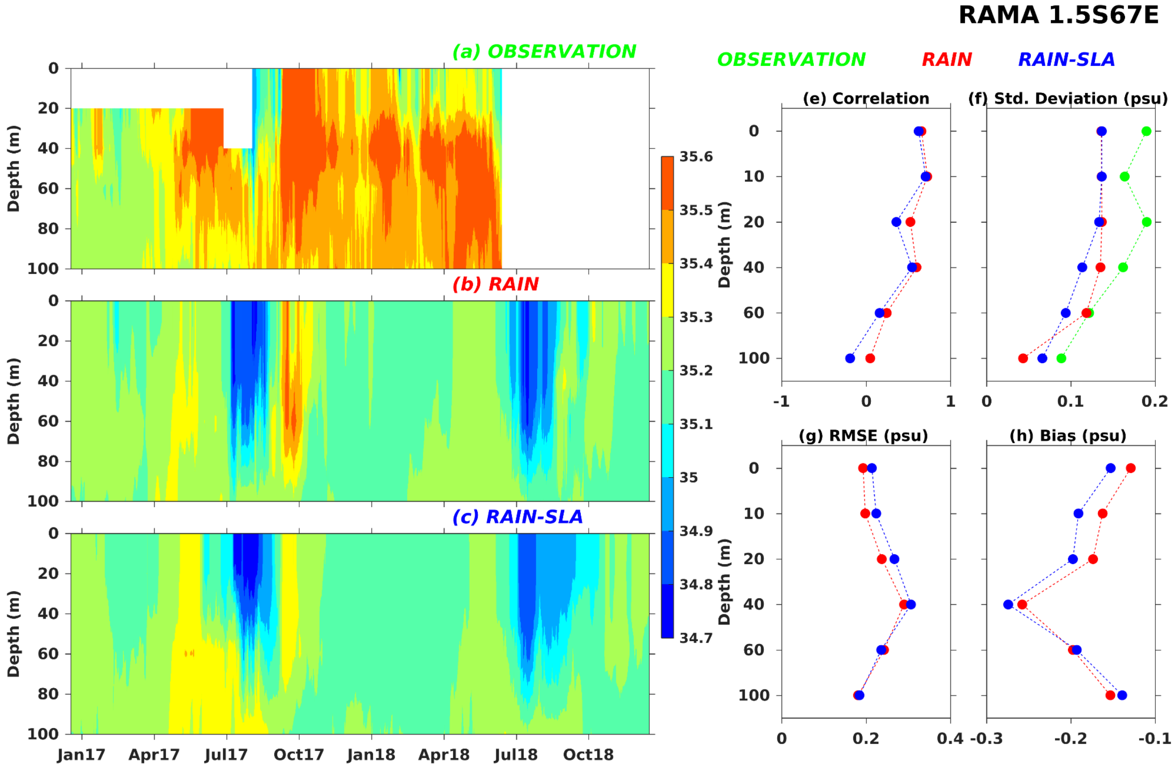

Figure 4.4: Time-depth section of temperature at 1.5° S, 67° E. from (a) RAMA, (b) RAIN and (c) RAIN-SLA. (e) Correlation of RAMA with RAIN (red) and RAIN-SLA (blue). (f) Standard deviation of RAMA (green), RAIN (red) and RAIN-SLA (blue). (g) RMSE with respect to RAMA for RAIN (red) and RAIN-SLA (blue). (h) Bias of RAIN (red) and RAIN-SLA (blue) with respect to RAMA. The white shades represent data unavailability.

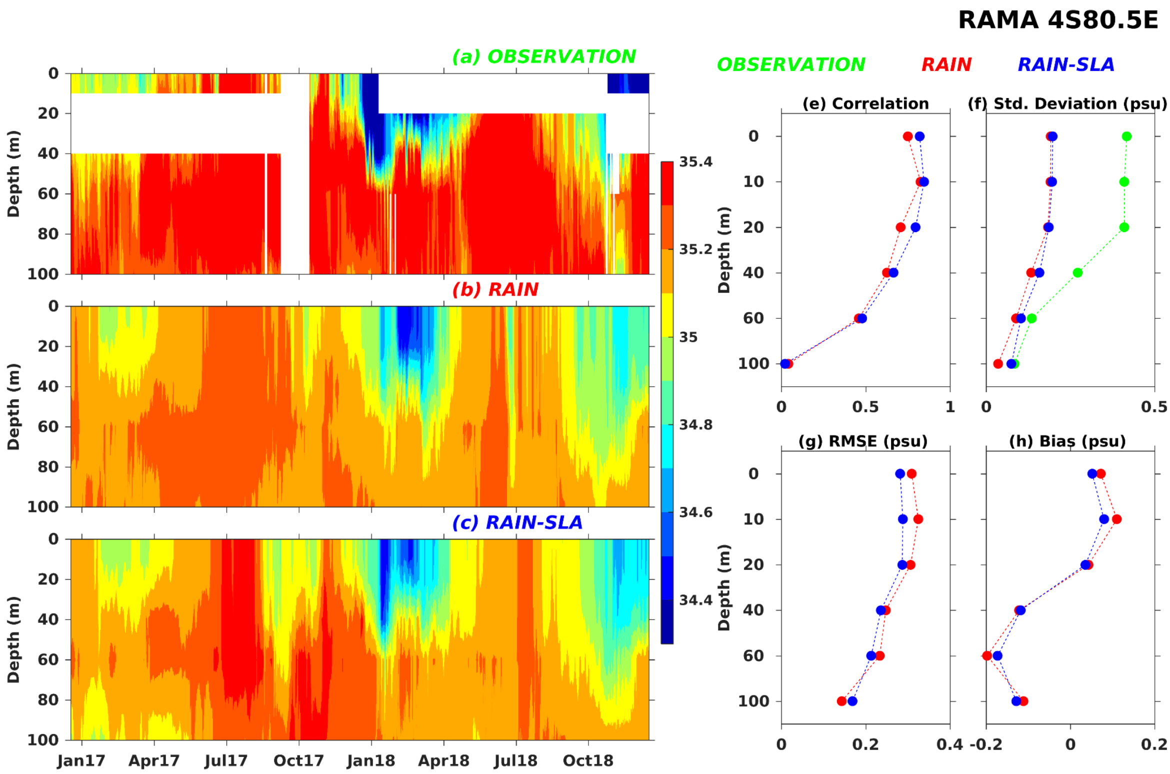

Figure 4.5: Time-depth section of temperature at 4° S, 80.5° E. from (a) RAMA, (b) RAIN and (c) RAIN-SLA. (e) Correlation of RAMA with RAIN (red) and RAIN-SLA (blue). (f) Standard deviation of RAMA (green), RAIN (red) and RAIN-SLA (blue). (g) RMSE with respect to RAMA for RAIN (red) and RAIN-SLA (blue). (h) Bias of RAIN (red) and RAIN-SLA (blue) with respect to RAMA. The white shades represent data unavailability.

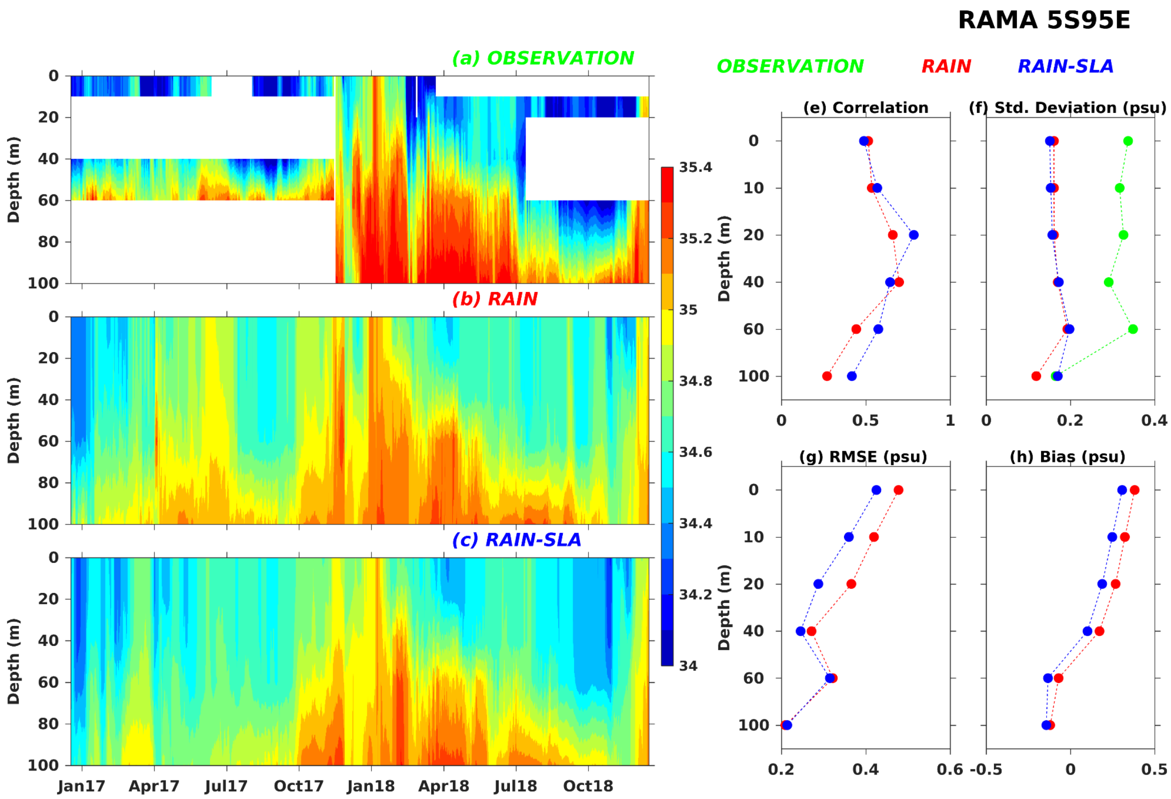

Figure 4.6: Time-depth section of temperature at 5º S, 95º E. from (a) RAMA, (b) RAIN and (c) RAIN-SLA. (e) Correlation of RAMA with RAIN (red) and RAIN-SLA (blue). (f) Standard deviation of RAMA (green), RAIN (red) and RAIN-SLA (blue). (g) RMSE with respect to RAMA for RAIN (red) and RAIN-SLA (blue). (h) Bias of RAIN (red) and RAIN-SLA (blue) with respect to RAMA. The white shades represent data unavailability.

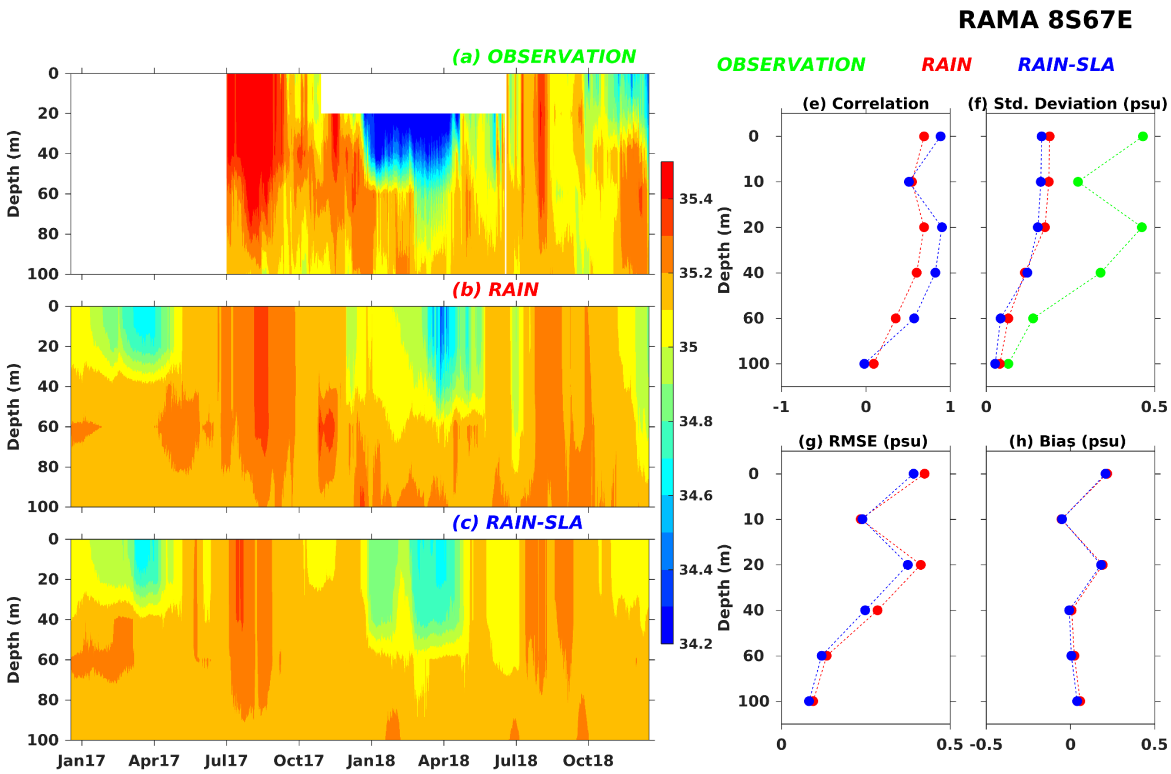

Figure 4.7: Time-depth section of temperature at 8° S, 67° E. from (a) RAMA, (b) RAIN and (c) RAIN-SLA. (e) Correlation of RAMA with RAIN (red) and RAIN-SLA (blue). (f) Standard deviation of RAMA (green), RAIN (red) and RAIN-SLA (blue). (g) RMSE with respect to RAMA for RAIN (red) and RAIN-SLA (blue). (h) Bias of RAIN (red) and RAIN-SLA (blue) with respect to RAMA. The white shades represent data unavailability.

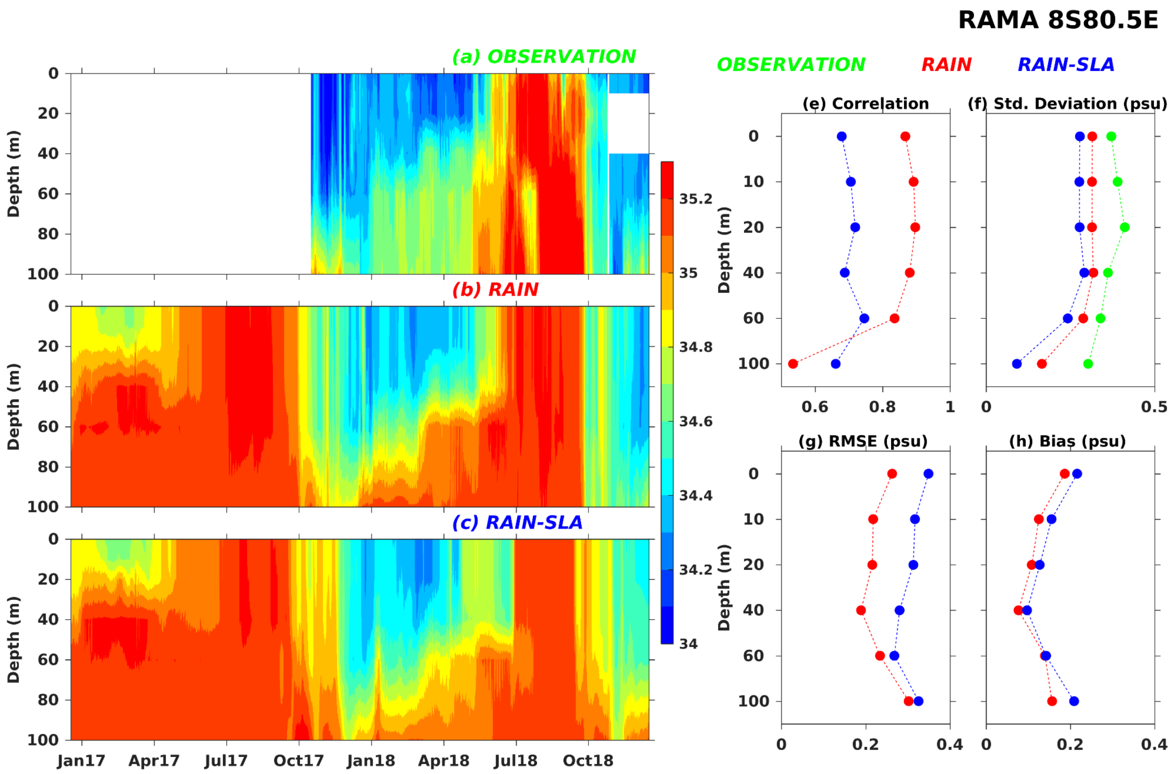

Figure 4.8: Time-depth section of temperature at 8° S, 80.5° E. from (a) RAMA, (b) RAIN and (c) RAIN-SLA. (e) Correlation of RAMA with RAIN (red) and RAIN-SLA (blue). (f) Standard deviation of RAMA (green), RAIN (red) and RAIN-SLA (blue). (g) RMSE with respect to RAMA for RAIN (red) and RAIN-SLA (blue). (h) Bias of RAIN (red) and RAIN-SLA (blue) with respect to RAMA. The white shades represent data unavailability.

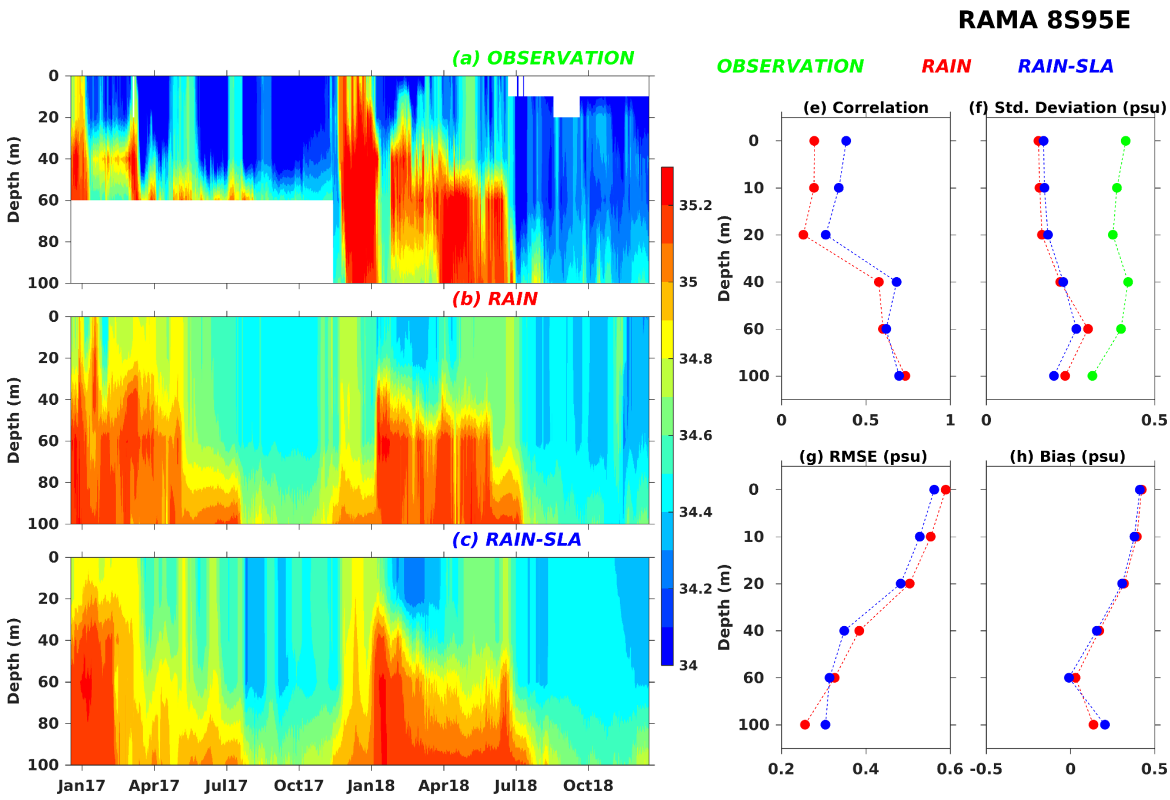

Figure 4.9: Time-depth section of temperature at 8° S, 95° E. from (a) RAMA, (b) RAIN and (c) RAIN-SLA. (e) Correlation of RAMA with RAIN (red) and RAIN-SLA (blue). (f) Standard deviation of RAMA (green), RAIN (red) and RAIN-SLA (blue). (g) RMSE with respect to RAMA for RAIN (red) and RAIN-SLA (blue). (h) Bias of RAIN (red) and RAIN-SLA (blue) with respect to RAMA. The white shades represent data unavailability.

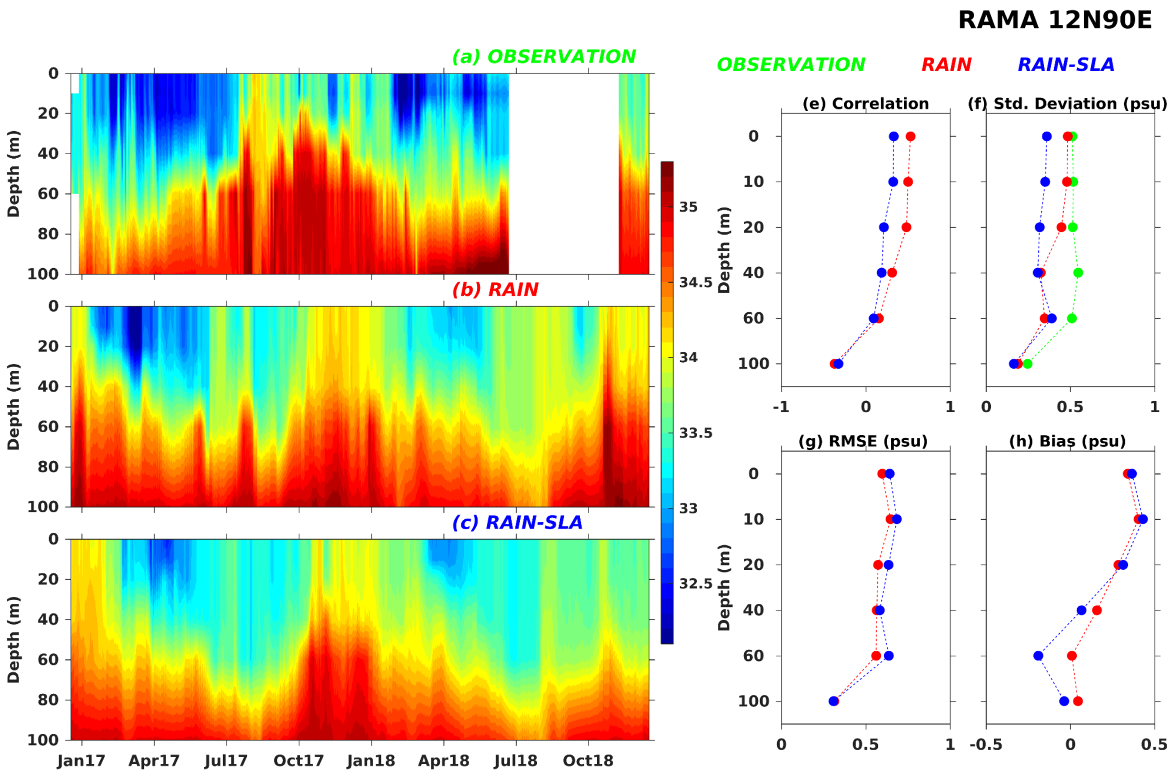

Figure 4.10: Time-depth section of temperature at 12° N, 90° E. from (a) RAMA, (b) RAIN and (c) RAIN-SLA. (e) Correlation of RAMA with RAIN (red) and RAIN-SLA (blue). (f) Standard deviation of RAMA (green), RAIN (red) and RAIN-SLA (blue). (g) RMSE with respect to RAMA for RAIN (red) and RAIN-SLA (blue). (h) Bias of RAIN (red) and RAIN-SLA (blue) with respect to RAMA. The white shades represent data unavailability.

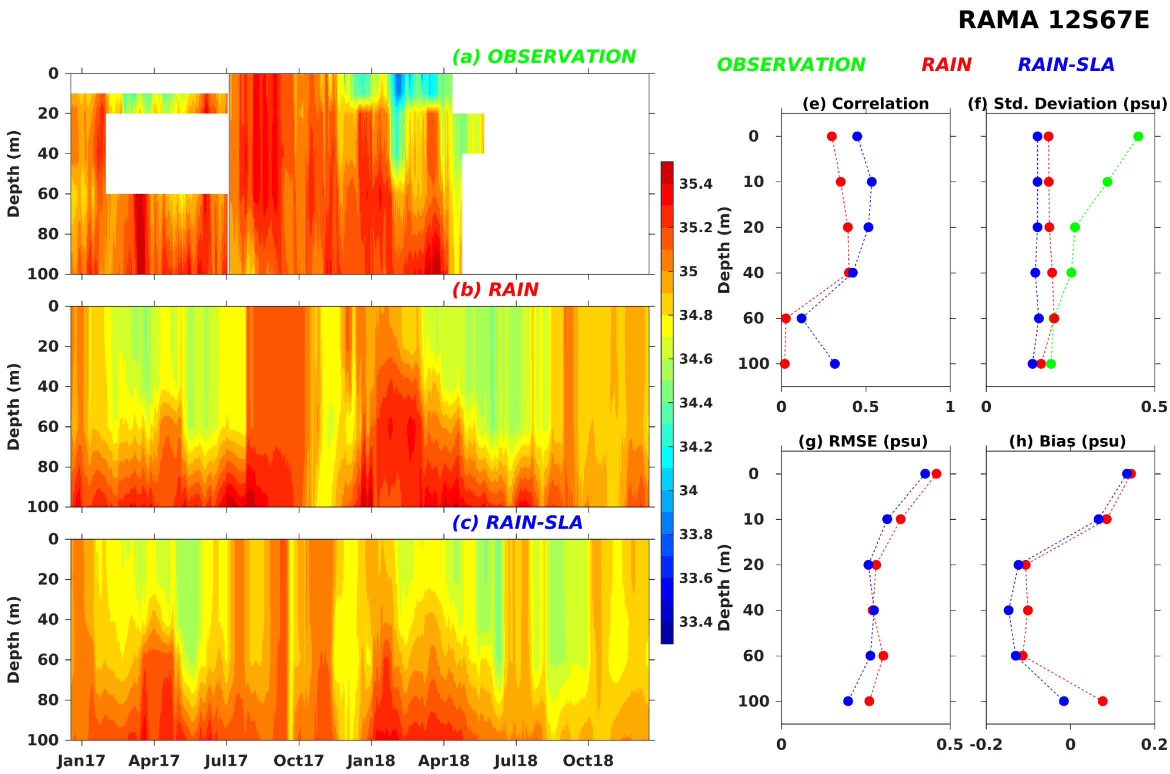

Figure 4.11: Time-depth section of temperature at 12^o S, 67^o E. from (a) RAMA, (b) RAIN and (c) RAIN-SLA. (e) Correlation of RAMA with RAIN (red) and RAIN-SLA (blue). (f) Standard deviation of RAMA (green), RAIN (red) and RAIN-SLA (blue). (g) RMSE with respect to RAMA for RAIN (red) and RAIN-SLA (blue). (h) Bias of RAIN (red) and RAIN-SLA (blue) with respect to RAMA. The white shades represent data unavailability.

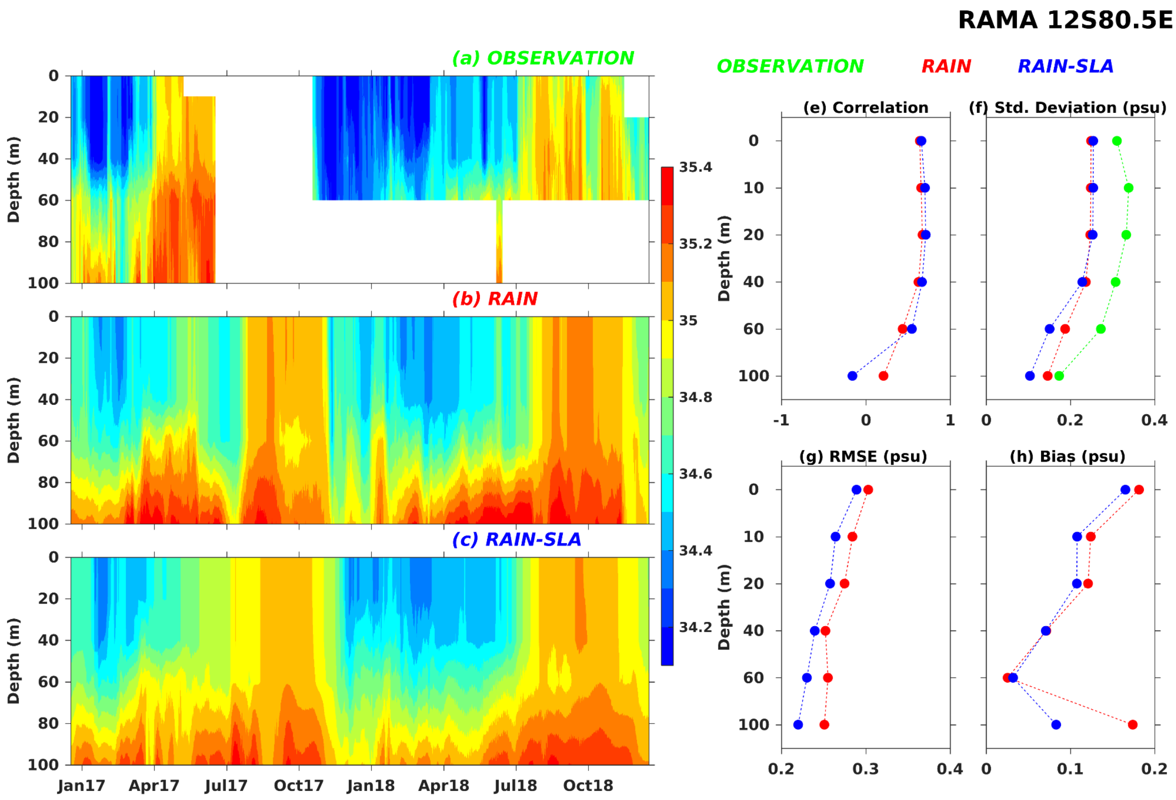

Figure 4.12: Time-depth section of temperature at 12° S, 80.5° E. from (a) RAMA, (b) RAIN and (c) RAIN-SLA. (e) Correlation of RAMA with RAIN (red) and RAIN-SLA (blue). (f) Standard deviation of RAMA (green), RAIN (red) and RAIN-SLA (blue). (g) RMSE with respect to RAMA for RAIN (red) and RAIN-SLA (blue). (h) Bias of RAIN (red) and RAIN-SLA (blue) with respect to RAMA. The white shades represent data unavailability.

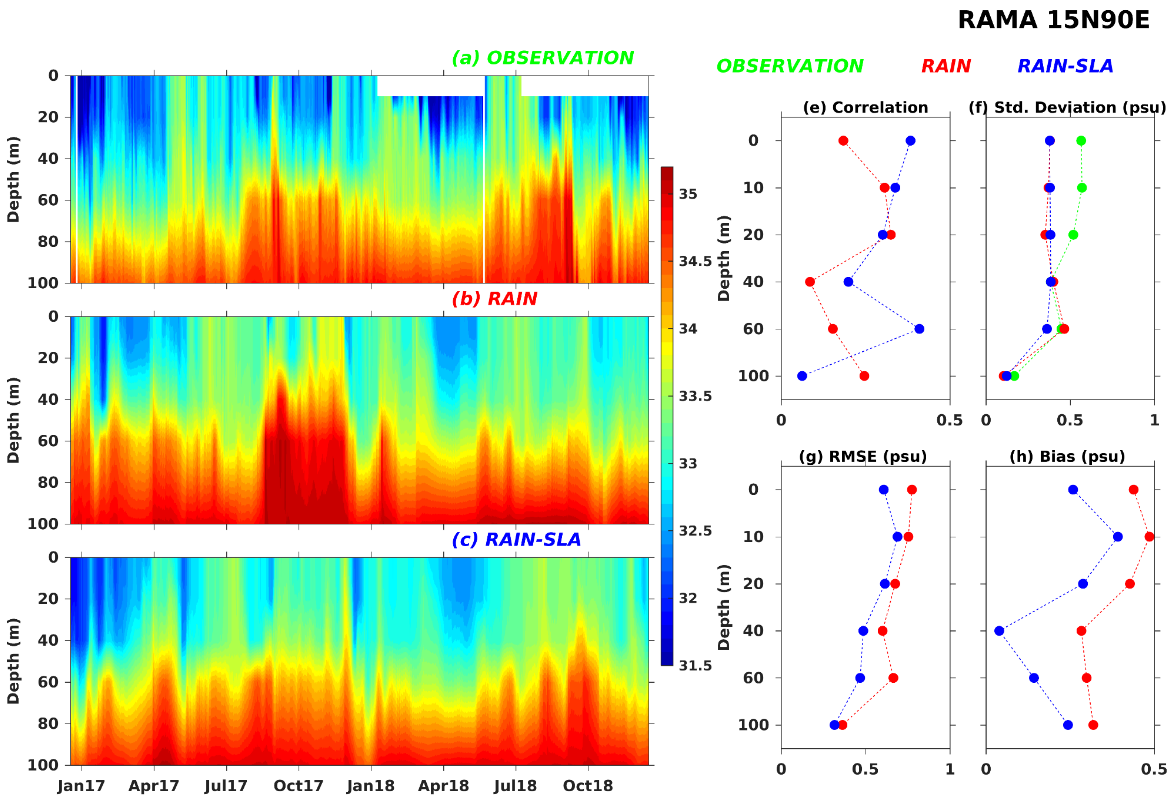

Figure 4.13: Time-depth section of temperature at 15° N, 90° E. from (a) RAMA, (b) RAIN and (c) RAIN-SLA. (e) Correlation of RAMA with RAIN (red) and RAIN-SLA (blue). (f) Standard deviation of RAMA (green), RAIN (red) and RAIN-SLA (blue). (g) RMSE with respect to RAMA for RAIN (red) and RAIN-SLA (blue). (h) Bias of RAIN (red) and RAIN-SLA (blue) with respect to RAMA. The white shades represent data unavailability.

4.3 Comparison with ARGO

Here we quantify the performance of all the three systems with respect to Argo floats in simulating the temperature of the oceans. Since Argo floats traverse in time, we divide the Indian Ocean into three broad regions - Arabian Sea, Bay of Bengal and Equatorial Indian Ocean and perform a collective analysis on the performance. Data from each region is concatenated and a daily Argo observation is obtained for each of the regions. In Fig.1.2, we plot the location of pop-up of Argo floats in the Northern and Equatorial Indian Ocean that were taken into consideration for this validation exercise.

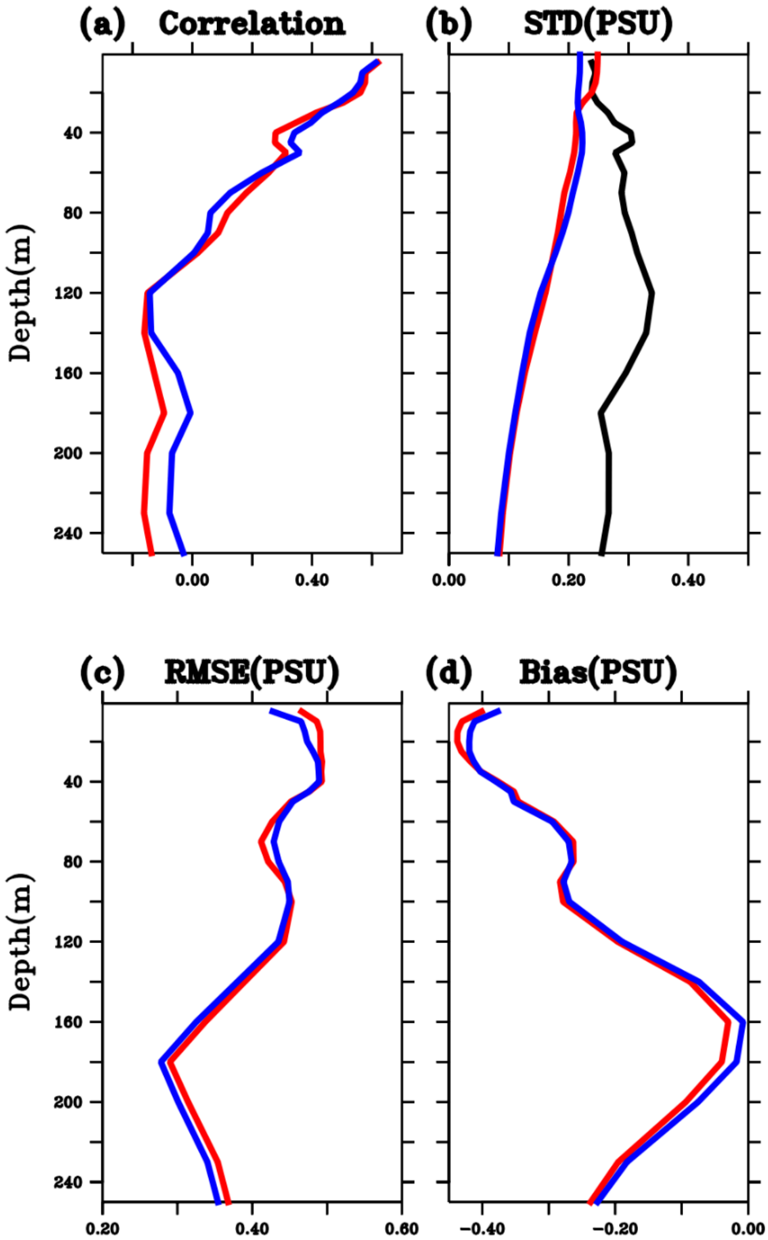

Figure 4.14: (a) Correlation of Argo floats with RAIN (red) and RAIN-SLA (blue) at vertical levels till 260m. (b) Standard deviation of Argo floats (black), RAIN (red) and RAIN-SLA (blue). (c) RMSE with respect to Argo floats for RAIN (red) and RAIN-SLA (blue) at vertical levels till 260m. (d) Bias of RAIN (red) and RAIN-SLA (blue) at vertical levels till 260m with respect to Argo floats in Arabian sea

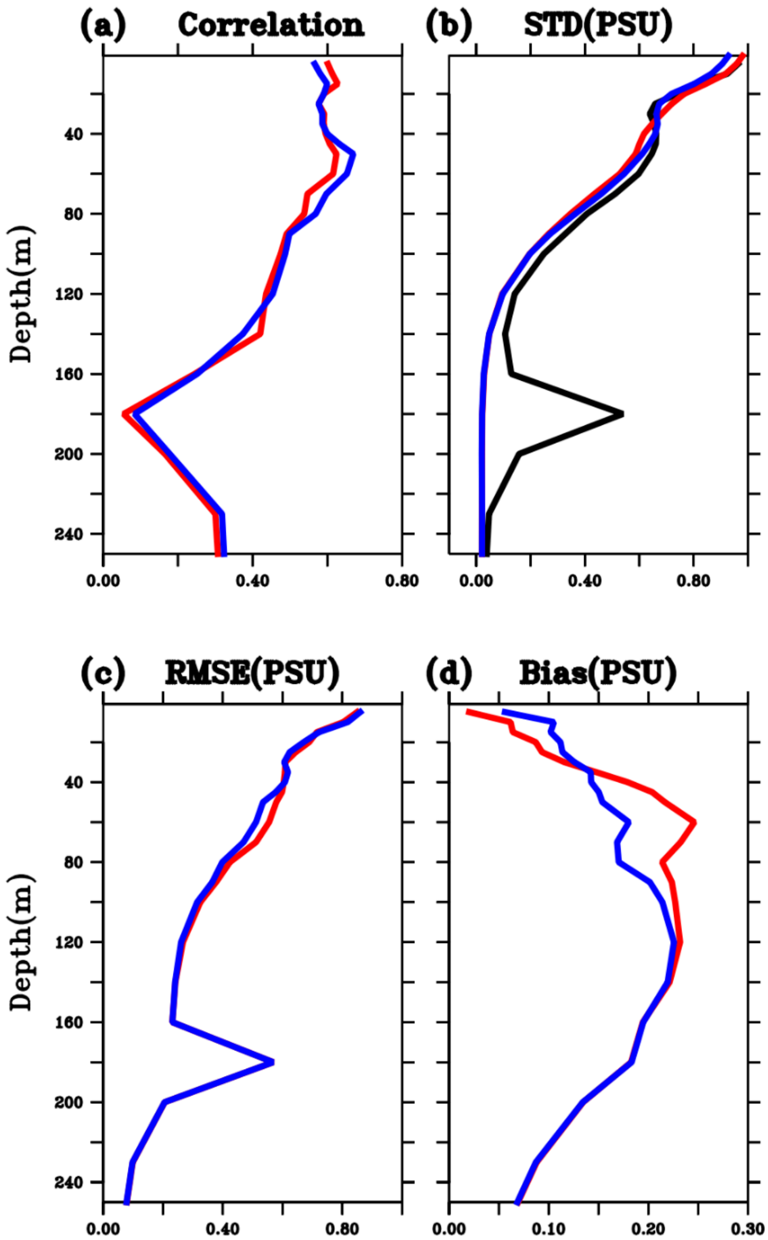

Figure 4.15: (a) Correlation of Argo floats with RAIN (red) and RAIN-SLA (blue) at vertical levels till 260m. (b) Standard deviation of Argo floats (black), RAIN (red) and RAIN-SLA (blue). (c) RMSE with respect to Argo floats for RAIN (red) and RAIN-SLA (blue) at vertical levels till 260m. (d) Bias of RAIN (red) and RAIN-SLA (blue) at vertical levels till 260m with respect to Argo floats in Arabian sea

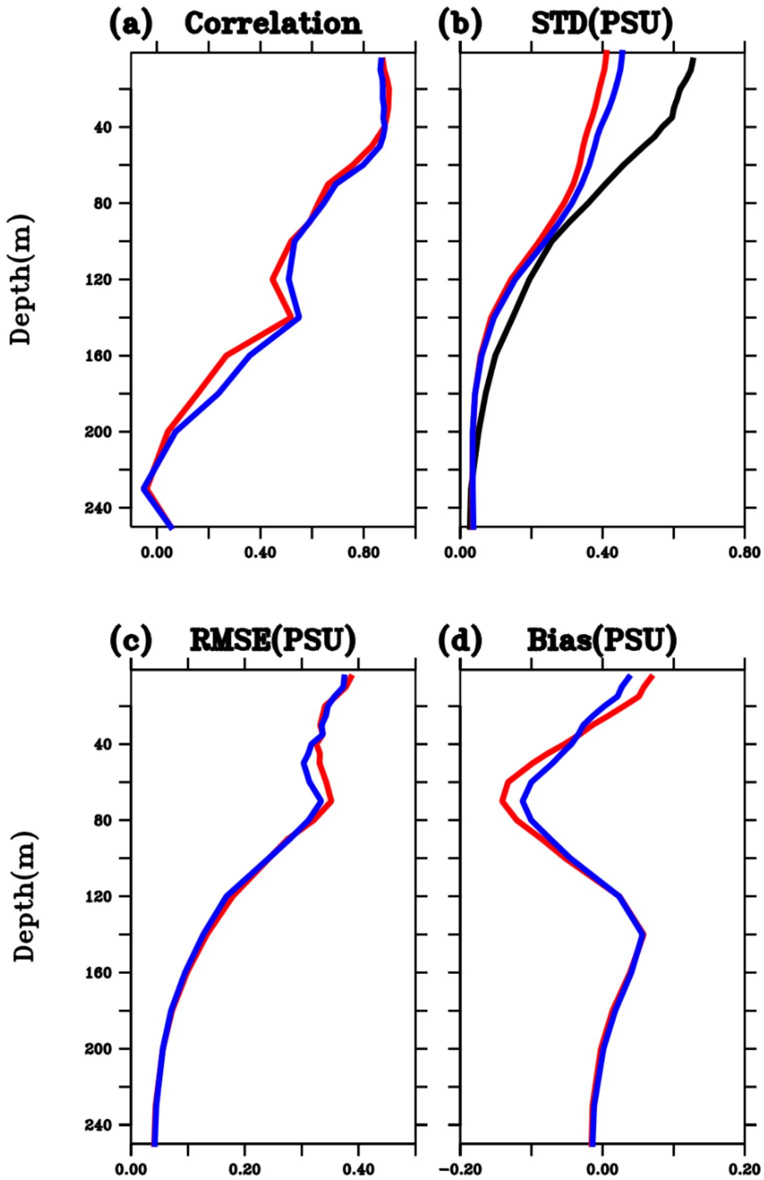

Figure 4.16: (a) Correlation of Argo floats with RAIN (red) and RAIN-SLA (blue) at vertical levels till 260m. (b) Standard deviation of Argo floats (black), RAIN (red) and RAIN-SLA (blue). (c) RMSE with respect to Argo floats for RAIN (red) and RAIN-SLA (blue) at vertical levels till 260m. (d) Bias of RAIN (red) and RAIN-SLA (blue) at vertical levels till 260m with respect to Argo floats in Arabian sea

4.4 Conclusion

We observe a mixed result in salinity improvement. There are some locations where the vertical profile of salinity is improved. Whereas at some locations, we see a slight degradation. Overall, the assimilation of SLA does not have any significant impact on salinity.

5 Sea Level Anomaly

5.1 Introduction

We validate sea level anomaly (SLA) obtained from RAIN and RAIN-SLA with respect to observations from Archiving Validation and Interpretation of Satellite Oceanography (AVISO) Altimetry [18]. We are interested in validating sea level anomaly and not sea surface height because of the mismatch in the model geoid and satellite derived geoid. It is also to be noted that SLA is an independent variable in RAIN and No SLA data has been assimilated in RAIN.

5.2 Comparison with AVISO

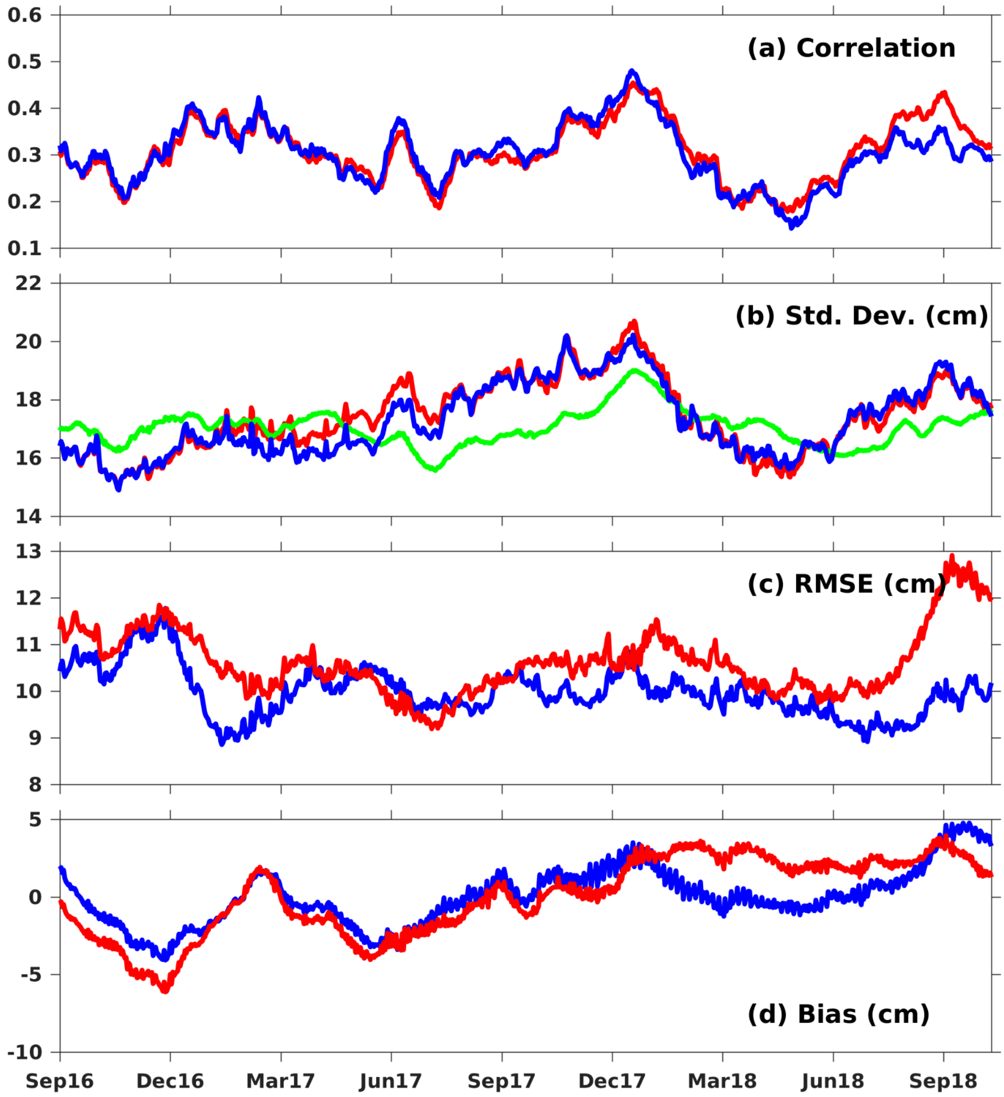

Figure 5.1: Temporal plot of (a) correlation, (b) standard deviation, (c) rmse and (d) bias from RAIN-SLA (blue), RAIN (red) and Observations (green). SLA Assimilation significantly improves the sea level anomaly by reducing rmse and bias. The standard deviation of observation in (b) is shown in green.

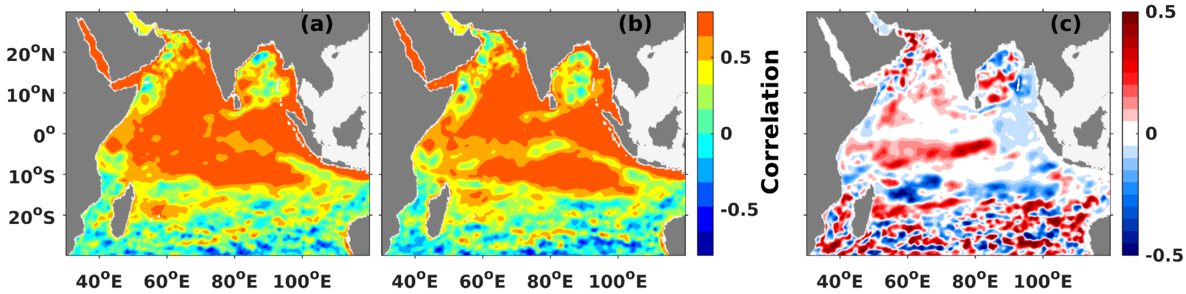

Figure 5.2: Spatial correlation of SLA from AVISO with SLA from (a) RAIN, (b) RAIN-SLA and (c) Difference. There is a marginal improvement in correlation due to assimilation.

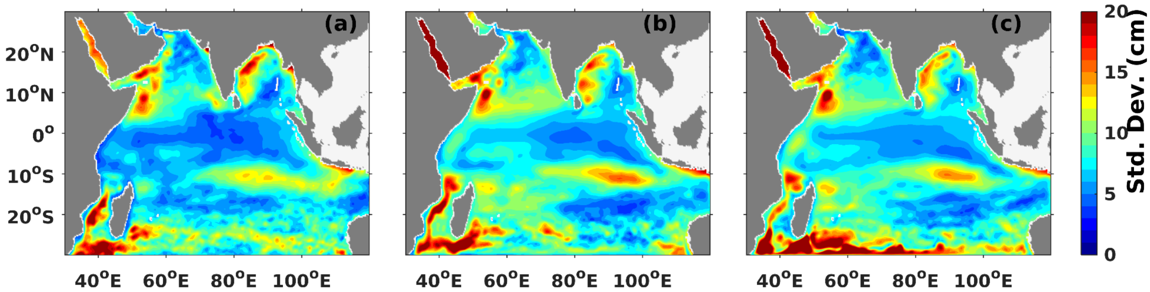

Figure 5.3: Spatial standard deviation of SLA from (a) Observation, (b) RAIN and (c) RAIN-SLA.

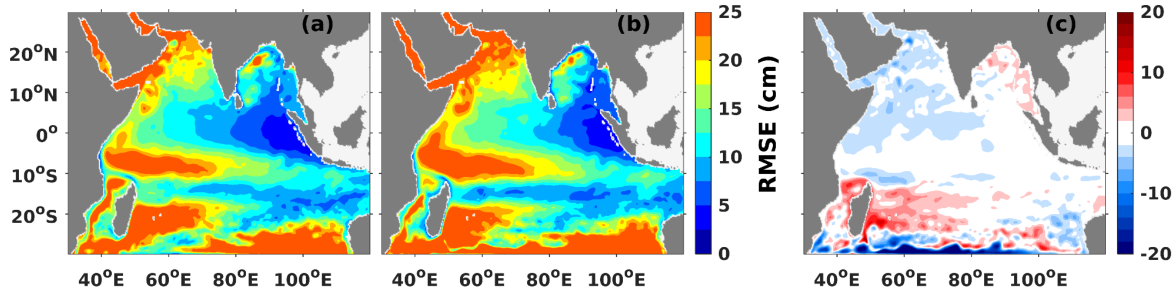

Figure 5.4: Spatial rmse of SLA from AVISO with SLA from (a) RAIN, (b) RAIN-SLA and (c) Difference.

5.3 Conclusion

We see that there is a notable improvement in the time series of rmse in SLA due to assimilation of SLA. Spatial correlation has improved in the North Indian Ocean.

6 Currents

6.1 Introduction

We look at the performance in simulating ocean currents in RAIN-SLA and compare it with RAIN. It is to be remembered that currents were not assimilated and hence are independent variables. We compare the performance against Ocean Surface Current Analysis Real-time (OSCAR), RAMA, Acoustic Doppler Current Profilers (ADCP) installed at various locations along the Indian coast (see Fig.1.1). We also compare against surface current observation from High Frequency RADAR installed along the coast of India. [19]

6.2 Comparison with OSCAR

We validate the performance of RAIN and RAIN-SLA against OSCAR currents and compare the performance. The model data from both the systems were projected on to the OSCAR grid and compared.

6.2.1 zonal current

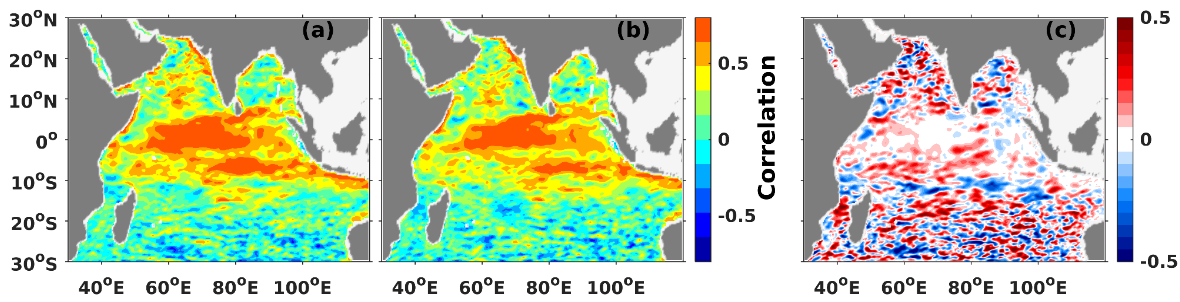

Figure 6.1: Spatial correlation with respect to OSCAR current of u component of the horizontal velocity from a) RAIN, (b) RAIN-SLA and (c) Difference

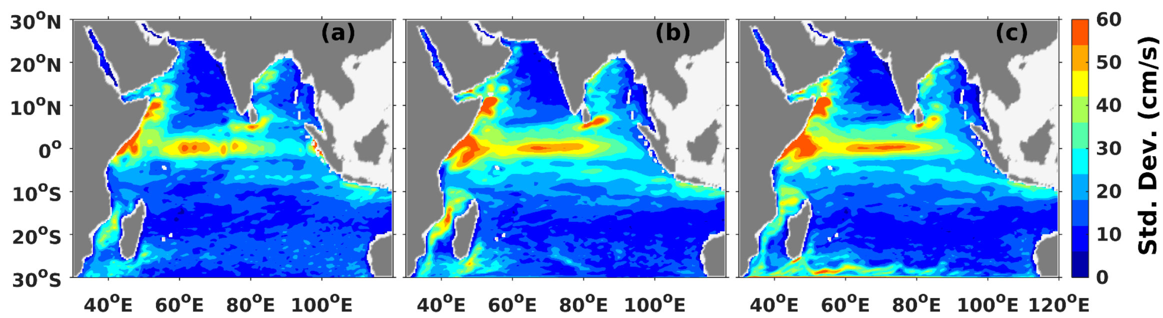

Figure 6.2: Spatial plot of standard deviation u component of the horizontal velocity from (a) OSCAR current, (b) RAIN and (c) RAIN-SLA

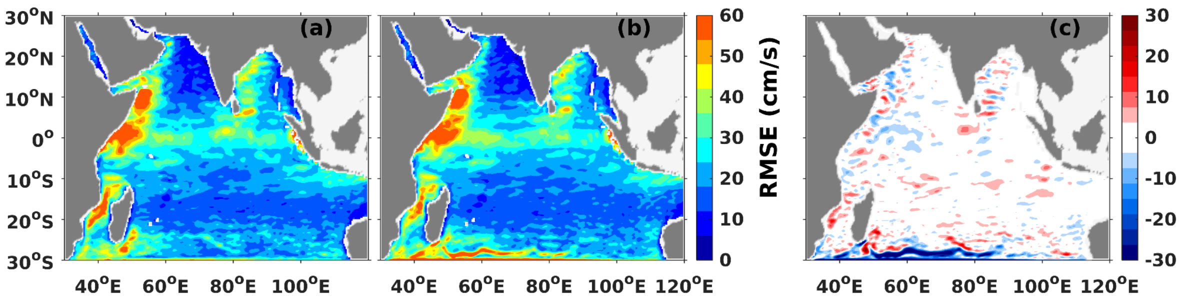

Figure 6.3: Spatial rmse with respect to OSCAR current of u component of the horizontal velocity from a) RAIN, (b) RAIN-SLA and (c) Difference

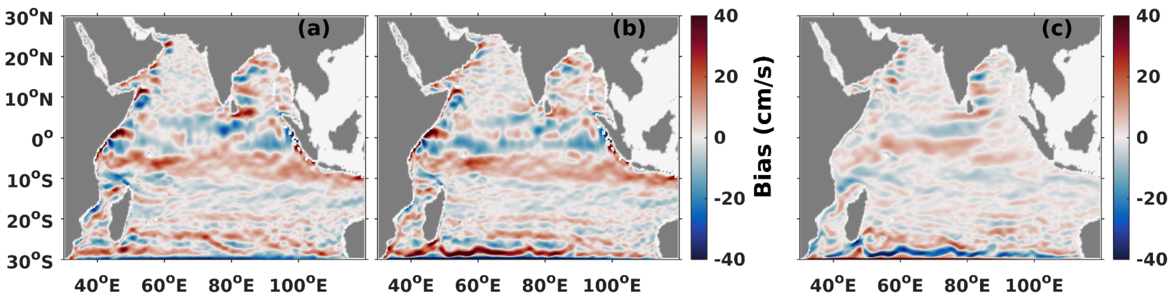

Figure 6.4: Spatial bias with respect to OSCAR current of u component of the horizontal velocity from a) RAIN, (b) RAIN-SLA and (c) Difference

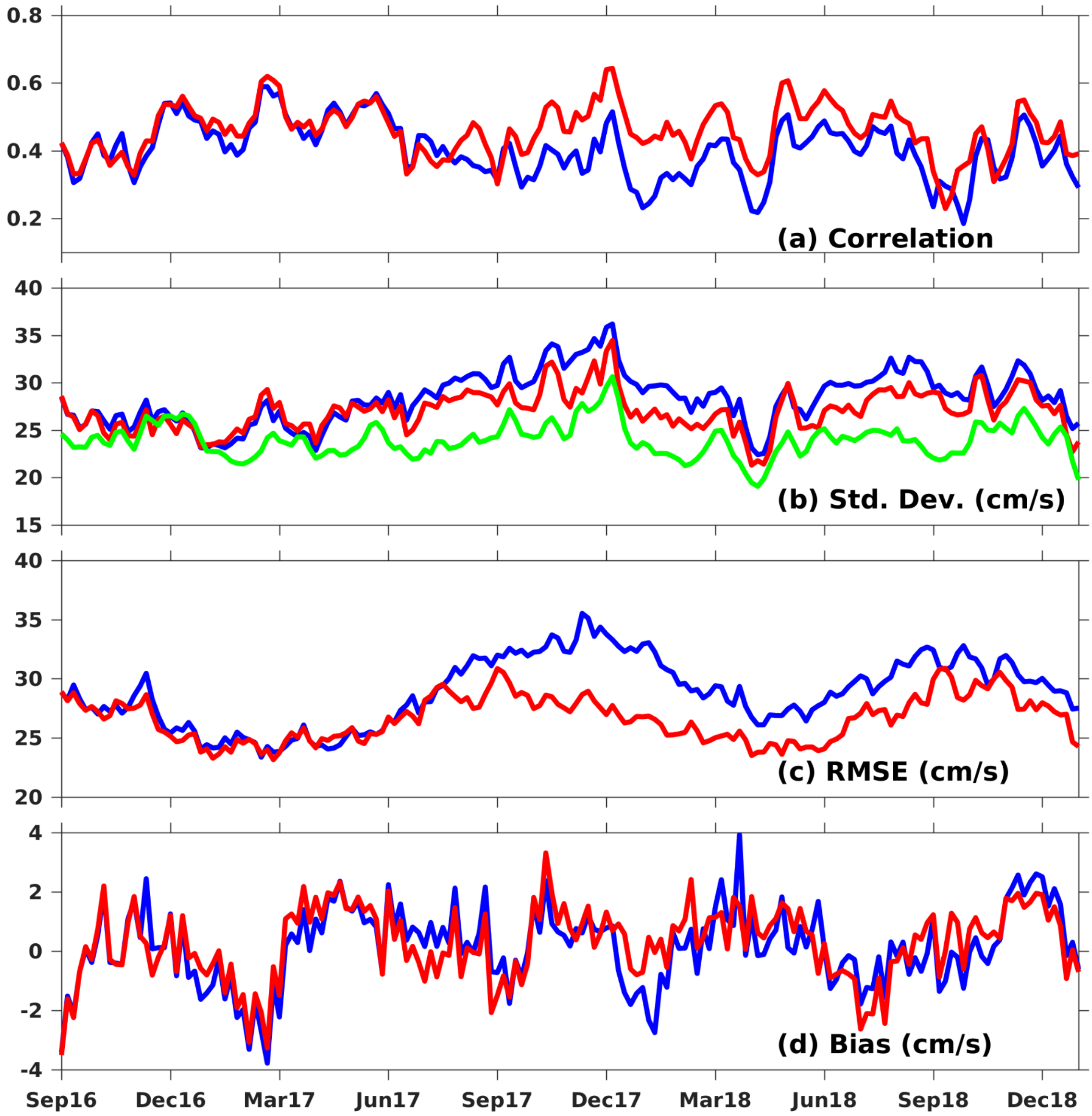

Figure 6.5: Temporal plot of (a) correlation, (b) standard deviation, (c) rmse and (d) bias in u from RAIN (red) and RAIN-SLA (blue) . The standard deviation of u in OSCAR is shown in green.

6.2.1 meridional current

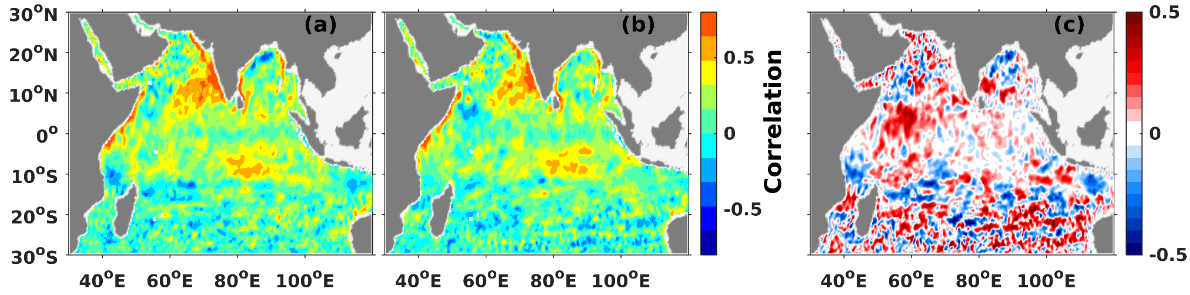

Figure 6.6: Spatial correlation with respect to OSCAR current of v component of the horizontal velocity from a) RAIN, (b) RAIN-SLA and (c) Difference

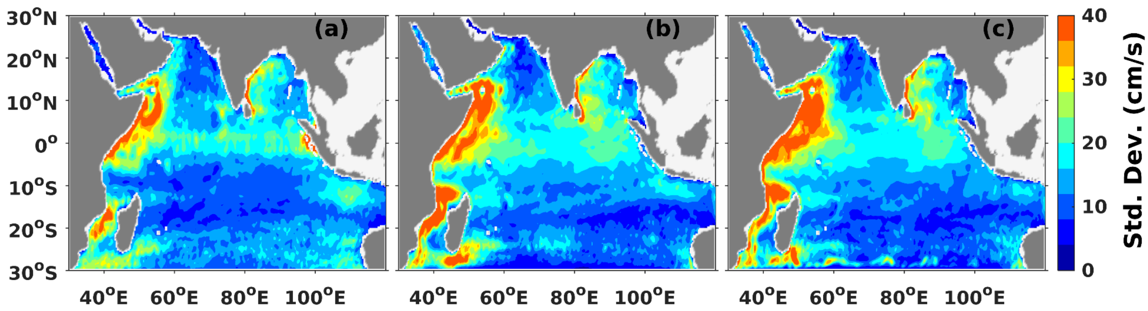

Figure 6.7: Spatial plot of standard deviation v component of the horizontal velocity from (a) OSCAR current, (b) RAIN and (c) RAIN-SLA

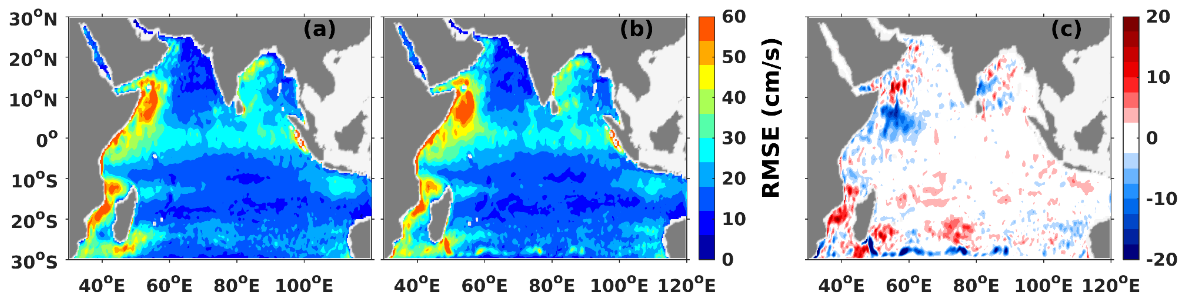

Figure 6.8: Spatial rmse with respect to OSCAR current of v component of the horizontal velocity from a) RAIN, (b) RAIN-SLA and (c) Difference

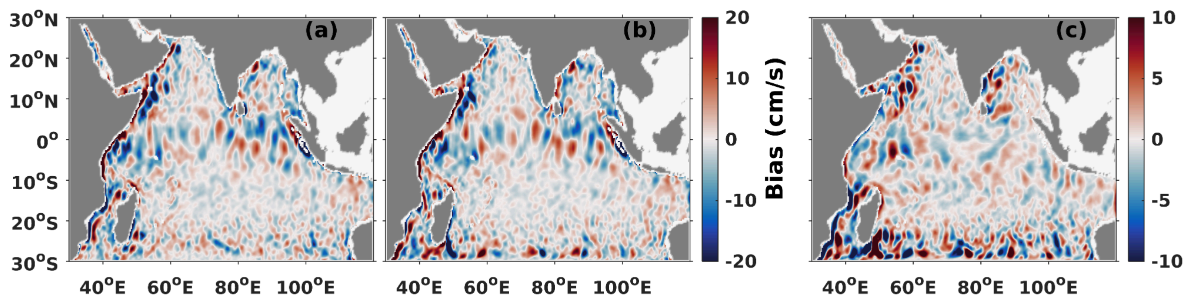

Figure 6.9: Spatial bias with respect to OSCAR current of v component of the horizontal velocity from a) RAIN, (b) RAIN-SLA and (c) Difference

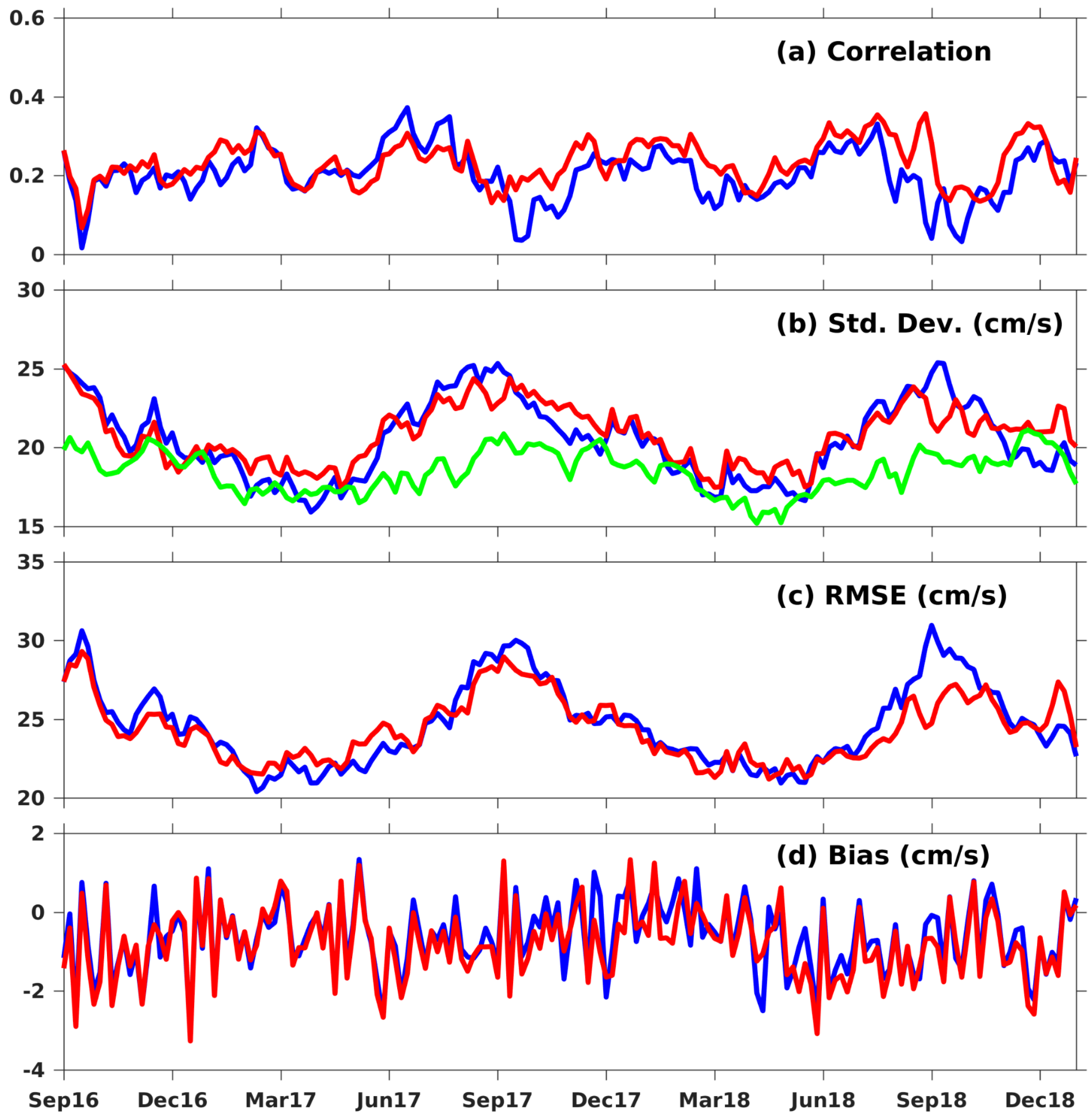

Figure 6.10: Temporal plot of (a) correlation, (b) standard deviation, (c) rmse and (d) bias in v from RAIN (red) and RAIN-SLA (blue) . The standard deviation of v in OSCAR is shown in green.

6.3 Comparison with RAMA ADCP

6.3.1 u current

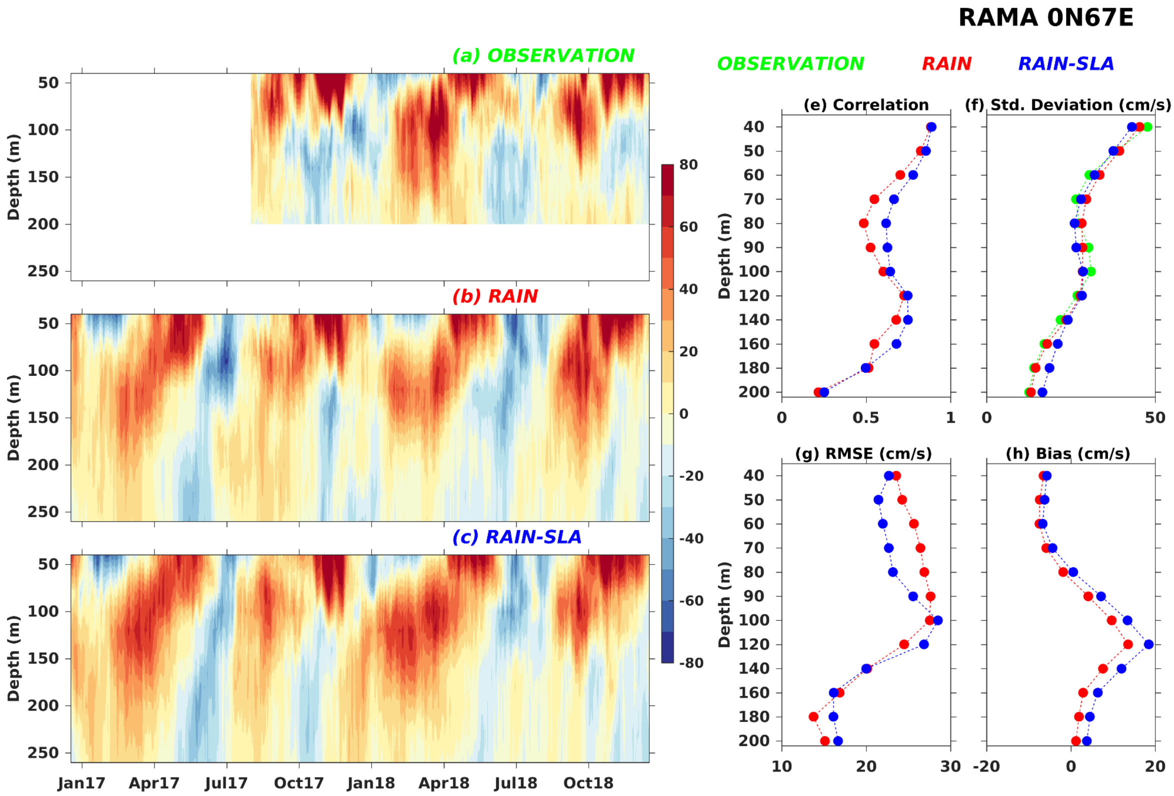

Figure 6.11: Time-depth section of temperature at 0° N, 67° E. from (a) RAMA, (b) RAIN and (c) RAIN-SLA. (e) Correlation of RAMA with RAIN (red) and RAIN-SLA (blue). (f) Standard deviation of RAMA (green), RAIN (red) and RAIN-SLA (blue). (g) RMSE with respect to RAMA for RAIN (red) and RAIN-SLA (blue). (h) Bias of RAIN (red) and RAIN-SLA (blue) with respect to RAMA. The white shades represent data unavailability.

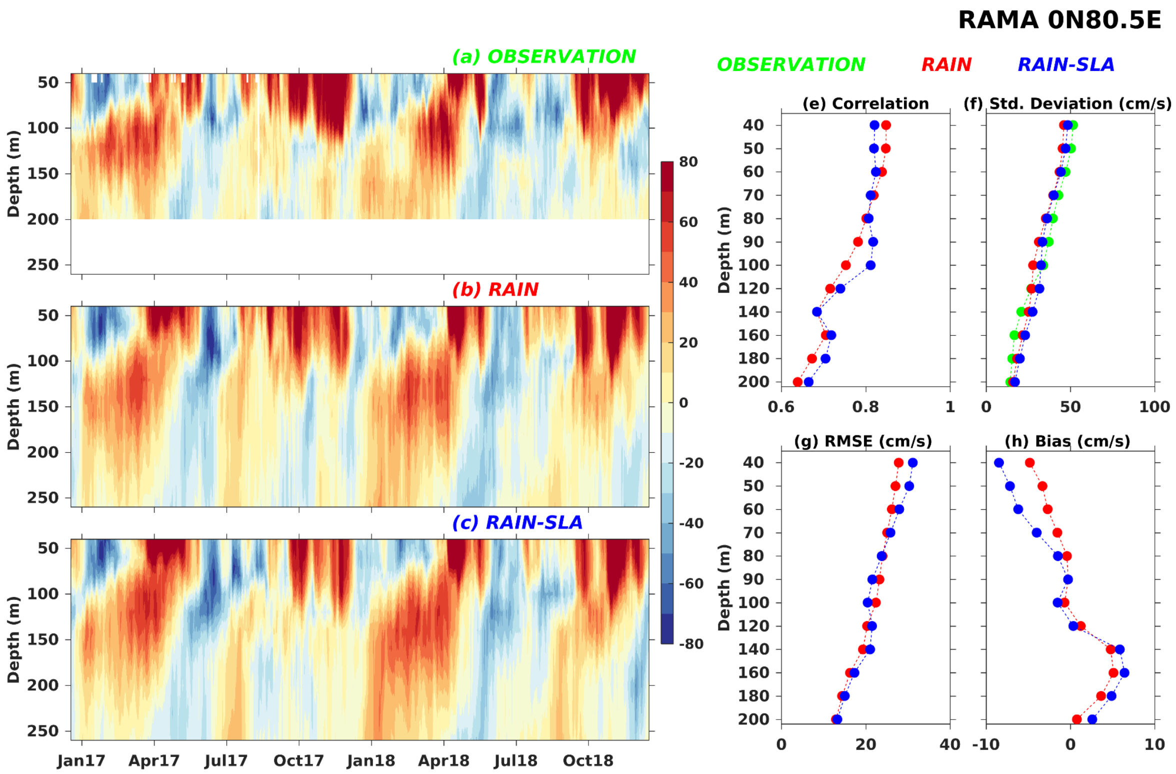

Figure 6.12: Time-depth section of temperature at 0° N, 80.5° E. from (a) RAMA, (b) RAIN and (c) RAIN-SLA. (e) Correlation of RAMA with RAIN (red) and RAIN-SLA (blue). (f) Standard deviation of RAMA (green), RAIN (red) and RAIN-SLA (blue). (g) RMSE with respect to RAMA for RAIN (red) and RAIN-SLA (blue). (h) Bias of RAIN (red) and RAIN-SLA (blue) with respect to RAMA. The white shades represent data unavailability.

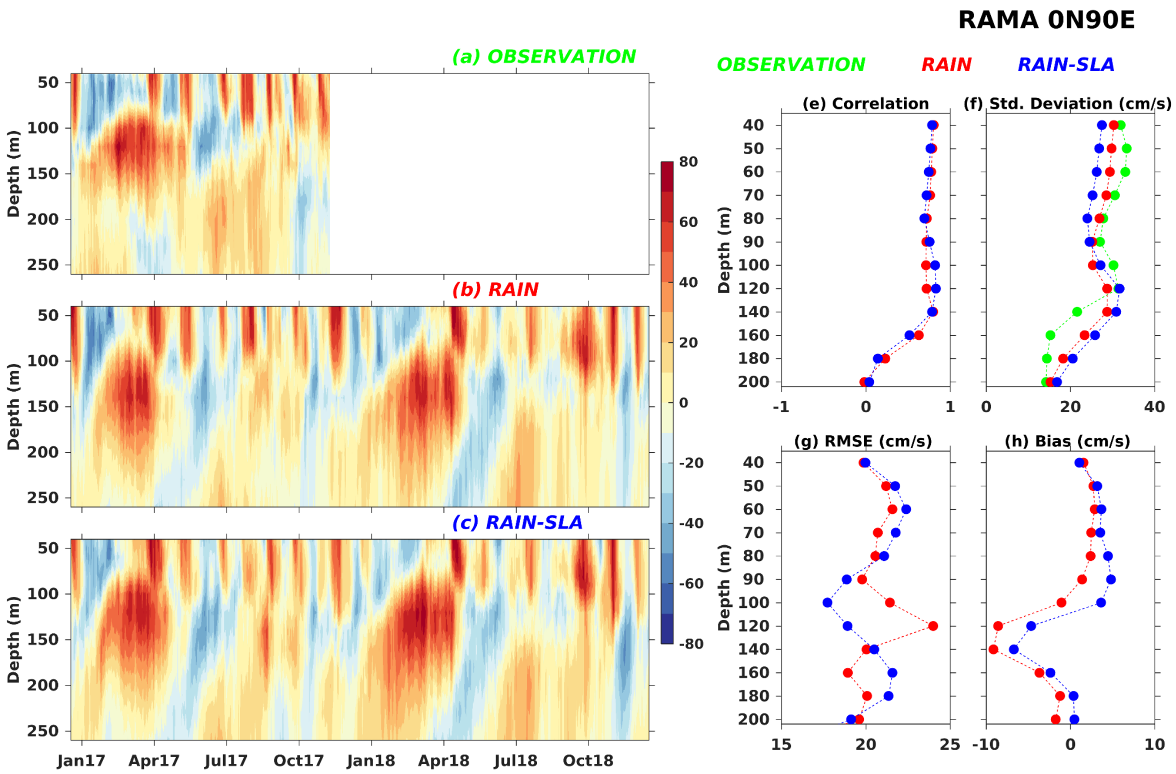

Figure 6.13: Time-depth section of temperature at 0° N, 90° E. from (a) RAMA, (b) RAIN and (c) RAIN-SLA. (e) Correlation of RAMA with RAIN (red) and RAIN-SLA (blue). (f) Standard deviation of RAMA (green), RAIN (red) and RAIN-SLA (blue). (g) RMSE with respect to RAMA for RAIN (red) and RAIN-SLA (blue). (h) Bias of RAIN (red) and RAIN-SLA (blue) with respect to RAMA. The white shades represent data unavailability.

6.3.2 v current

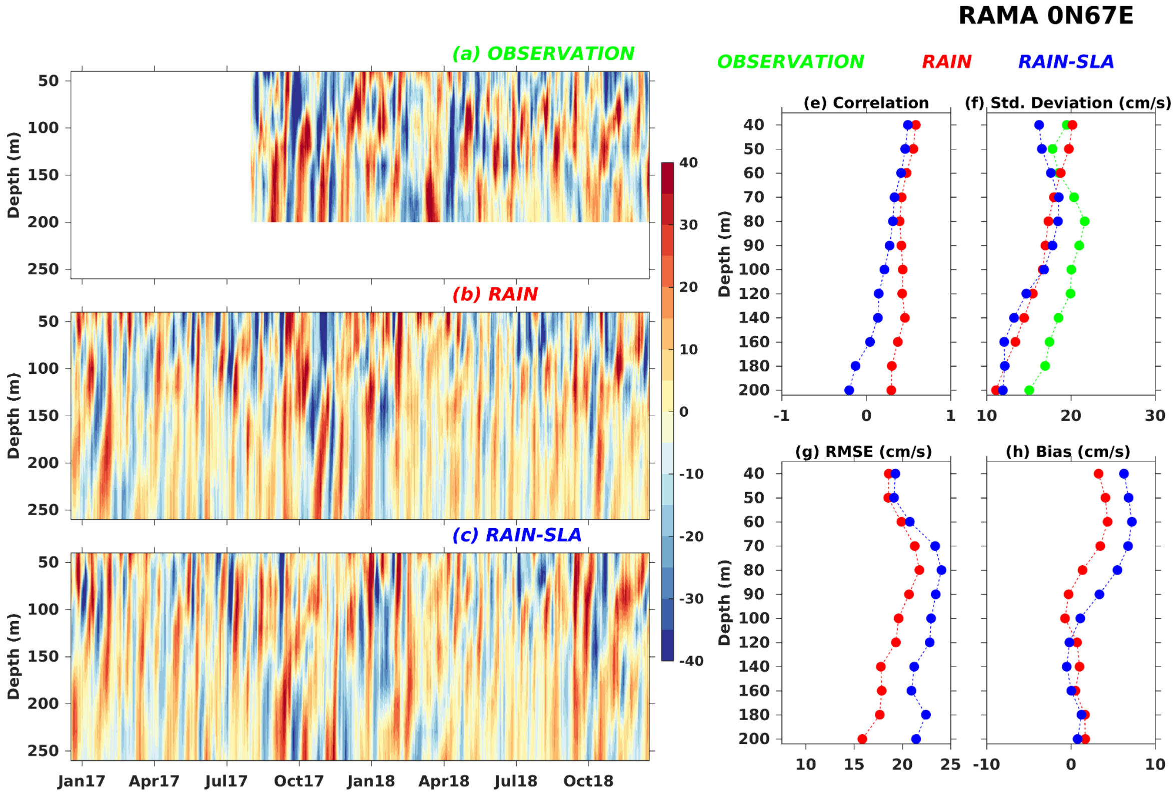

Figure 6.14: Time-depth section of temperature at 0° N, 67° E. from (a) RAMA, (b) RAIN and (c) RAIN-SLA. (e) Correlation of RAMA with RAIN (red) and RAIN-SLA (blue). (f) Standard deviation of RAMA (green), RAIN (red) and RAIN-SLA (blue). (g) RMSE with respect to RAMA for RAIN (red) and RAIN-SLA (blue). (h) Bias of RAIN (red) and RAIN-SLA (blue) with respect to RAMA. The white shades represent data unavailability.

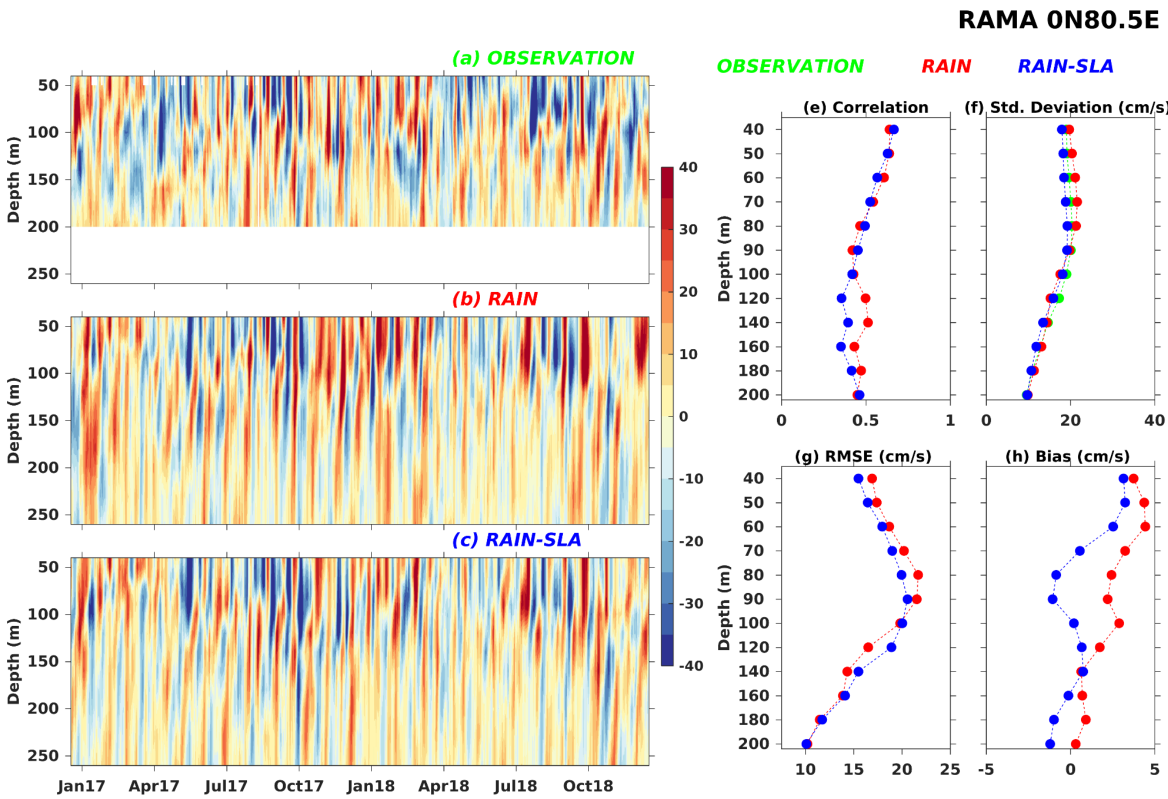

Figure 6.15: Time-depth section of temperature at 0° N, 80.5° E. from (a) RAMA, (b) RAIN and (c) RAIN-SLA. (e) Correlation of RAMA with RAIN (red) and RAIN-SLA (blue). (f) Standard deviation of RAMA (green), RAIN (red) and RAIN-SLA (blue). (g) RMSE with respect to RAMA for RAIN (red) and RAIN-SLA (blue). (h) Bias of RAIN (red) and RAIN-SLA (blue) with respect to RAMA. The white shades represent data unavailability.

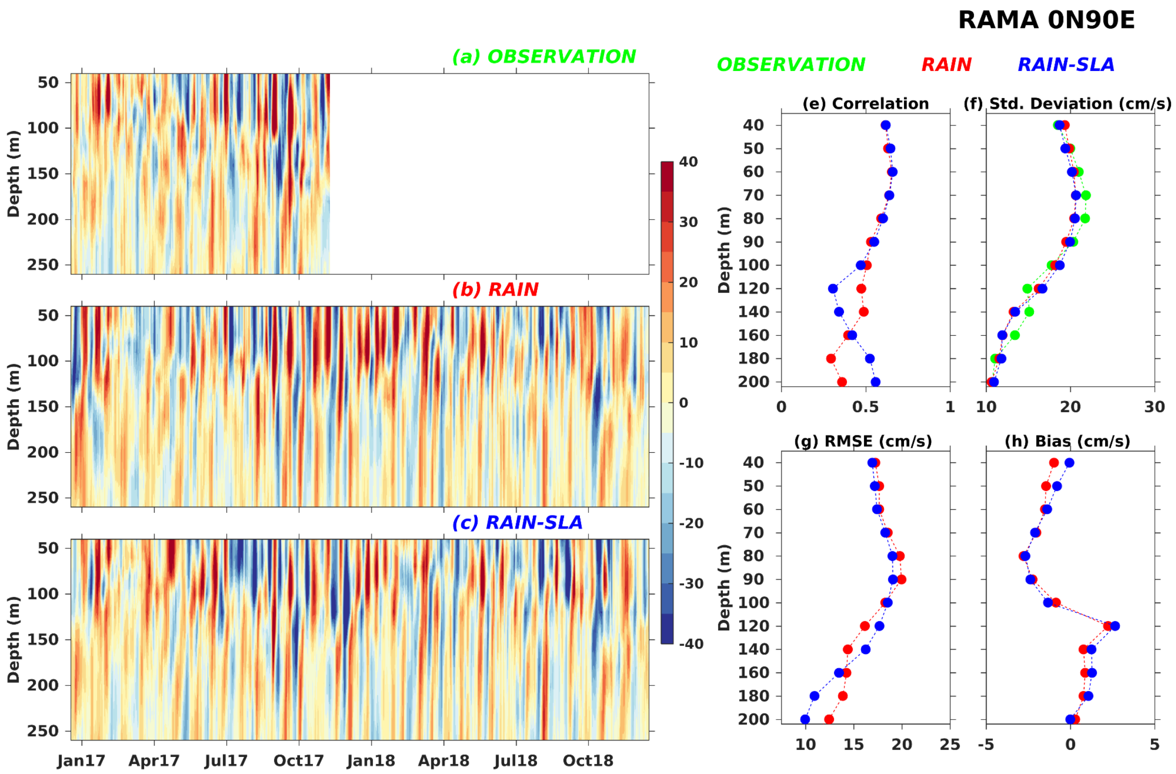

Figure 6.16: Time-depth section of temperature at 0° N, 90° E. from (a) RAMA, (b) RAIN and (c) RAIN-SLA. (e) Correlation of RAMA with RAIN (red) and RAIN-SLA (blue). (f) Standard deviation of RAMA (green), RAIN (red) and RAIN-SLA (blue). (g) RMSE with respect to RAMA for RAIN (red) and RAIN-SLA (blue). (h) Bias of RAIN (red) and RAIN-SLA (blue) with respect to RAMA. The white shades represent data unavailability.

6.4 Comparison with RAMA surface current

6.4.1 u current

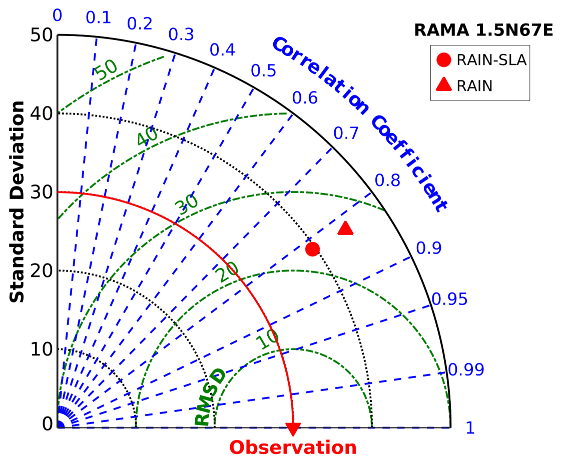

Figure 6.17: Taylor Diagram of surface U current from RAIN-SLA and RAIN with respect to RAMA mooring at 1.5° N, 67° E.

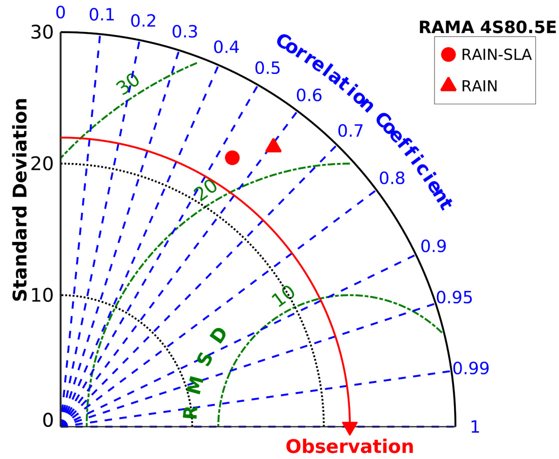

Figure 6.18: Taylor Diagram of surface U current from RAIN-SLA and RAIN with respect to RAMA mooring at 4° S, 80.5° E.

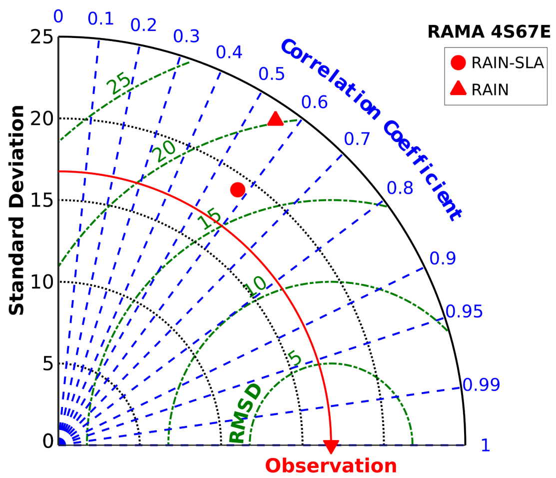

Figure 6.19: Taylor Diagram of surface U current from RAIN-SLA and RAIN with respect to RAMA mooring at 4° S, 67° E.

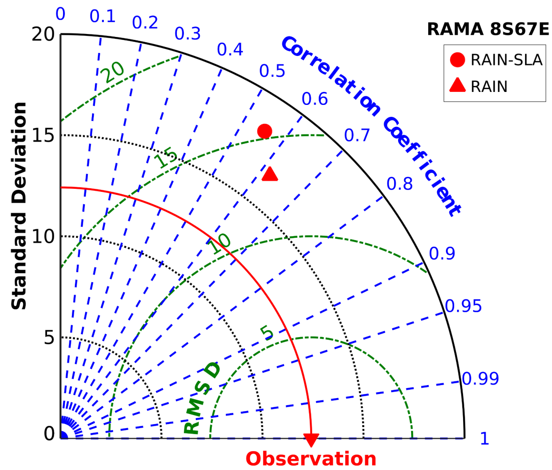

Figure 6.20: Taylor Diagram of surface U current from RAIN-SLA and RAIN with respect to RAMA mooring at 8° S, 67° E.

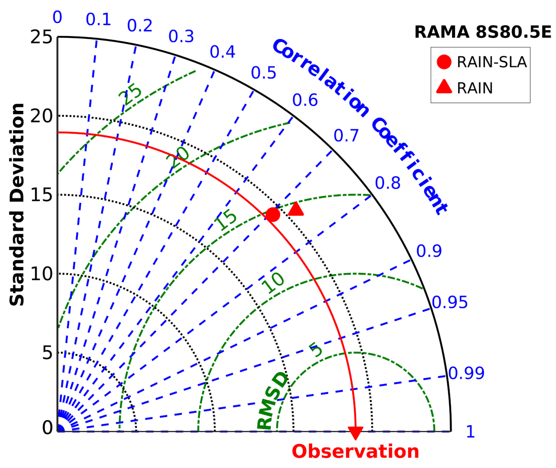

Figure 6.21: Taylor Diagram of surface U current from RAIN-SLA and RAIN with respect to RAMA mooring at 8° S, 80.5° E.

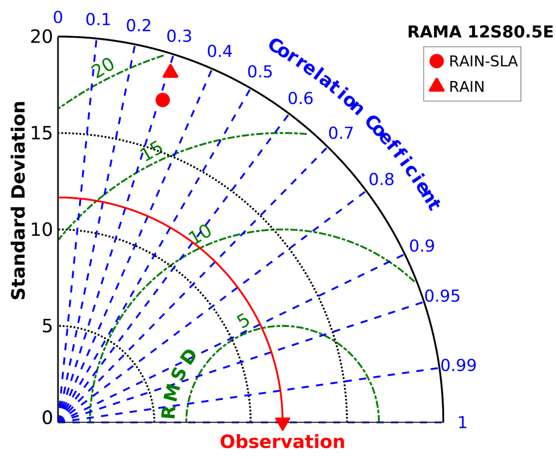

Figure 6.22: Taylor Diagram of surface U current from RAIN-SLA and RAIN with respect to RAMA mooring at 12° S, 80.5° E.

6.4.2 v current

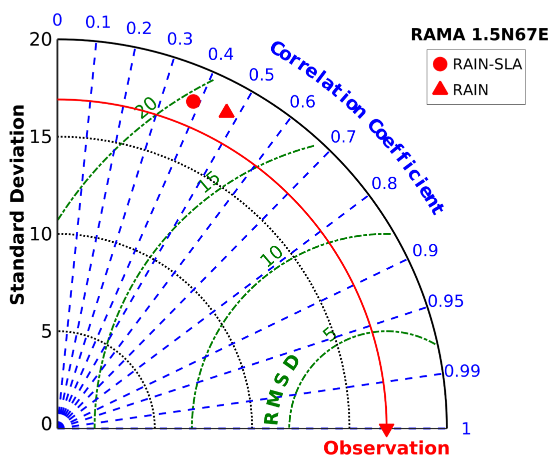

Figure 6.23: Taylor Diagram of surface V current from RAIN-SLA and RAIN with respect to RAMA mooring at 1.5° N, 67° E.

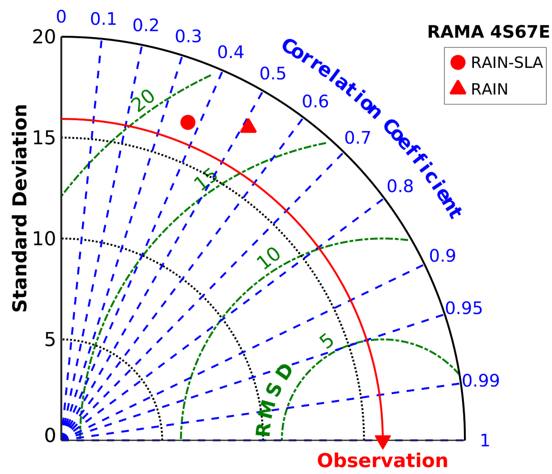

Figure 6.24: Taylor Diagram of surface V current from RAIN-SLA and RAIN with respect to RAMA mooring at 4° S, 67° E.

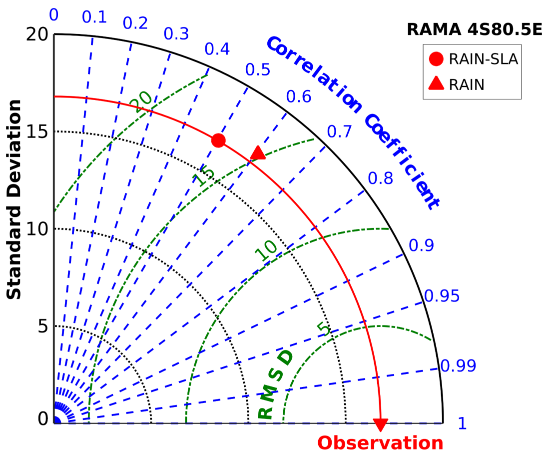

Figure 6.25: Taylor Diagram of surface V current from RAIN-SLA and RAIN with respect to RAMA mooring at 4° S, 80.5° E.

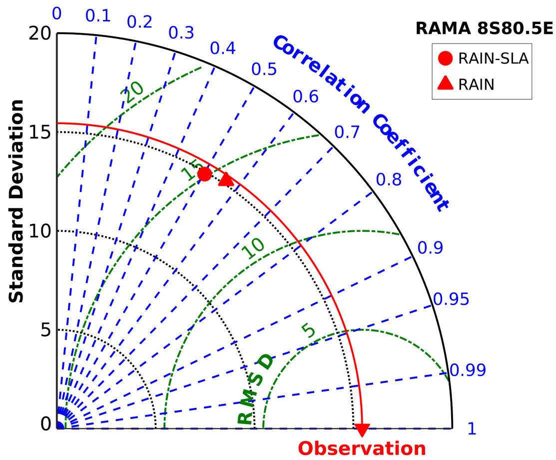

Figure 6.26: Taylor Diagram of surface V current from RAIN-SLA and RAIN with respect to RAMA mooring at 8° S, 80.5° E.

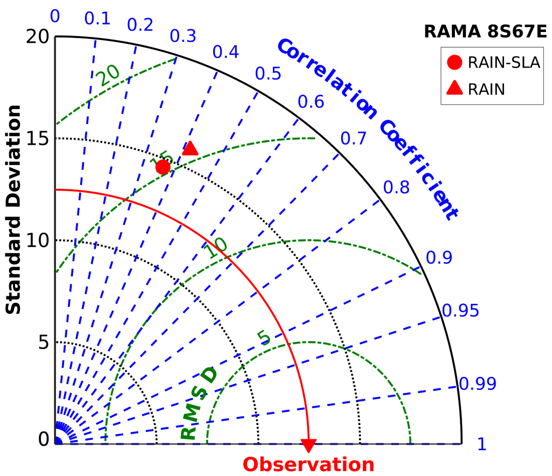

Figure 6.27: Taylor Diagram of surface V current from RAIN-SLA and RAIN with respect to RAMA mooring at 8° S, 67° E.

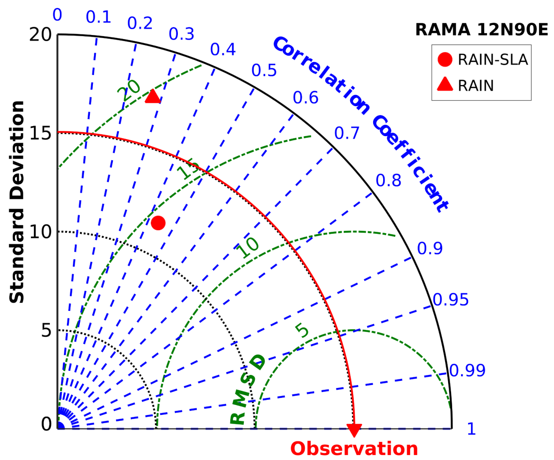

Figure 6.28.: Taylor Diagram of surface V current from RAIN-SLA and RAIN with respect to RAMA mooring at 12° N, 90° E.

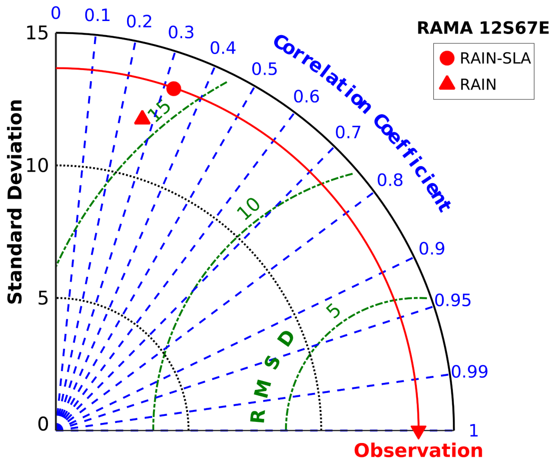

Figure 6.29: Taylor Diagram of surface V current from RAIN-SLA and RAIN with respect to RAMA mooring at 12° S, 67° E.

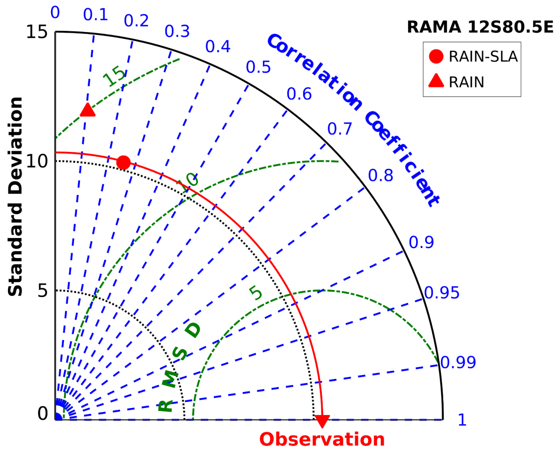

Figure 6.30: Taylor Diagram of surface V current from RAIN-SLA and RAIN with respect to RAMA mooring at 12° S, 80.5° E.

6.5 Comparison with HF Radar surface currents

6.5.1 u current

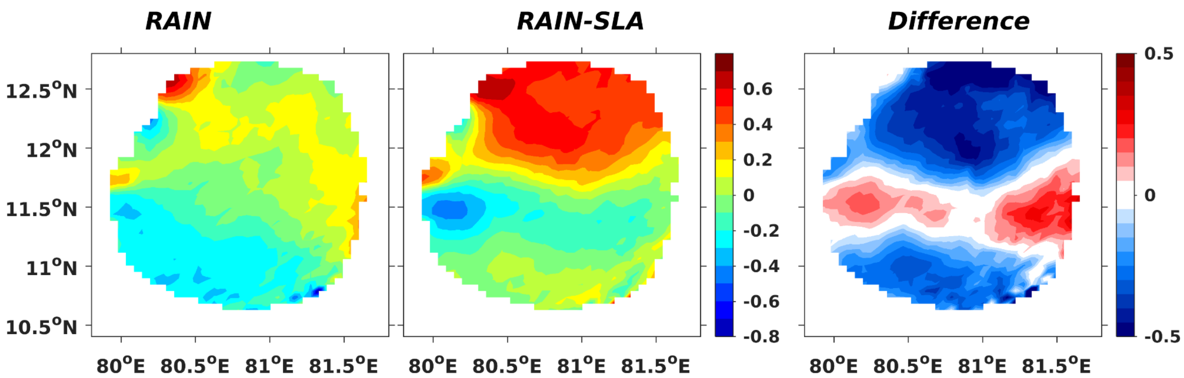

Figure 6.31: Spatial correlation with respect to u component of the horizontal velocity of Tamil Nadu HF radar from a) RAIN, (b) RAIN-SLA and (c) Difference

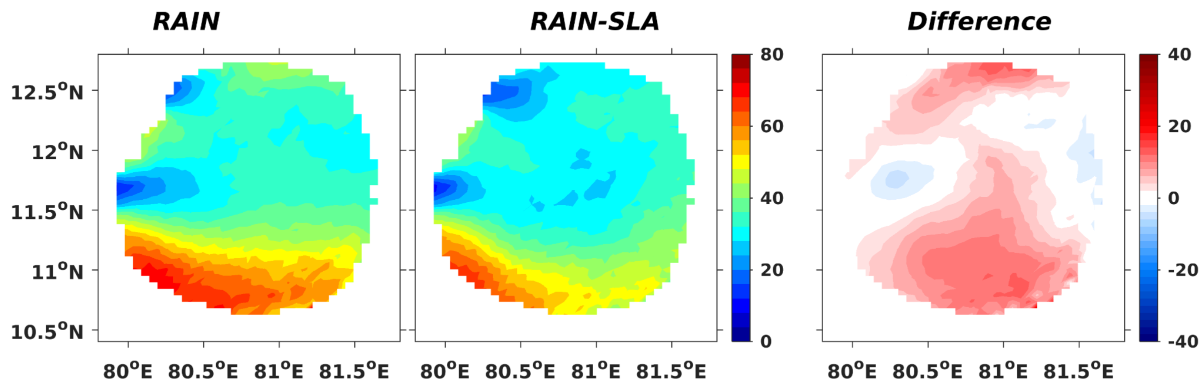

Figure 6.32: Spatial RMSE with respect to u component of the horizontal velocity of Tamil Nadu HF radar from a) RAIN, (b) RAIN-SLA and (c) Difference

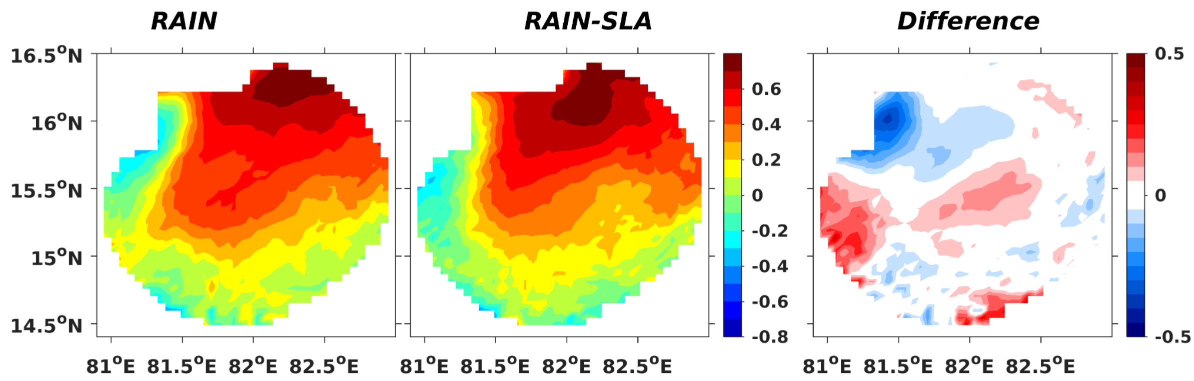

Figure 6.33: Spatial correlation with respect to u component of the horizontal velocity of Andhra Pradesh HF radar from a) RAIN, (b) RAIN-SLA and (c) Difference

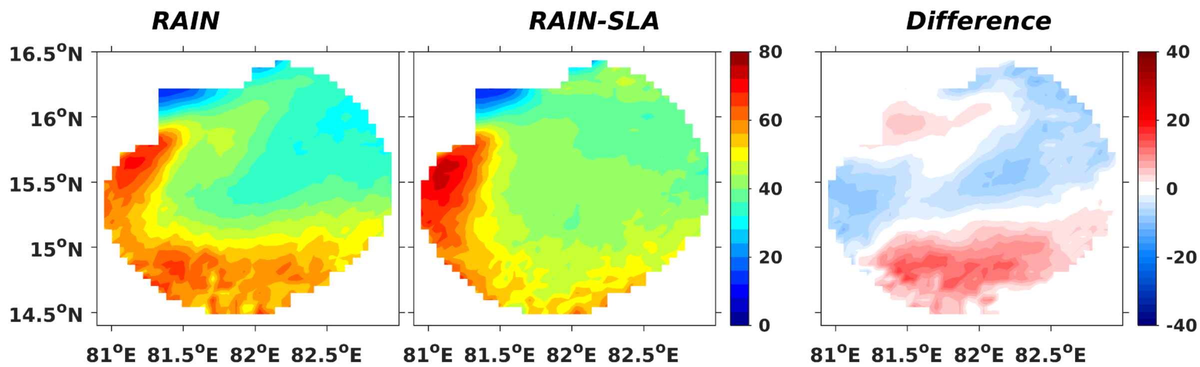

Figure 6.34: Spatial RMSE with respect to u component of the horizontal velocity of Andhra Pradesh HF radar from a) RAIN, (b) RAIN-SLA and (c) Difference

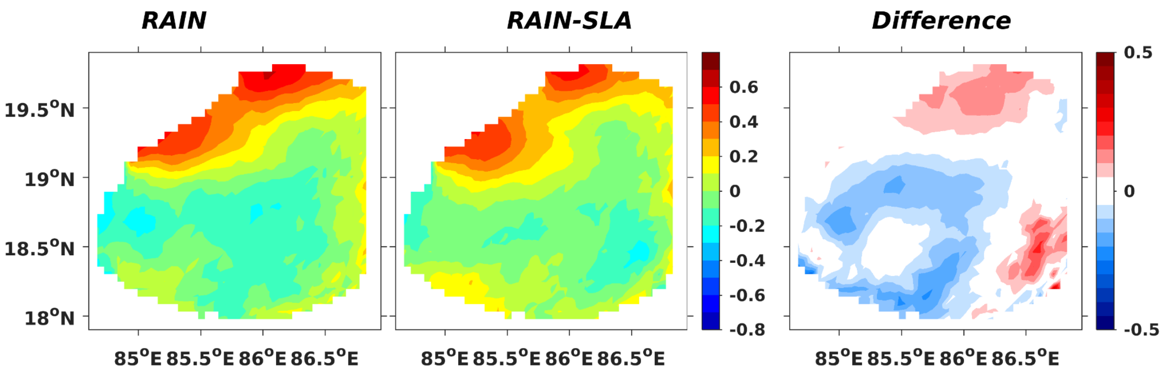

Figure 6.35: Spatial correlation with respect to u component of the horizontal velocity of Odisha HF radar from a) RAIN, (b) RAIN-SLA and (c) Difference

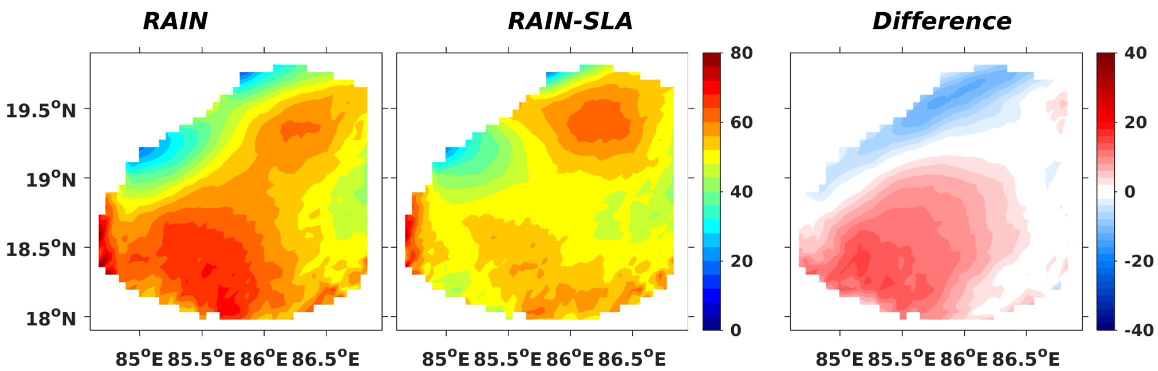

Figure 6.36: Spatial RMSE with respect to u component of the horizontal velocity of Odisha HF radar from a) RAIN, (b) RAIN-SLA and (c) Difference

6.5.2 v current

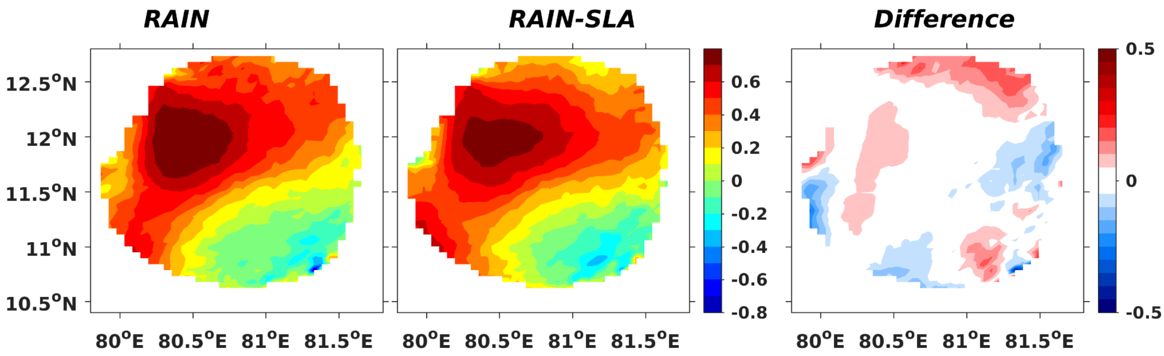

Figure 6.37: Spatial correlation with respect to v component of the horizontal velocity of Tamil Nadu HF radar from a) RAIN, (b) RAIN-SLA and (c) Difference

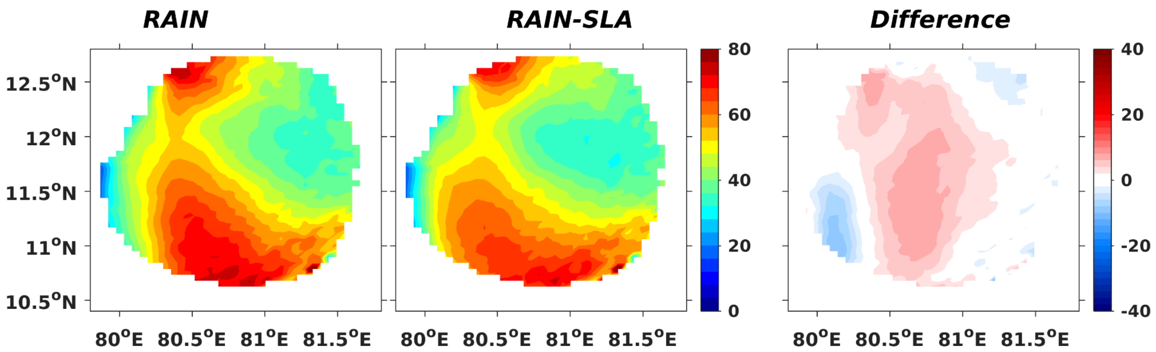

Figure 6.38: Spatial RMSE with respect to v component of the horizontal velocity of Tamil Nadu HF radar from a) RAIN, (b) RAIN-SLA and (c) Difference

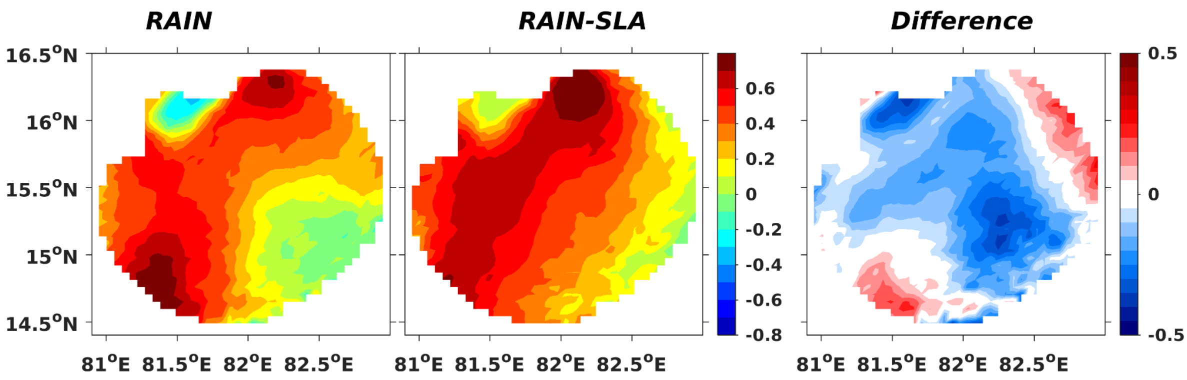

Figure 6.39: Spatial correlation with respect to v component of the horizontal velocity of Andhra Pradesh HF radar from a) RAIN, (b) RAIN-SLA and (c) Difference

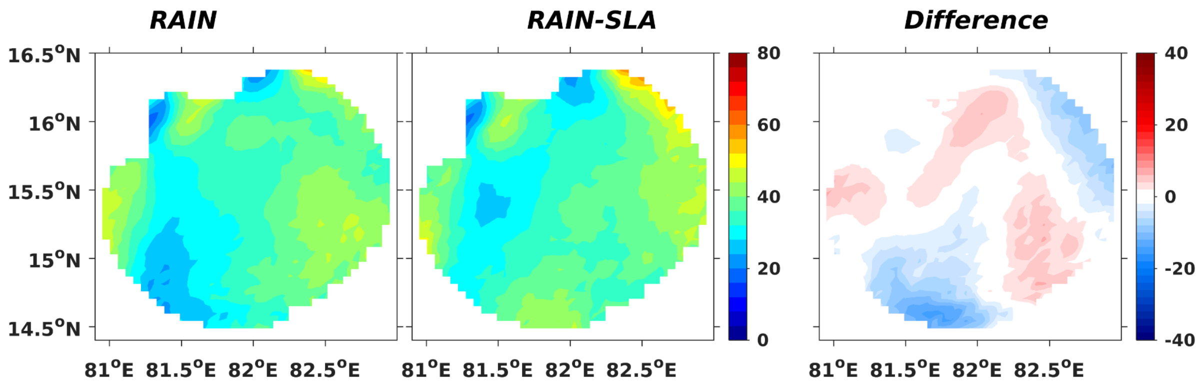

Figure 6.40: Spatial RMSE with respect to v component of the horizontal velocity of Andhra Pradesh HF radar from a) RAIN, (b) RAIN-SLA and (c) Difference

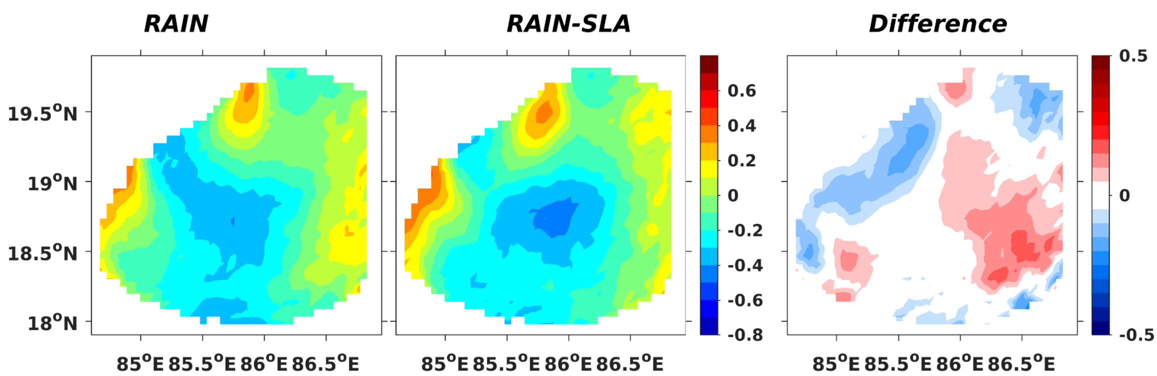

Figure 6.41: Spatial correlation with respect to v component of the horizontal velocity of Odisha HF radar from a) RAIN, (b) RAIN-SLA and (c) Difference

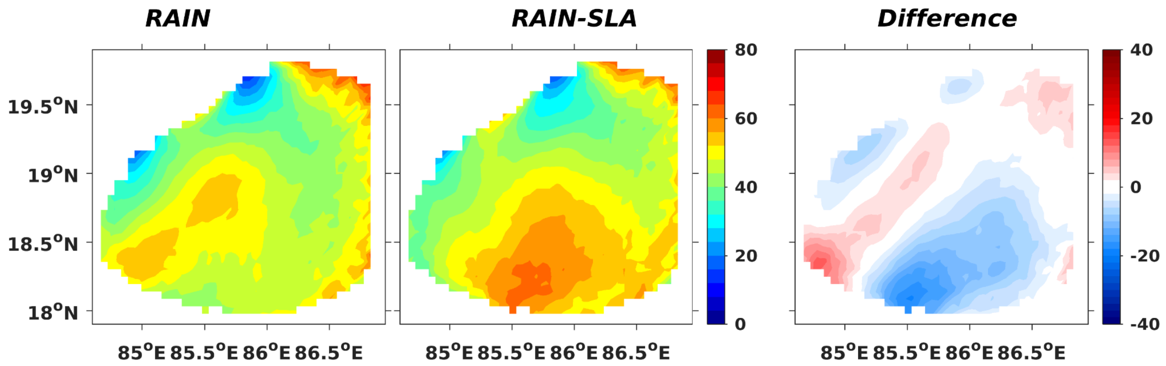

Figure 6.42: Spatial RMSE with respect to v component of the horizontal velocity of Odisha HF radar from a) RAIN, (b) RAIN-SLA and (c) Difference

6.6 Comparison with Coastal ADCP

6.6.1 Deep Ocean

We first consider the comparison with respect to ADCPs located in relatively part of the ocean.

Bhatkal ADCP

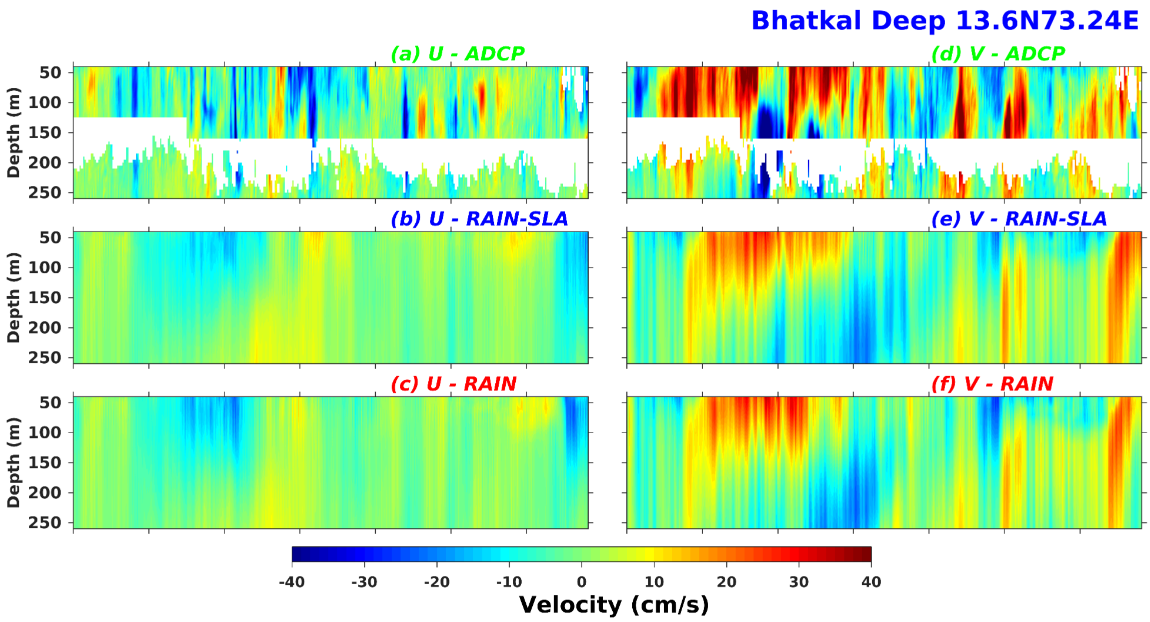

Figure 6.43: (a,d) u,v from ADCP (b,e) u,v from RAIN-SLA. (c,f) u,v from RAIN at Bhatkal

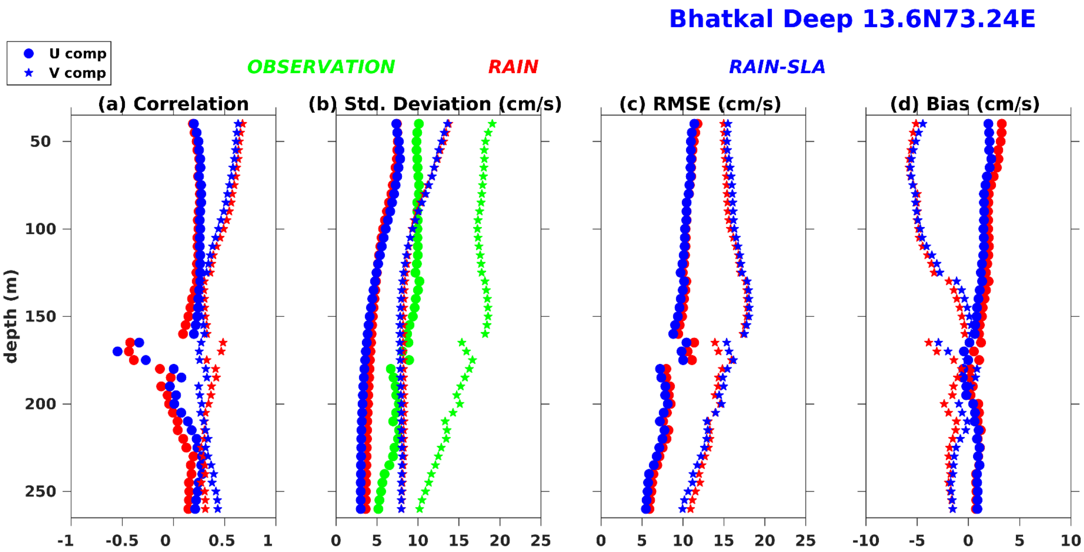

Figure 6.44: (a) Correlation of u(solid circle) and v(star) from RAIN (red) and RAIN-SLA(blue) with ADCP observations at Bhatkal. (b) Standard deviation of u(solid circle) and v(star) in RAIN(red), RAIN-SLA(blue) and ADCP(green). (c) rmse of u(solid circle) and v(star) from RAIN(red) and RAIN-SLA(blue) with respect to ADCP observations. (d) bias of u(solid circle) and v(star) from RAIN(red) and RAIN-SLA(blue) with respect to ADCP observations.

Goa ADCP

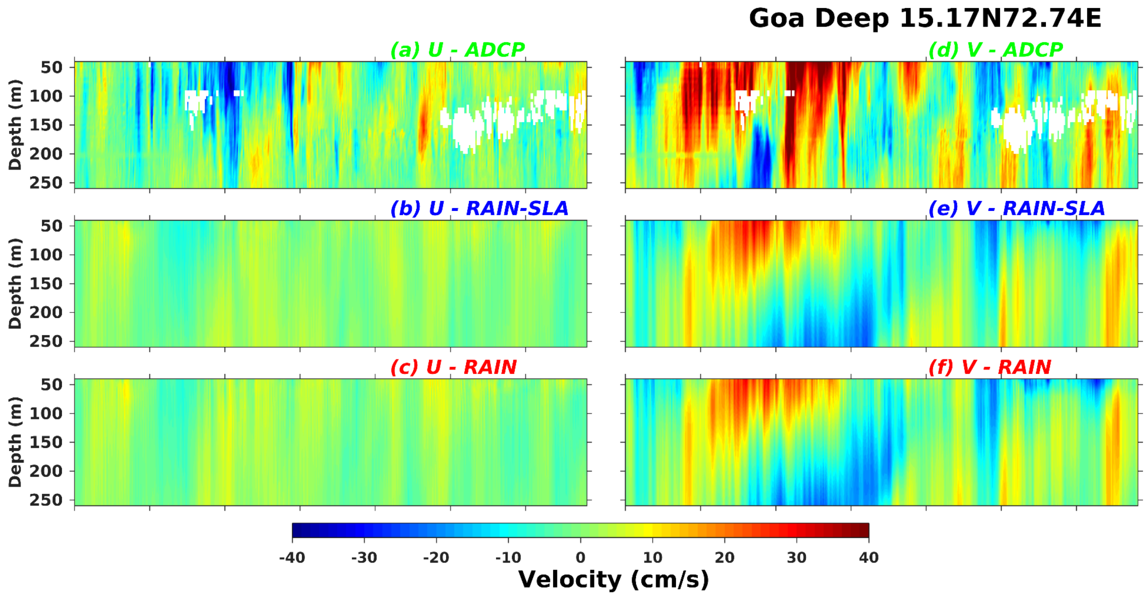

Figure 6.45: (a,d) u,v from ADCP (b,e) u,v from RAIN-SLA. (c,f) u,v from RAIN at Goa

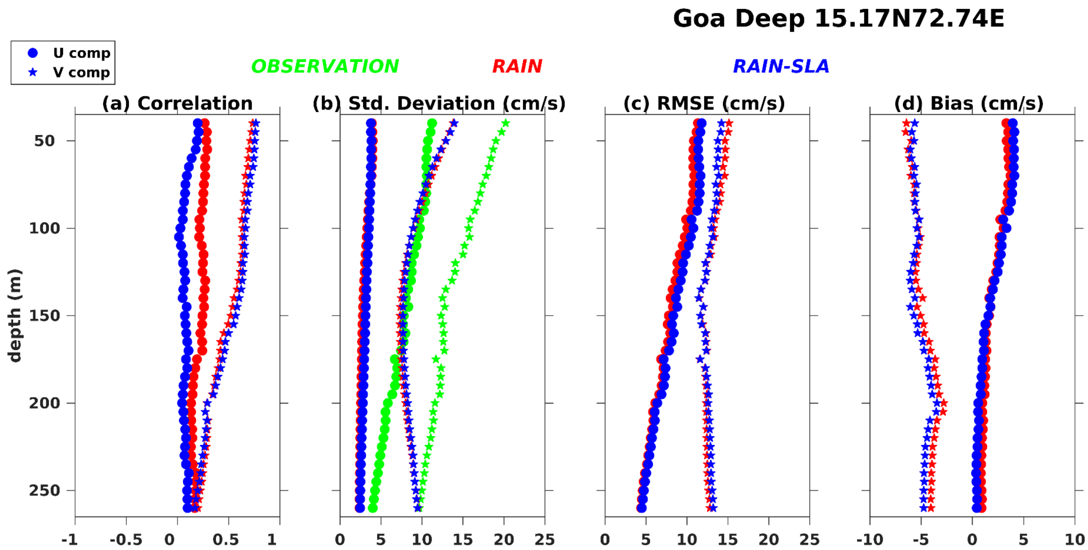

Figure 6.46: (a) Correlation of u(solid circle) and v(star) from RAIN (red) and RAIN-SLA(blue) with ADCP observations at Goal. (b) Standard deviation of u(solid circle) and v(star) in RAIN(red), RAIN-SLA(blue) and ADCP(green). (c) rmse of u(solid circle) and v(star) from RAIN(red) and RAIN-SLA(blue) with respect to ADCP observations. (d) bias of u(solid circle) and v(star) from RAIN(red) and RAIN-SLA(blue) with respect to ADCP observations.

Vizag ADCP

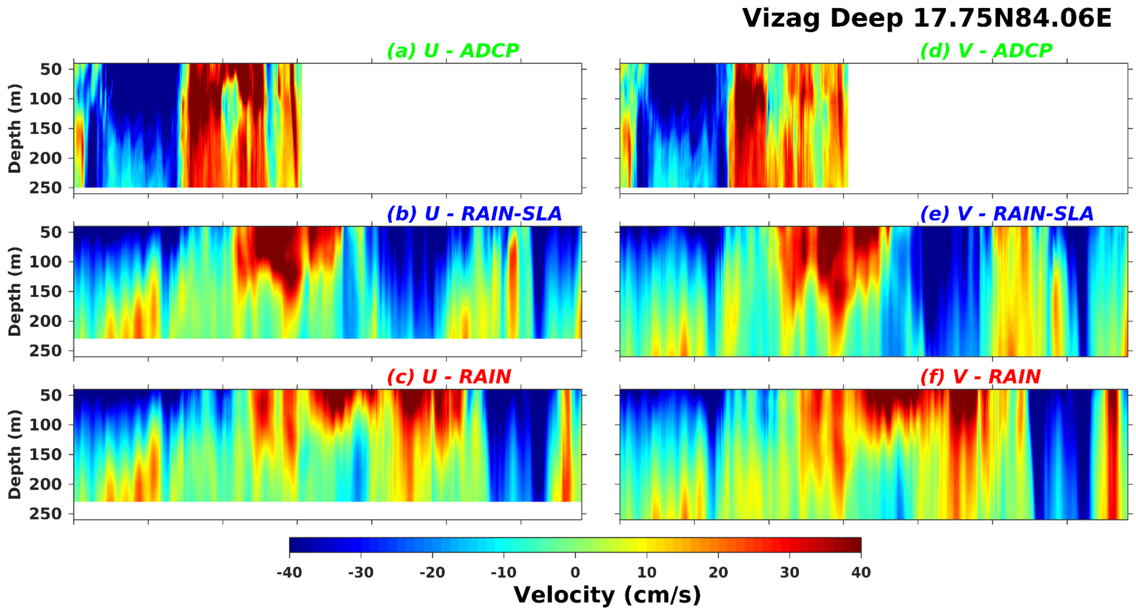

Figure 6.47: (a,d) u,v from ADCP (b,e) u,v from RAIN-SLA. (c,f) u,v from RAIN at Vizag

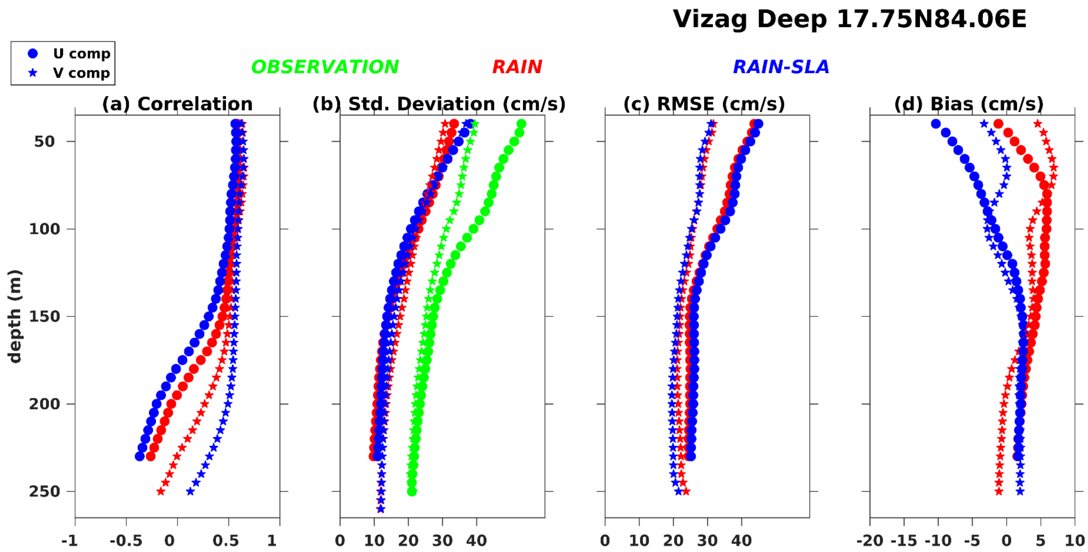

Figure 6.48: (a) Correlation of u(solid circle) and v(star) from RAIN (red) and RAIN-SLA(blue) with ADCP observations at Vizag. (b) Standard deviation of u(solid circle) and v(star) in RAIN(red), RAIN-SLA(blue) and ADCP(green). (c) rmse of u(solid circle) and v(star) from RAIN(red) and RAIN-SLA(blue) with respect to ADCP observations. (d) bias of u(solid circle) and v(star) from RAIN(red) and RAIN-SLA(blue) with respect to ADCP observations.

Paradeep ADCP

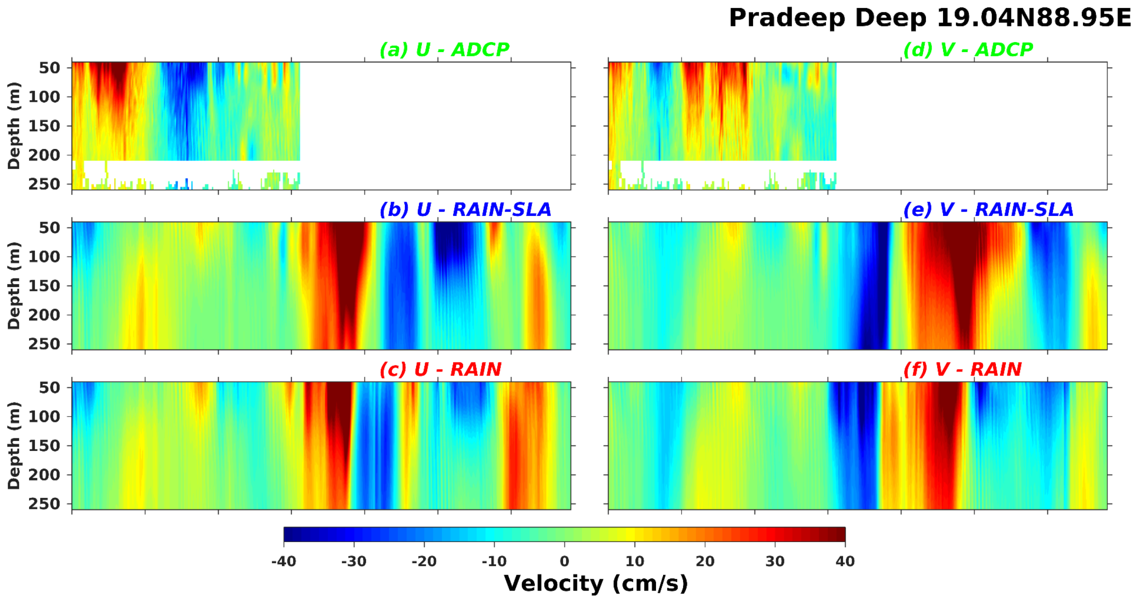

Figure 6.49: (a,d) u,v from ADCP (b,e) u,v from RAIN-SLA. (c,f) u,v from RAIN at Pradeep

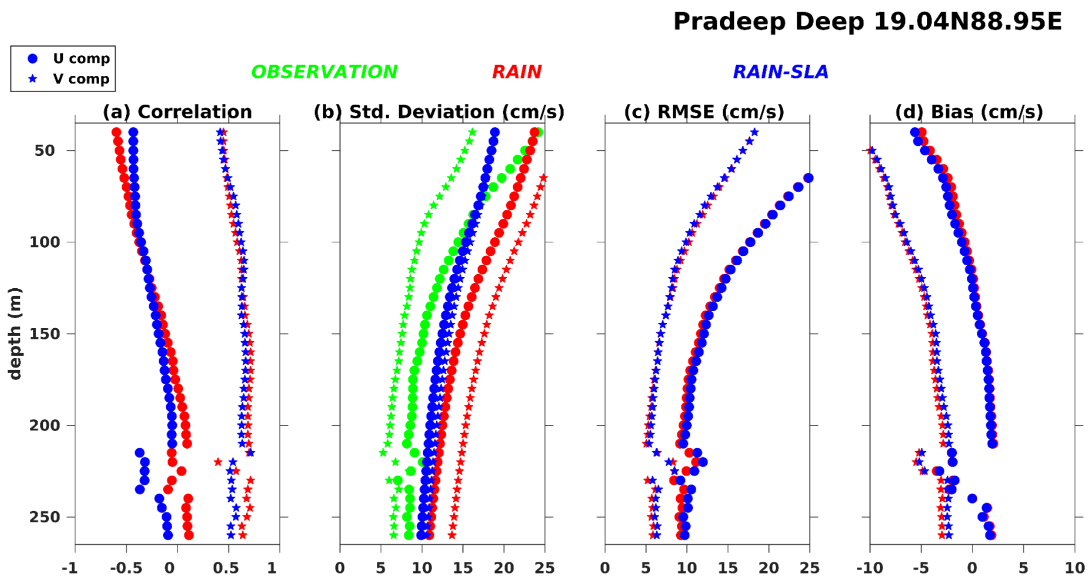

Figure 6.50: (a) Correlation of u(solid circle) and v(star) from RAIN (red) and RAIN-SLA(blue) with ADCP observations at Pradeep. (b) Standard deviation of u(solid circle) and v(star) in RAIN(red), RAIN-SLA(blue) and ADCP(green). (c) rmse of u(solid circle) and v(star) from RAIN(red) and RAIN-SLA(blue) with respect to ADCP observations. (d) bias of u(solid circle) and v(star) from RAIN(red) and RAIN-SLA(blue) with respect to ADCP observations.

Mumbai ADCP

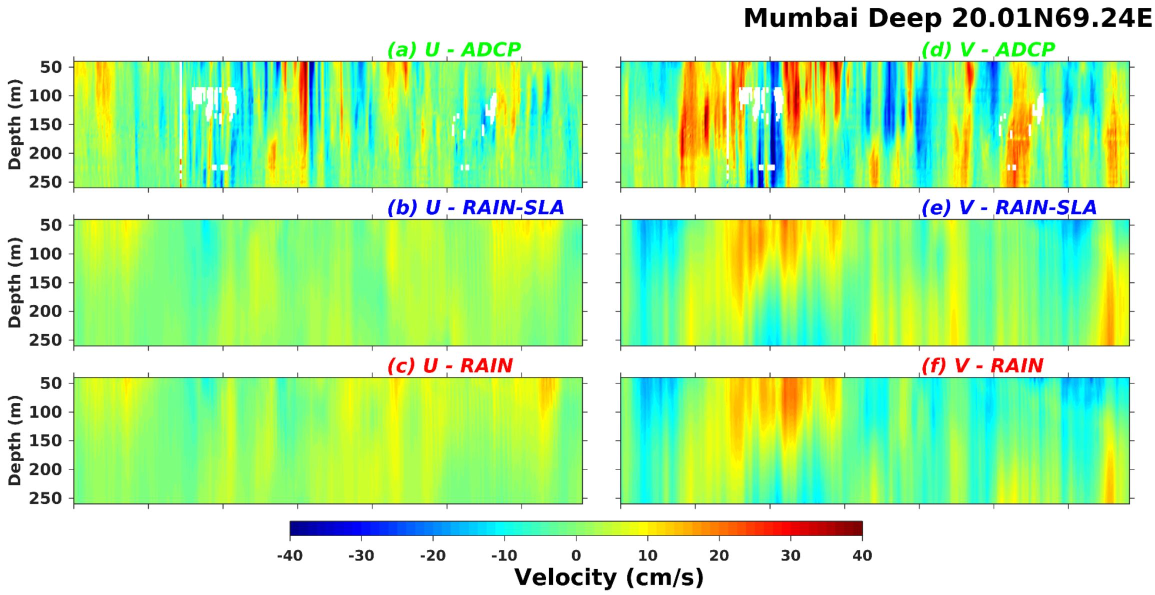

Figure 6.51: (a,d) u,v from ADCP (b,e) u,v from RAIN-SLA. (c,f) u,v from RAIN at Mumbai

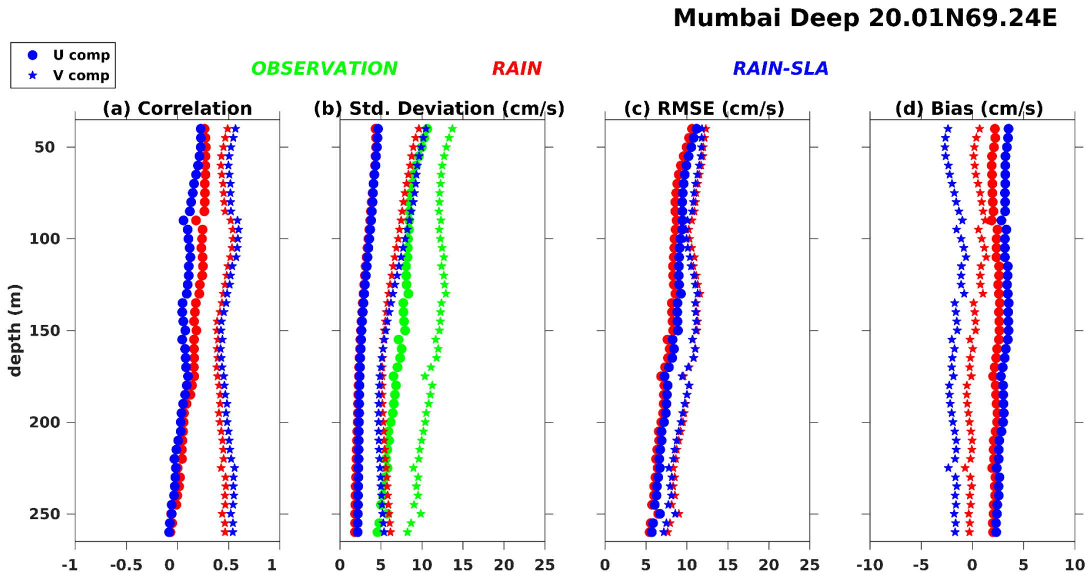

Figure 6.52: (a) Correlation of u(solid circle) and v(star) from RAIN (red) and RAIN-SLA(blue) with ADCP observations at Mumbai. (b) Standard deviation of u(solid circle) and v(star) in RAIN(red), RAIN-SLA(blue) and ADCP(green). (c) rmse of u(solid circle) and v(star) from RAIN(red) and RAIN-SLA(blue) with respect to ADCP observations. (d) bias of u(solid circle) and v(star) from RAIN(red) and RAIN-SLA(blue) with respect to ADCP observations.

Kanyakumari ADCP

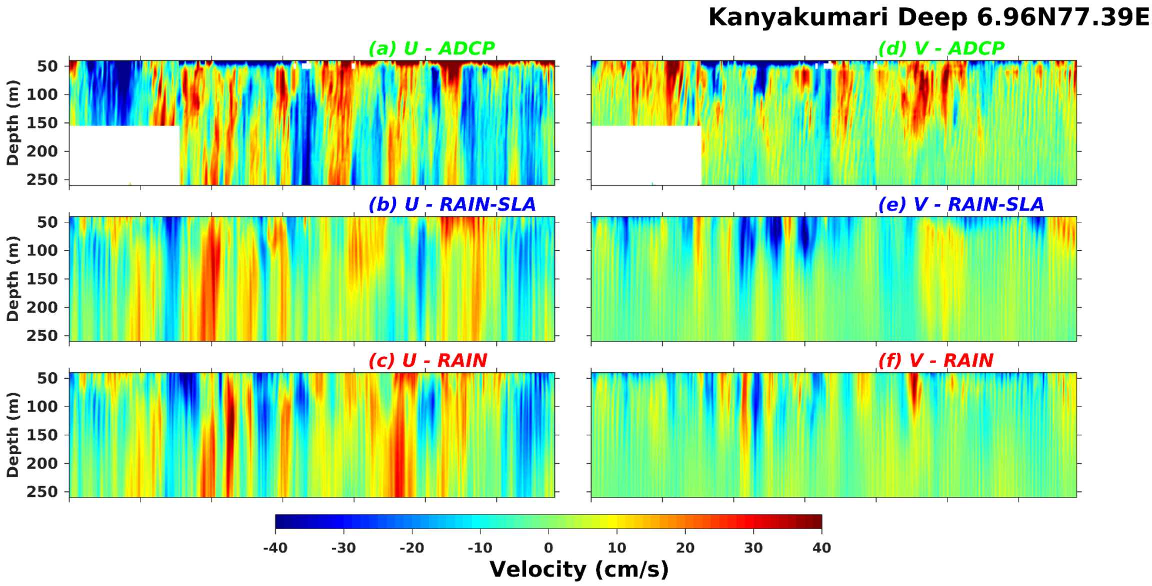

Figure 6.53: (a,d) u,v from ADCP (b,e) u,v from RAIN-SLA. (c,f) u,v from RAIN at Kanyakumari

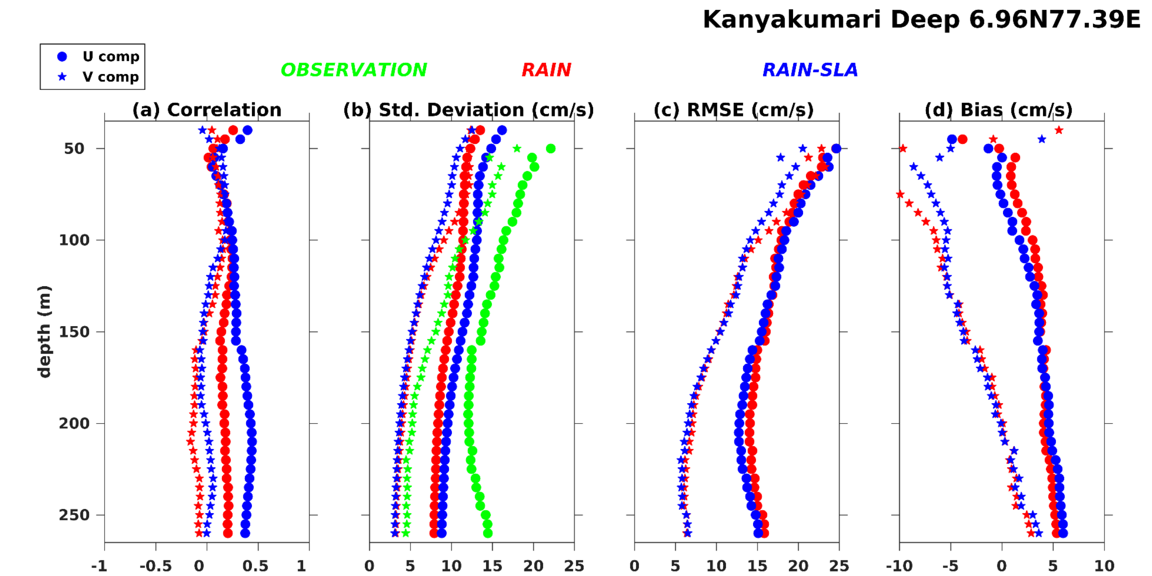

Figure 6.54: (a) Correlation of u(solid circle) and v(star) from RAIN (red) and RAIN-SLA(blue) with ADCP observations at Kanyakumari. (b) Standard deviation of u(solid circle) and v(star) in RAIN (red), RAIN-SLA (blue) and ADCP (green). (c) rmse of u(solid circle) and v(star) from RAIN (red) and RAIN-SLA (blue) with respect to ADCP observations. (d) bias of u(solid circle) and v(star) from RAIN (red) and RAIN-SLA (blue) with respect to ADCP observations.

Kollam ADCP

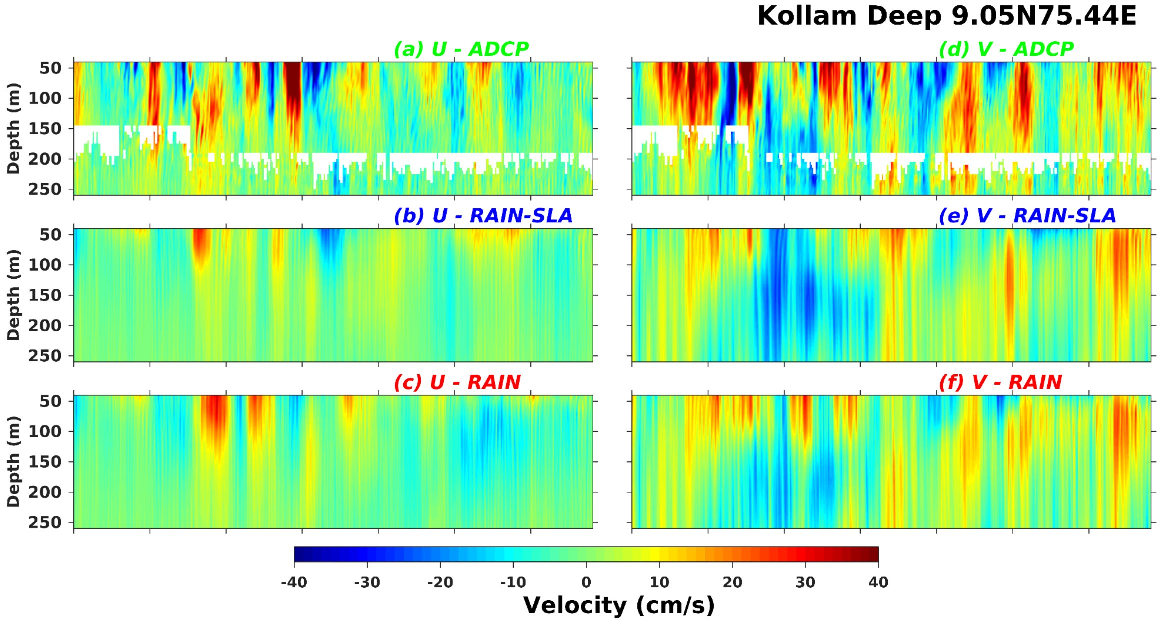

Figure 6.55: (a,d) u,v from ADCP (b,e) u,v from RAIN-SLA. (c,f) u,v from RAIN at Kollam

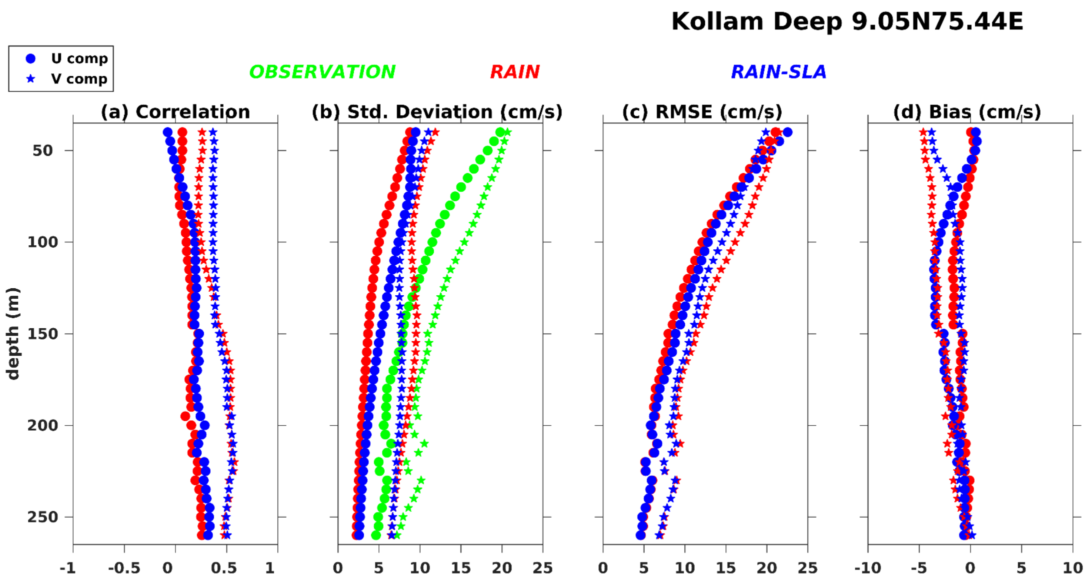

Figure 6.56: (a) Correlation of u(solid circle) and v(star) from RAIN (red) and RAIN-SLA(blue) with ADCP observations at Kollam. (b) Standard deviation of u(solid circle) and v(star) in RAIN(red), RAIN-SLA(blue) and ADCP(green). (c) rmse of u(solid circle) and v(star) from RAIN(red) and RAIN-SLA(blue) with respect to ADCP observations. (d) bias of u(solid circle) and v(star) from RAIN(red) and RAIN-SLA(blue) with respect to ADCP observations.

6.6.2 Shallow Ocean

We now consider the performance of RAIN and RAIN-SLA in the shallow ocean.

Bhatkal ADCP

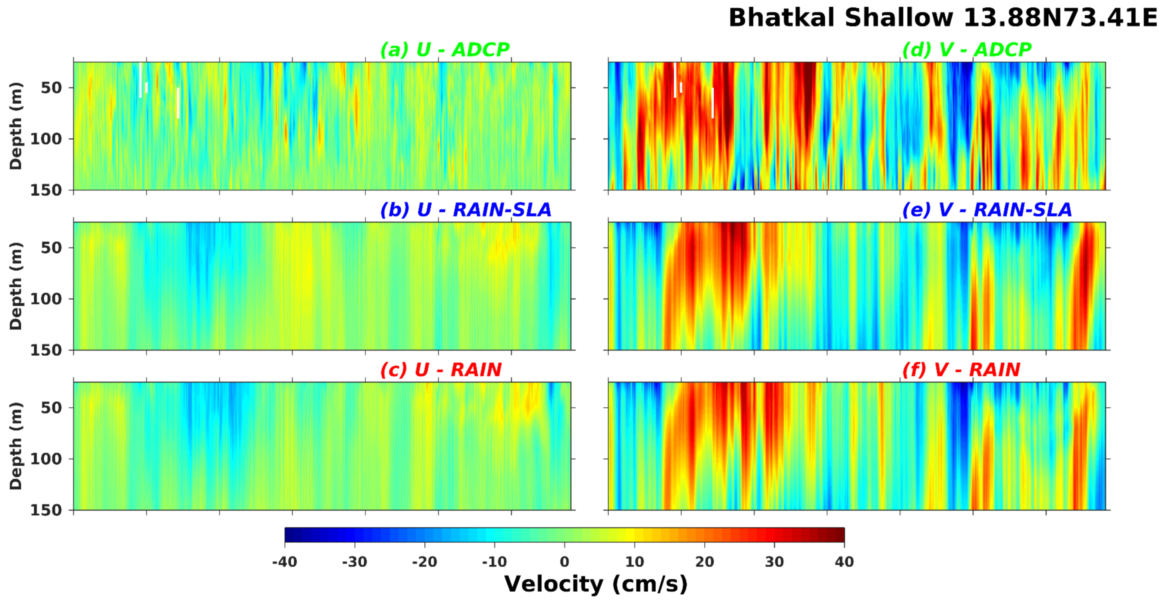

Figure 6.57: (a,d) u,v from ADCP (b,e) u,v from RAIN-SLA. (c,f) u,v from RAIN at Bhatkal

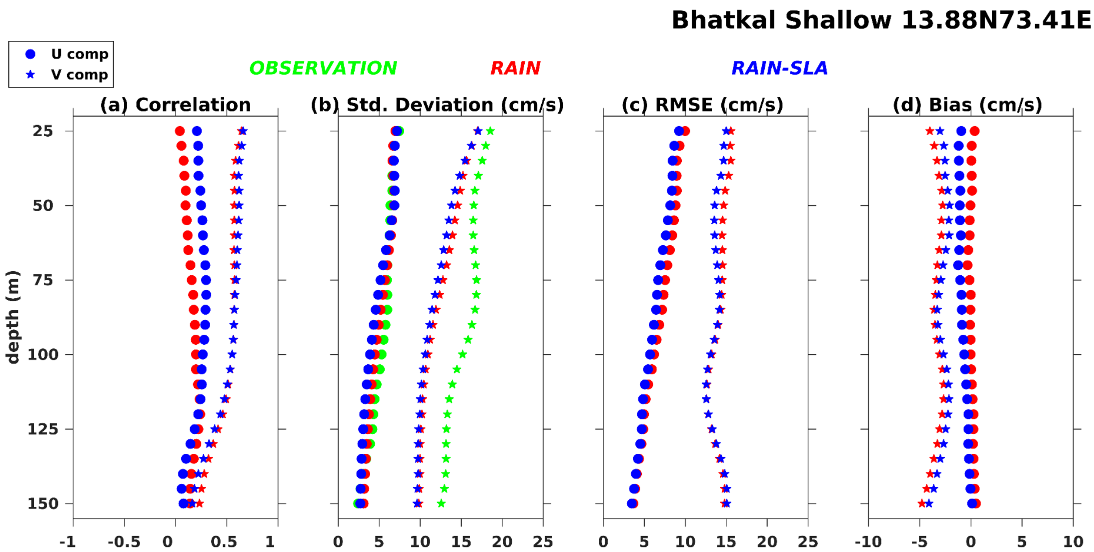

Figure 6.58: (a) Correlation of u(solid circle) and v(star) from RAIN (red) and RAIN-SLA(blue) with ADCP observations at Bhatkal. (b) Standard deviation of u(solid circle) and v(star) in RAIN(red), RAIN-SLA(blue) and ADCP(green). (c) rmse of u(solid circle) and v(star) from RAIN(red) and RAIN-SLA(blue) with respect to ADCP observations. (d) bias of u(solid circle) and v(star) from RAIN(red) and RAIN-SLA(blue) with respect to ADCP observations.

Goa ADCP

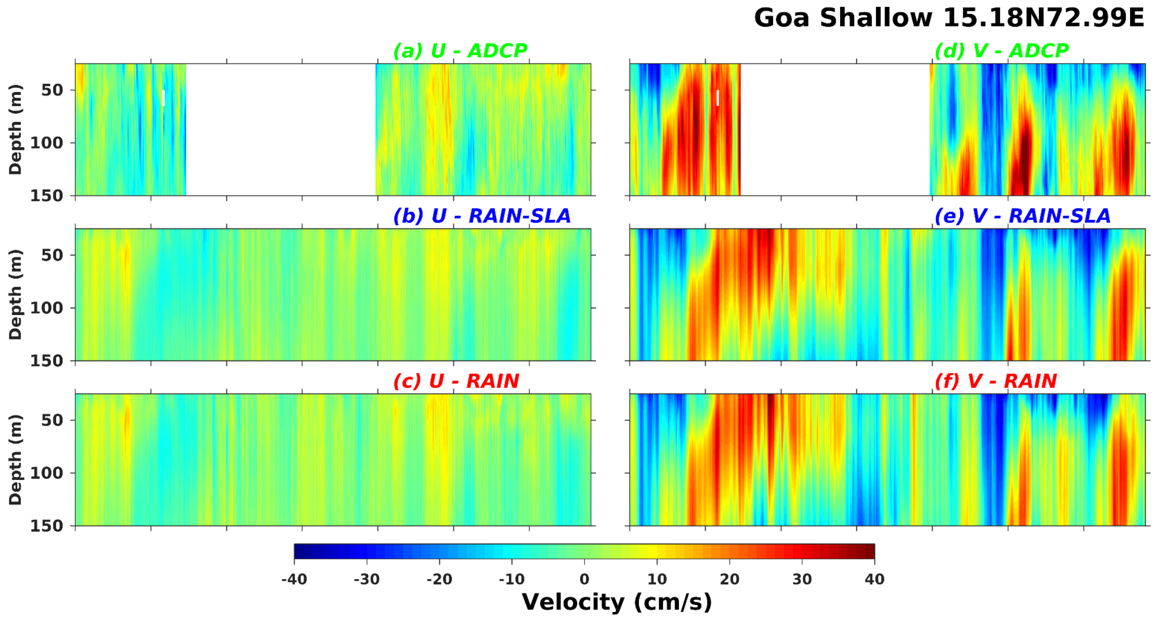

Figure 6.59: (a,d) u,v from ADCP (b,e) u,v from RAIN-SLA. (c,f) u,v from RAIN at Goa

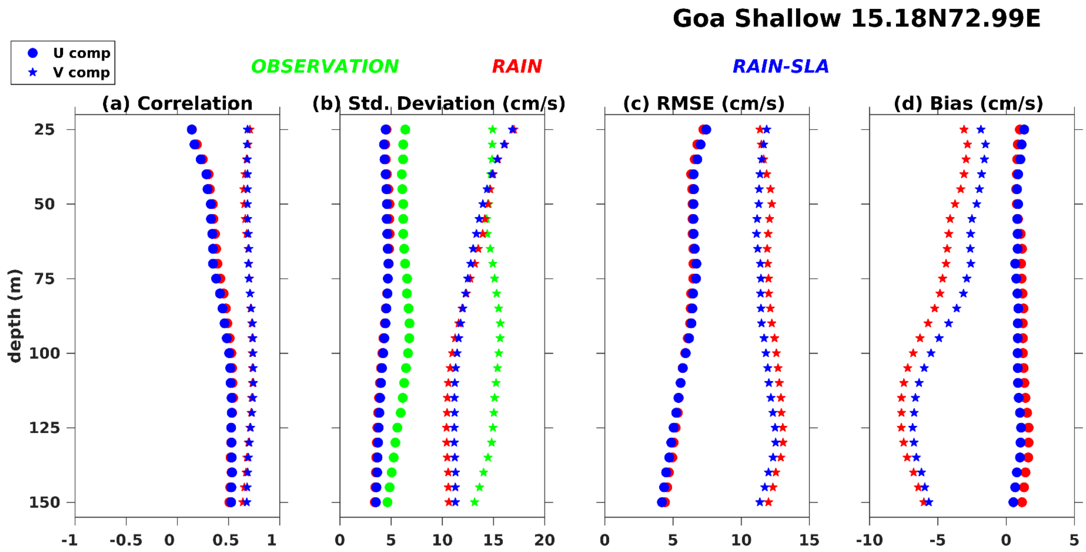

Figure 6.60: (a) Correlation of u(solid circle) and v(star) from RAIN (red) and RAIN-SLA(blue) with ADCP observations at Goa. (b) Standard deviation of u(solid circle) and v(star) in RAIN(red), RAIN-SLA(blue) and ADCP(green). (c) rmse of u(solid circle) and v(star) from RAIN(red) and RAIN-SLA(blue) with respect to ADCP observations. (d) bias of u(solid circle) and v(star) from RAIN(red) and RAIN-SLA(blue) with respect to ADCP observations.

Gopalpur ADCP

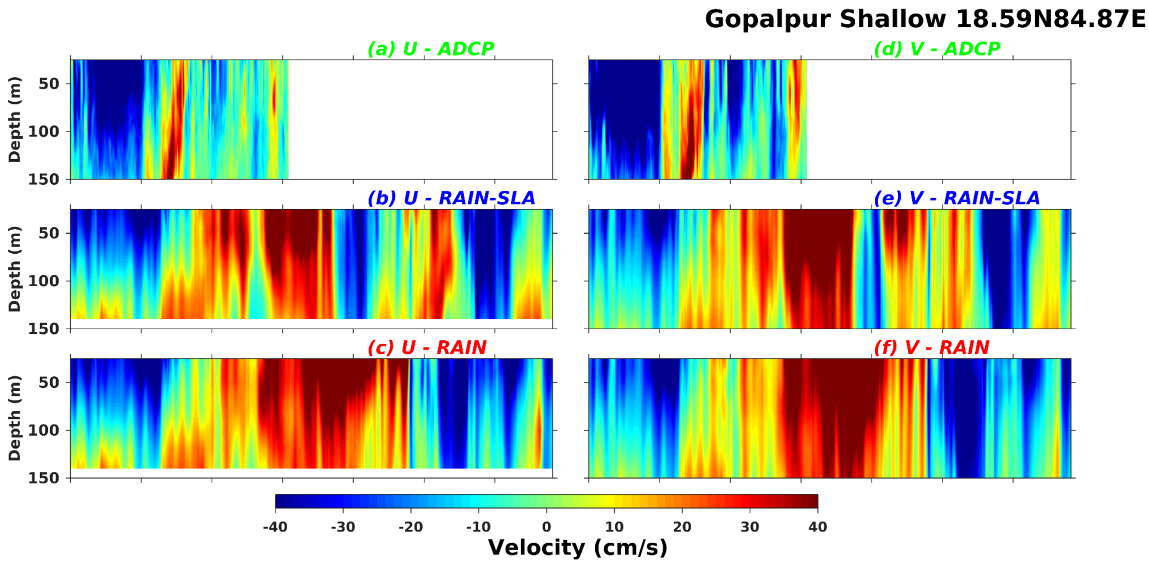

Figure 6.61: (a,d) u,v from ADCP (b,e) u,v from RAIN-SLA. (c,f) u,v from RAIN at Gopalpur

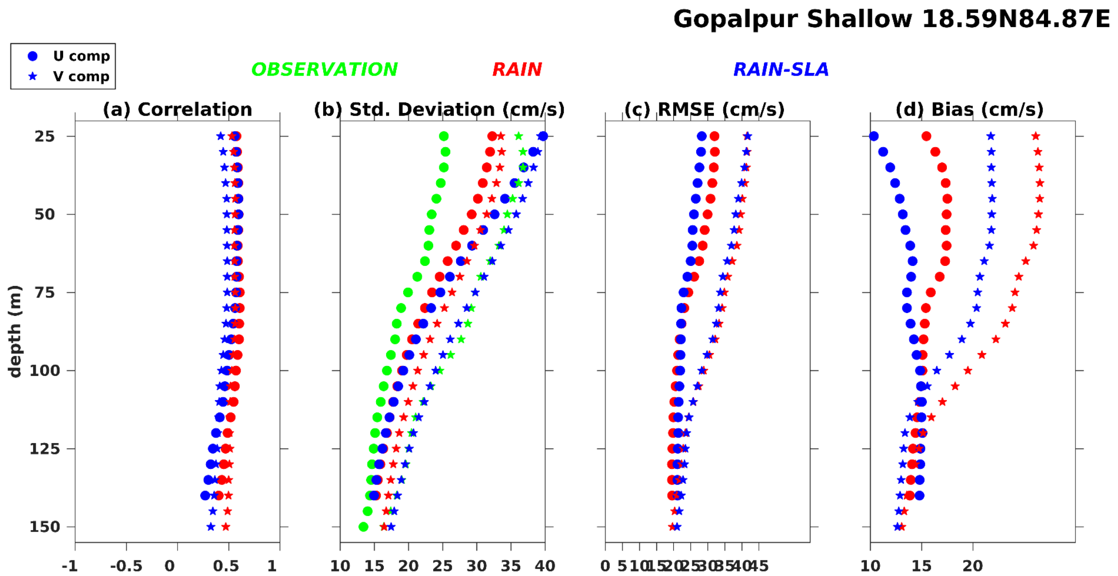

Figure 6.62: (a) Correlation of u(solid circle) and v(star) from RAIN (red) and RAIN-SLA(blue) with ADCP observations at Gopalpur. (b) Standard deviation of u(solid circle) and v(star) in RAIN(red), RAIN-SLA(blue) and ADCP(green). (c) rmse of u(solid circle) and v(star) from RAIN(red) and RAIN-SLA(blue) with respect to ADCP observations. (d) bias of u(solid circle) and v(star) from RAIN(red) and RAIN-SLA(blue) with respect to ADCP observations.

Vizag ADCP

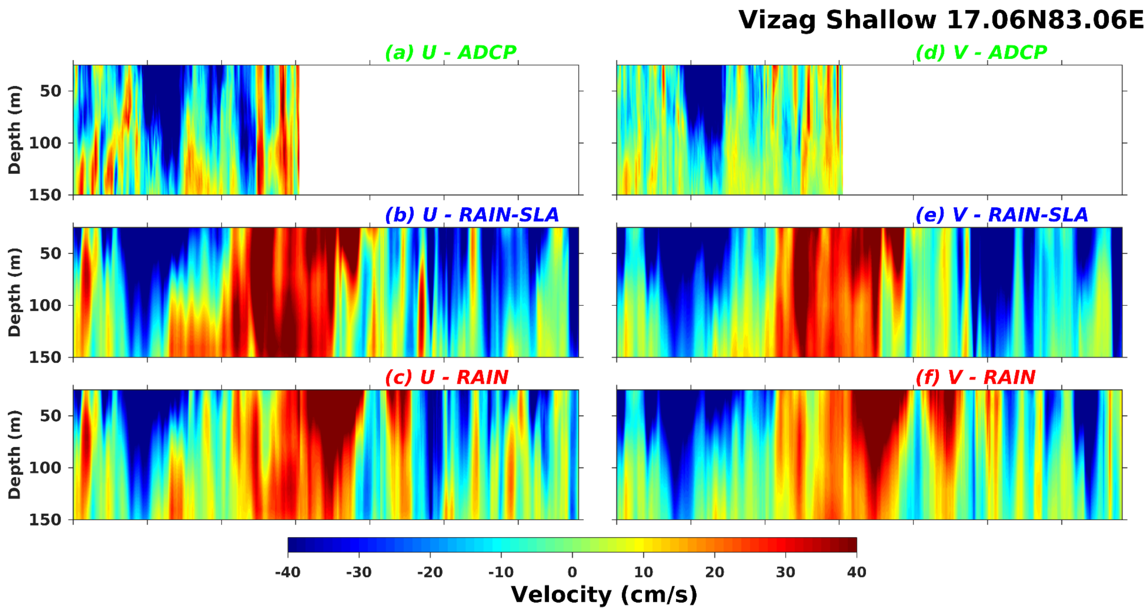

Figure 6.63: (a,d) u,v from ADCP (b,e) u,v from RAIN-SLA. (c,f) u,v from RAIN at Vizag

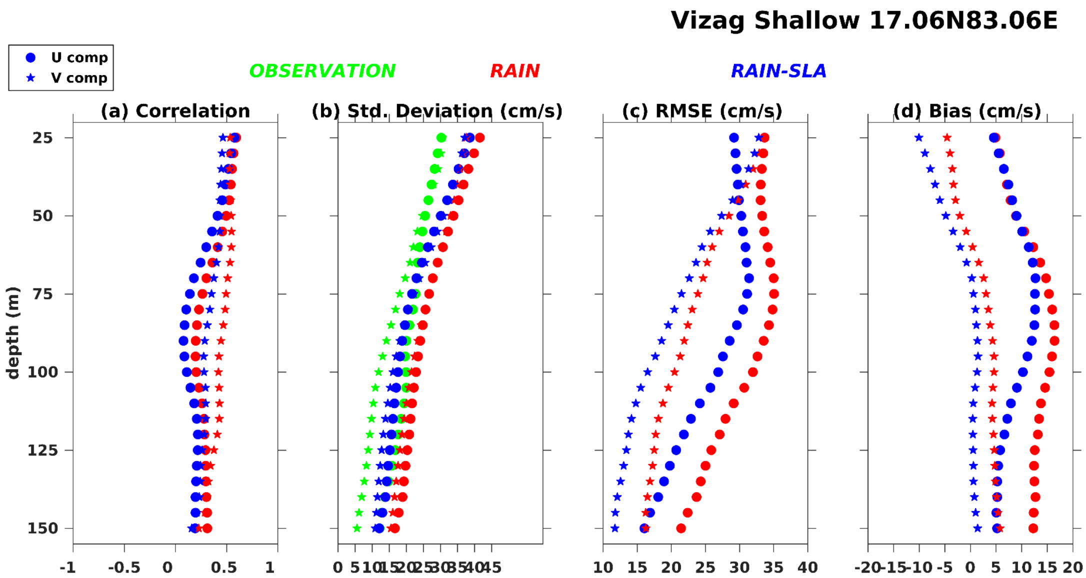

Figure 6.64: (a) Correlation of u(solid circle) and v(star) from RAIN (red) and RAIN-SLA(blue) with ADCP observations at Vizag. (b) Standard deviation of u(solid circle) and v(star) in RAIN(red), RAIN-SLA(blue) and ADCP(green). (c) rmse of u(solid circle) and v(star) from RAIN(red) and RAIN-SLA(blue) with respect to ADCP observations. (d) bias of u(solid circle) and v(star) from RAIN(red) and RAIN-SLA(blue) with respect to ADCP observations.

6.7 Conclusion

Assimilation of SLA has improved the currents significantly across various in-situ locations as seen from comparisons with ADCPs stationed close to the coasts. The correlations have improved and the RMSEs have decreased. Most of the improvement in the ADCP comparison is in the RMSE. Comparison with HF-RADAR also indicates that the assimilation of SLA has improved the coastal currents.

7 Bottom Pressure values

7.1 Introduction

INCOIS has deployed several bottom pressure recorders (BPRs) across the Indian Ocean for detecting tsunamis. In-situ BPRs anchored on the ocean floor measure the total pressure caused by the weight of the oceanic and atmospheric column above it. In normal mode of operation, BPR samples every 15 minutes and transmits every hour. We however compare daily-averaged bottom pressure values from the BPRs with the daily averaged bottom pressure estimated offline from RAIN and RAIN-SLA.

7.2 Comparison with Observations

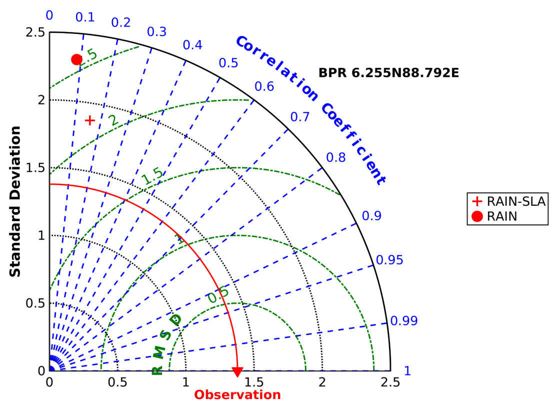

Figure 7.1 : Taylor Diagram of bottom pressure from RAIN-SLA and RAIN with respect to BPR mooring at 6.255° N, 88.792° E

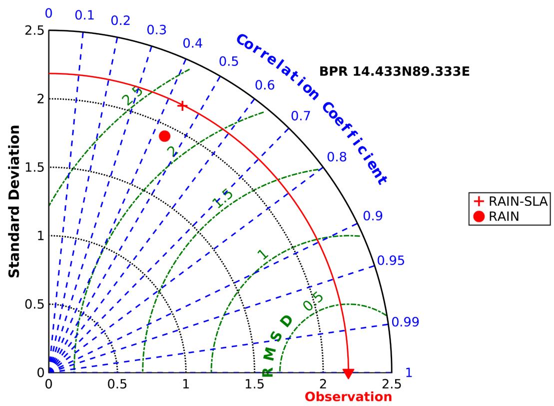

Figure 7.2 : Taylor Diagram of bottom pressure from RAIN-SLA and RAIN with respect to BPR mooring at 14.433° N, 89.333° E

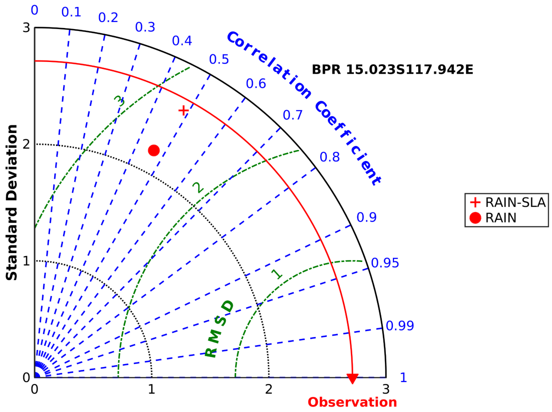

Figure 7.3 :Taylor Diagram of bottom pressure from RAIN-SLA and RAIN with respect to BPR mooring at 15.023° S, 117.942° E

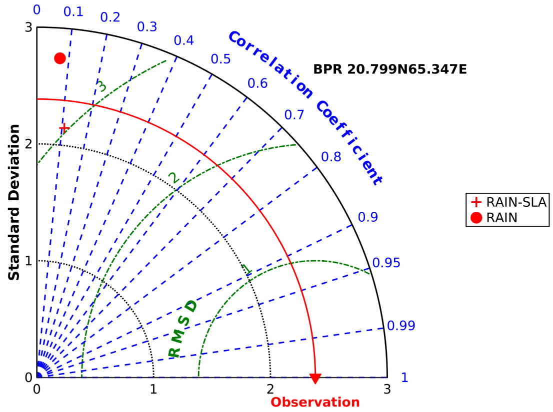

Figure 7.4 :Taylor Diagram of bottom pressure from RAIN-SLA and RAIN with respect to BPR mooring at 20.799° N, 65.347° E

7.3 Conclusion

We observe a marked improvement in bottom pressure estimation, as expected, once SLA is assimilated across three of the locations out of four.

8 Discussion & Summary

The existing operational RAIN set-up is augmented with assimilation of satellite track data of sea level anomaly. This assimilation has been done in two steps. In step one, we assimilate all available in-situ temperature and salinity profiles along with satellite track data of SST. Thereafter, we estimate the steric height from the analysis so obtained. Since the sea level anomaly output from ROMS does not contain steric height information, we deduct this steric height from the observations and assimilate the residue to the model using LETKF. This system (RAIN-SLA), using 40 ensembles, is run for two years - from September 2016 to December 2018. We comprehensively compare RAIN-SLA with a similar system except that SLA is not assimilated in the second system.

The comparison of the two systems reveal that assimilating SLA in the existing systems brings in the following characteristics :

1) There is a slight improvement in SST across the Indian Ocean.
2) There is no significant improvement or degradation in the temperature and salinity profiles.
3) Most profound improvements are seen in currents which is an independent variable.
4) The bottom pressure of the ocean, which is an independent variable, improves across multiple locations.

References

[1] Song, Y. and D. B. Haidvogel, *A semi-implicit ocean circulation model using a generalized topography-following coordinate system,* J. Comp. Phys., 115 (1), 228-244 (1994).

[2] Haidvogel, D. B. and A. Beckmann, *Numerical Ocean Circulation Modeling. Series on Environmental Science and Management* Vol. 2, Imperial College Press, 319 pp (2004).

[3] Haidvogel, D. B., H. G. Arango, K. Hedstrom, A. Beckmann, P. Malanotte-Rizzoli, and A. F. Shchepetkin, *Model evaluation experiments in the North Atlantic Basin: Simulations in nonlinear terrain-following coordinates*, Dyn. Atmos. Oceans, 32, 239-281 (2000).

[4] Shchepetkin, A. F., and J. C. McWilliams, *The Regional Ocean Modeling System: A splitexplicit, free-surface, topography following coordinates ocean model,* Ocean Modelling, 9, 347-404 (2005).

[5] P.A. Francis et al, *The Indian Ocean Forecast System,* Current Science, 104, 1354-1368 (2013).

[6] P.A. Francis et al, *High-Resolution Operational Ocean Forecast and Reanalysis System for the Indian Ocean,* Bulletin of the American Meteorological Society, E1340-E1356 (2020).

[7] Balaji, B., Deepsankar, B., Paul, B., Sanikommu Sivareddy, P.A. Francis, Abhisek Chatterjee, and Arya Paul, *LETKF-ROMS: An improved predictability system for the Indian Ocean.* Technical Report, ESSO-INCOIS-MDG-TR- 03, 96 pages. (2018).

[8] Baduru, B., B. Paul, D. S. Banerjee, S. Sanikommu, and A. Paul, *Ensemble based regional ocean data assimilation system for the Indian Ocean: Implementation and evaluation.* Ocean Modelling, 143, 101470. (2019).

[9] Sanikommu, S., D. S. Banerjee, B. Baduru, B. Paul, A. Paul, K. Chakraborty, and I. Hoteit, *Impact of dynamical representational errors on an Indian Ocean ensemble data assimilation system.* Quarterly Journal of the Royal Meteorological Society, 145, 3680 - 3691, (2019).

[10] Hunt, Brian R., Eric J. Kostelich, and Istvan Szunyogh. *Efficient data assimilation for spatiotemporal chaos: A local ensemble transform Kalman filter.* Physica D: Nonlinear Phenomena 230(1-2) 112-126. (2007)

[11] Fu, W. *On the Role of Temperature and Salinity Data Assimilation to Constrain a Coupled PhysicalBiogeochemical Model in the Baltic Sea.* J. Phys. Oceanography, 46, 713729, (2016). https://doi.org/10.1175/JPO-D-15-0027.1

[12] Ott, E., Hunt, B. R., Szunyogh, I., Zimin, A. V., Kostelich, E. J., Corazza, M., Yorke, J. A. *A local ensemble Kalman filter for atmospheric data assimilation.* Tellus A, 56(5), 415-428 (2004).

[13] Bishop, Craig H., Brian J. Etherton, and Sharanya J. Majumdar. *Adaptive sampling with the ensemble transform Kalman filter. Part I: Theoretical aspects.* Monthly weather review

129(3), 420-436, (2001).

[14] McPhaden, M.J., Meyers, G., Ando, K., Masumoto, Y., Murty, V.S.N., Ravichandran, M., Syamsudin, F., Vialard, J., Yu, L., Yu, W., *RAMA: The research moored array for african-asian-Australian monsoon analysis and prediction.* Bulletin of the American Meteorological Society 90, 459 - 480. (2009).

[15] Reynolds, R.W., Smith, T.M., Liu, C., Chelton, D.B., Casey, K.S., Schlax, M.G., *Daily high-resolution-blended analyses for sea surface temperature.* Journal of Climate. 20, 5473–5496. (2007).

[16] Levitus, Sydney, et al. ”World ocean atlas 2009.” (2002)

[17] Levitus, Sydney, et al. *Global ocean heat content 19552008 in light of recently revealed instrumentation problems.* Geophysical Research Letters, 36, 7, (2009).

[18] The Ssalto/Duacs altimeter products were produced and distributed by the Copernicus Marine and Environment Monitoring Service (CMEMS)(http://www.marine.copernicus.eu).

[19] Jena, B. K., Anuraj, K. S., Suseentharan, V., Tushar, Kukadiya, Karthikeyan, T. *Indian coastal ocean radar network.* Current Science, 116(3), 372–378. (2019).